NSF/CEE-82054

UILU-ENG-82-2014

PB83-144624

CIVIL ENGINEERING STUDIES

STRUCTURAL RESEARCH SERIES NO. 502

AN ANALYTICAL STUDY OF THE INTERACTION OF FRAMES AND INFILL MASONRY WALLS

by

C. E. RIVERO

and

W. H. WALKER

A Technical Report of
Research Supported by the
NATIONAL SCIENCE FOUNDATION
under Grant Nos. ENV 77-07190
and
PFR 80-02582

DEPARTMENT OF CIVIL ENGINEERING
UNIVERSITY OF ILLINOIS
AT URBANA-CHAMPAIGN
URBANA, ILLINOIS

SEPTEMBER 1982

AN ANALYTICAL STUDY OF THE INTERACTION OF FRAMES AND INFILL MASONRY WALLS

BY

C. E. RIVERO

and

W. H. WALKER

A Report on a Research Project Sponsored by the
NATIONAL SCIENCE FOUNDATION
Research Grant Nos. ENV 77-07190 and PFR 80-02582

University of Illinois at Urbana-Champaign
Urbana, Illinois
September 1982

ACKNOWLEDGMENT

This investigation was part of a research program sponsored by the National Science Foundation under Grant ENV 77-07190, "Engineering Design For Natural Hazards". Any opinions, findings, and conclusions or recommendations expressed in this publication are those of the author and do not necessarily reflect the views of the National Science Foundation. The report was prepared as a doctoral dissertation by C. E. Rivero under the supervision of W. H. Walker, Associate Professor of Civil Engineering, and was submitted to the Graduate College of the University of Illinois at Urbana-Champaign in partial fulfillment of the requirements for the Ph.D. degree.

The development of the computer program and the numerical results as presented in this report were obtained with the use of the CDC Cyber 175 and IBM 4341 computers, and the Zeta 1453B plotting device. These facilities are supported by the Computing Services Office (CSO) of the University of Illinois. Partial computer service funding was provided by the Research Board of the Graduate College of the University of Illinois.

The authors wish to thank Professor D.A.W. Pecknold for his constructive comments throughout the study. The authors are also grateful for the assistance provided by the CSO Systems Consulting staff and to Dr. J. M. Nau for providing the computer programs for the spectrum plots and the plotting programs for the time history response.

TABLE OF CONTENTS

Page

LIST OF TABLES

LIST OF FIGURES

Page

CHAPTER 1

INTRODUCTION

1.1 Introductory Remarks

Infill walls have, for many years, formed an integral part of buildings. Their use, as well as their size, shape, and material composition have been largely based on their architectural function. The use of these walls mainly as architectural elements considerably simplified their structural design. This design was usually done by the architect.

In the typical design process structural engineers seldom knew where these partitions would go and since they served no structural purpose, they were largely ignored in the design of the main structural configuration. Yet engineers recognized the fact that these partitions could influence the behavior of the main structure especially when these walls were used to infill the space between two columns. In order to take this effect into account two basic assumptions were usually made about the structural behavior of these walls or partitions:

1. The wall tended to behave as a short beam, mainly in shear, being very stiff in its own plane and relatively flexible normal to its own plane.
2. The wall was essentially a brittle element whose lateral load capacity was small compared to the

lateral load capacity of the frame that surrounded it.

The first of these assumptions was based mainly on the height to width ratio of the wall which was usually less than one. The second assumption was based on the material properties of the wall which usually consisted of materials weak in tension and shear. One of the most widely used materials for these partitions was, and still is, unreinforced masonry which has a very brittle behavior in both tension and shear.

Although these assumptions seemed quite reasonable, they ignored the confining effect that the frame had on the wall. This fact, as will be seen, invalidated the assumptions and radically altered the behavior of the frame that enclosed the wall. The behavior of the frame-infill-wall system is relatively complex and as yet not fully understood. Therefore, at the present time a full explanation of its behavior cannot be given. Only the most relevant and well understood facts that affect the frame wall interaction will be discussed.

To understand the overall behavior of the frame-infill-wall system one should look at the boundary conditions that the frame imposes on the wall when a lateral load is applied. Before any load is applied the infill wall may be assumed continuous with the floor system while a gap or space may be assumed to exist between the wall and columns that surround it. These assumptions are based on widely used construction techniques for the

placement of these walls. As a first observation, these walls are usually placed after the main structural elements have undergone most of their initial dead load deformation. This usually precludes any frame wall interaction due to the dead load of the structure. In addition, as these walls are placed in the structure a gap is usually left between the frame and wall to allow for ambient changes in both humidity and temperature. Usually some material is placed in the gaps that exist between the frame and wall. This material is usually weak in tension with a relatively low modulus of elasticity.

Due to the existence of the gaps, the frame is initially free to deform without any constraints. Had the frame been continuous with the wall tension, compression, and shear stresses would develop at their common boundary. This indicates that in regions where tension would be developed, if the system were continuous, the gap size would increase while in the areas of compression the gaps either diminish or are totally closed creating an interaction between the wall and frame.

The amount of contact between the frame and wall, if linear elastic conditions are assumed, depends on the stresses at the frame wall boundary and the amount of loading present. Properly analyzed, the interaction between the frame and infill makes the overall problem nonlinear even when a linear elastic, small displacement theory is used. This nonlinearity may be explained as follows. Boundary conditions imposed on the wall by the frame

depend to a great extent on the magnitude of the load while the rigidity of the whole system depends on the boundary conditions and contact stresses between the frame and wall. It is this interdependence which makes the rigidity of the frame-infill-wall system a function of the displacement.

As the load increases, additional nonlinearities may come into play as the frame imposes a lateral load on the wall. Under typical conditions the infill tends to behave as a short, unreinforced masonry beam which usually results in a tensile failure at the base of the wall. Under unconfined conditions the wall would not be able to sustain any additional loading in fact, the load level would drop, in spite of the fact that the wall is virtually intact. When used as an infill the wall is not totally free to move, the frame confines and constrains its movement and usually forces the wall to change its mode of behavior. The wall usually changes from a flexural-shear behavior to an approximately axial compressive behavior across the diagonal of the frame. At this point the wall has not only altered its internal stress pattern but also its failure criteria from its weakest mode in tension and shear to its most efficient form of carrying load, compression. As a consequence of this change in behavior, the infill wall, not only alters its own stress pattern, but also modifies the fundamental frequency and behavior of the frame that surrounds it.

The fact that the behavior of the frame may be substantially modified by the presence of the infill points to the need of studying this phenomenon both analytically and experimentally under static and dynamic loads.

1.2 Object and Scope

One of the most severe loadings a frame-infill-wall system may experience is that due to a large earthquake. There are numerous examples of frames, although properly designed to resist earthquake loading when acting alone, being severely damaged due to the presence of infilled walls acting in the plane of the frame. Therefore, to design rationally an infill frame against earthquake loading the presence of these partitions should be taken into account in the design process. To accomplish this goal two basic steps should be taken:

1. Develop the techniques necessary to take explicitly into account, during the analysis and design process, the stiffening effect of these walls and their localized effect on the frame that surrounds it. These techniques should be developed so as to use the same assumptions common to the design process.
2. Under seismic loading, study the effect of these partitions on the maximum distortions and forces in the surrounding frame.

This research will deal mainly with the second step just outlined. Since the present design philosophy in earthquake engineering is based on allowing inelastic deformations to dissipate energy, the study of the frame-infill-wall system, under seismic loading, should include the inelastic domain.

The main objective of this research will be to develop an analytical model of the frame-infill-wall system to study its behavior versus that of the open frame. The scope of the model will include nonlinear behavior of the frame, wall, and their interaction under seismic loading. The research should include the effect of the frequency content of the earthquake, and the effect of the wall on the columns and girders that surround it.

1.3 Review of Previous Research

The literature that deals specifically with the frame-infill-wall system is extensive, dating back to at least 1957[8]. A review of all the available literature on the subject will not be done here, for most of the literature does not deal directly with the interaction problem. A good review of the different aspects of the overall problem may be found in Refs.[31,41,42]. Only that part of the literature which has a direct bearing on the development of the model will be reviewed herein.

Apparently the first attempt at studying the frame-infill-wall system while taking into account the change in behavior of the

wall was made by Stafford Smith [58,59,60]. By studying a simple one story frame with an infilled wall, Smith developed what could be called the "Equivalent Strut Method". This method consists of the replacement of the infilled wall with an equivalent diagonal bracing element. The area and therefore the stiffness of this element is dependent on the relative rigidity of the frame versus the infilled wall. The area of the bracing element was determined by multiplying the thickness of the wall by an equivalent width of wall which acts in compression along the diagonal of the frame. To arrive at this equivalent width Smith developed formulas that related the equivalent width to the amount of contact area that is developed at the frame wall boundary. This formula was expressed in terms of the structural characteristics and dimensions of both the frame and infill wall.

The advent of the finite element method allowed several researchers to make a more detailed model of the infilled wall and to specify with greater accuracy the boundary conditions imposed on the wall by the frame. This step was especially important for unreinforced masonry walls.

Storm [61] represented the wall as an assembly of bricks but he did not represent the mortar joints between the bricks or between the infill wall and frame as an independent set of elements. This brought on the problem of continuity. Whenever the stresses between the bricks exceeded the failure stress for the joints the two degrees of freedom would become independent

forcing a reformulation of the whole problem. In spite of this drawback the crack pattern of the model seemed to follow the test results reasonably well not only in the masonry infilled panel but also at its interface with the frame. From this study it was evident that the crack pattern in the masonry required a different approach to that normally used in the study of concrete. The need for a different approach is due in part to the inhomogeneity of masonry which tends to create preferred planes of failure along its mortar joints.

Franklin [19] represented the wall as an assembly of elements. He provided equivalent stiffness values to represent the masonry and used link elements to represent the contact stresses and compatibility between the frame and wall. He approached the modeling of the wall by dividing it into elements which were larger than the bricks but smaller than the whole wall. He also provided a brittle-type material model for the wall element to represent the masonry. The link elements provided the interaction between the frame and the wall. The failure model seemed too stiff, for the wall remained continuous with the frame almost up to failure. This seems to be in contradiction with the expected behavior of the material that is usually placed in the gaps between the frame and infill. The possible difficulty might be found in the tensile versus bond failure of this type of material. The concept of the overall model provided a promising approach to the handling of the frame-infill-wall interaction.

Page [46,47] developed a model for masonry. Modeling the brick and joints individually, he overcame most of the drawbacks of the model used by Storm. He represented the mortar by using joint elements similar to those developed in rock mechanics and allied disciplines. This model allowed for cracking along mortar joints to occur without having the problem of compatibility. The proposed model makes it easy to handle most of the cracking problems in masonry. This is especially true when reverse loading is applied. Page used the model to predict the behavior of several test specimens. The results given by the model seem to follow fairly well the behavior of the test and the crack pattern which was produced. Of all the proposed models this one has the greatest versatility with respect to loading and boundary conditions, and is the most sophisticated model of a masonry wall available in the present literature.

All of the previously cited references have the common factor of dealing specifically with monotonic loading. In spite of this, some of the models have been used as the basis for the development of new models to study static reverse loading as well as dynamic loading.

Klinger [31] used the diagonal strut concept to try to predict the behavior of the frame-infill-wall system under static reversed loading. Based on his own experiments Klinger developed a load displacement curve under reversed loading for the

equivalent diagonal element. He encountered the problem that to represent the wall under reverse loading two elements were needed, one across each diagonal. This related the damage to one diagonal element when loading in one direction to the damage suffered by the cross diagonal in the previous loading cycle. The finite element method made the handling of this problem difficult due to the independence of the two elements. He solved the problem by making assumptions on how the damage suffered by the diagonal element in one direction affected the behavior of the other diagonal element. The assumptions made were based on the maximum displacements suffered by the structure.

Kost [33] studied the gaps between the frame and wall under dynamic loading for structures which always remained elastic. To carry out the study Kost created gap elements to monitor the behavior of the space between the infill wall and frame. He based the model on nodal compatibility of the frame and infill wall. Whenever the frame and wall came into contact at a specific node he provided a relatively stiff spring as a link to guarantee compatibility between the frame and infill. This approach, although approximate in nature, facilitated the computations because the original set of equations at the beginning of the solution applied throughout the whole process. It is not clear from the work how the author determines when the gaps that are closed become open or how he keeps track of the gap size. This is an important question if the structure undergoes permanent deformations. Although the author considered only elastic

structures this method showed the effect of the gaps on the dynamic behavior of the frame-infill-wall system.

1.4 Notation

The symbols used in this study are defined in the text when they first appear. These symbols are listed here to provide an easy reference of all the symbols defined.

a_1, a_2	constants for Rayleigh type damping
$\{a\}$	acceleration vector
$\{*a\}$	vector of the increment in acceleration
$[A]$	dynamic matrix
$\{B\}$	dynamic load vector
$[C]$	damping matrix
c_i	modal damping corresponding to mode i
$\{*d\}$	vector of the increment in displacement
$\{*d_1\}$	vector of the increment in displacements of the structure degrees of freedom
$\{*d_2\}$	vector of the increment in displacements of the boundary degrees of freedom
F_i	control point for the failure surface
f'	compressive strength of masonry
f_t	tensile strength of masonry
I	number of dynamic degrees of freedom
$[K']$	reduced stiffness matrix
$[K_{ij}]$	submatrix, where i and j may be 1 or 2
k_i	modal stiffness corresponding to mode i

[M]	mass matrix
m_i	modal mass corresponding to mode i
M_y	yield moment
m	constant
n_1	normal stress control point in joint failure surface
n_i	damping ratio corresponding to mode i
n	constant
p_i	circular frequency corresponding to mode i
[Q]	modal matrix, matrix formed by the mode shapes
q	a constant in Newmark's integration scheme
{res}	total residual force vector
{R}	ground influence vector
s_1	shear stress control point in joint failure surface
{TIF}	total inertial force vector
{TDF}	total damping force vector
{TEF}	total external force vector
{TIR}	total internal force vector
*t	time interval, or integration time step
{v}	velocity vector
{*v}	vector of the increment in velocity
θ	angle with respect to the mortar joints at which the principal stresses occur

CHAPTER 2

MECHANICAL MODEL

2.1 Introduction

The modeling of the frame-infill-wall problem may be classified into two broad categories: the equivalent diagonal strut method, and the finite element method. Each one of these methods has advantages and disadvantages which make each one well suited for specific but different conditions. It must be observed that the equivalent strut method only provides an analysis of the interaction between the frame and infill wall. Once this analysis is carried out the strut method must rely on a more general technique such as the finite element method to analyze the structure as a whole. This division in the analysis distinguishes the equivalent strut method from the finite element technique.

The equivalent diagonal strut has the great advantage of simplicity. Without increasing the number of degrees of freedom used in the analysis of the structure, it provides a simple method of taking walls into account. However, the indirect provision for handling the frame-wall interaction with this method does lack versatility. Unless additional validation studies are done, the method has a limited application whenever the conditions under which it was derived are considerably

altered. Any attempt at using this approach for dynamic analysis immediately runs into the problem of providing an overall load-displacement curve, under reverse loading, for the diagonal element. The development of this curve may be quite difficult, especially for masonry walls, and specifically when the boundary conditions of the frame-infill-wall system change considerably under load reversal.

The finite element technique easily overcomes most of the disadvantages of the strut method. It allows for great flexibility especially in the modeling of the wall and its interaction with the frame. With adequate modeling of the material behavior of its various parts the frame-infill-wall system may be studied with greater accuracy and detail. This allows for more flexibility in the study of its behavior under varied loading patterns, boundary conditions and structural forms. However, the versatility gained in using the finite element method may be overshadowed by the need to use a large number of degrees of freedom to model the masonry wall adequately. In the specific case of dynamic behavior the number of degrees of freedom could be excessive.

The advantages and disadvantages of the two approaches for the modeling of the frame-infill-wall system suggest the need to develop a model to study this problem under nonlinear dynamic loads. This model should have the versatility of the finite element method while reducing the number of degrees of freedom needed to model the frame-infill-wall system.

2.2 Development of Model

The development of the model and its characteristics may be divided into two areas for discussion. The first area deals with the topological development, specifically with the representation of the structural configuration and the problems related to it. The second area deals with the material model development to describe the behavior and characteristics of the materials that make up the structure. The topological development will be treated in this chapter and the material model will be described in Chapter 3.

2.2.1 Columns and Beams

Columns and beams will be represented by line elements, placed along the centerlines of the members. Column elements will have moment, shear, and axial load capacity. The axial load, shear, and moment will be interdependent with respect to the stability of the element. Beams will have the same characteristics as the columns except that the axial behavior may be constrained when the problem being analyzed allows this approximation or requires it. All inelastic behavior will be concentrated at nonlinear hinges located at the end of the elements. These hinges have zero length and allow for plastic rotation to take place.

2.2.2 Wall

The modeling of the wall may be divided into three basic areas:

1. Boundary between frame and wall.
2. Cracking in the wall itself.
3. Uncracked behavior of the specific wall segment.

The boundary between the frame and wall will be modeled by two types of elements which may be called "gap elements" and "joint elements", respectively. They will reflect, as their names suggest, the conditions that exist at the frame wall boundary at any given time.

The gap elements will model the space that exists between the frame and wall, usually found on the sides and top of the wall. The element will keep track of the gaps and determine when the frame and wall come into contact, forcing continuity of the frame and infill wall at that point.

The joint elements will model the boundary between the frame and wall where continuity is initially assumed. This element permits the representation of mortar joints at the base of the wall. It allows continuity up to a certain stress then permits a change in behavior similar to the gap element.

The uncracked wall itself is represented as an assemblage of triangular elements. Since the study will focus mainly on masonry walls, cracking along mortar joints becomes an important factor.

A joint element is placed at the edge of each wall element to approximately represent the cracking in the masonry wall. Each wall element represents several bricks and joints. It is assumed that all cracking in the wall is concentrated along the boundaries of the wall elements where the joint elements are located. The shape of the wall element is taken to be a triangle. When representing a rectangular section of the infill wall, this shape allows for cracking across the diagonals as well as along the boundaries of the rectangle.

A schematic representation of the wall model as applied to a specific wall section is shown in Fig. 2.1. This figure shows how the three elements which have already been defined are assembled to form the overall model for the wall. A more detailed application of the model is illustrated in Fig. 2.2 through 2.4 taken from Ref.[18]. These figures represent the development of the cracking patterns in the three specimens which were tested to their ultimate capacity. On these figures the proposed wall model has been superimposed as a series of triangles. Two of the specimens, Fig. 2.2 and 2.3, consisted of a simple frame infilled by a masonry wall while the third, Fig. 2.4, consisted of a simple frame infilled by a masonry wall with an opening in the center of the wall. The numbering scheme found in each figure represents the order in which the cracks appeared on the specimen as the lateral load was applied. It may be seen that cracking and separation along the boundary in the test specimen may be modeled by the proposed gap and joint elements. The cracking in the wall

itself may be approximately modeled by the cracking along the boundary of the wall elements using the proposed joint element. As may be seen from the figures some of the real cracks, as represented by the numbering scheme, coincide with the predetermined crack pattern of the proposed model while other real crack patterns may only be modeled approximately.

The use of joint elements to simulate cracking in the wall is based on the need for practicality and simplicity. The treatment of cracking as a continuum property within a finite element is a difficult problem, especially when reverse loading is considered. This treatment is even more difficult when a material like masonry is being modeled. Masonry tends to crack along its mortar joints with little damage to the surrounding bricks. When the load is reversed these cracks close and the masonry strength is essentially unaffected. This fact makes the cracking of masonry a difficult problem to model as a continuum.

2.3 Assumptions

The postulated models for the beams, columns, and walls may now be assembled to form the frame-infill-wall structure. To accomplish this step certain assumptions and requirements should be made. These assumptions should allow as much flexibility as possible in representing the structure and should enable the application of dynamic loads.

The assumptions are:

1. Torsional effects are neglected; therefore the representation of the structure is limited to the plane of the wall.
2. The connecting points or nodes of the structure will have a maximum of three degrees of freedom, two translations which are mutually perpendicular and one rotation.
3. The relative angle of the members meeting at a node is constant throughout the analysis.
4. Masses may be specified for each degree of freedom.
5. All dynamic loads on the structure are induced by boundary accelerations.
6. Only one boundary acceleration may be a specified but several points may have said acceleration.
7. Small deformations are assumed in the analysis so the equations of equilibrium may be based on the initial configuration.
8. The instantaneous stiffness matrix and nonlinear properties of the structure are assumed constant during each time step.
9. Only kinematic boundary conditions may be specified.
10. The kinematic boundary conditions may be specified independently of the point at which the external acceleration is specified.

Based on these assumptions and requirements, Fig. 2.5 shows an example of the modeling of a three story structure. In this case masses were assumed concentrated at the story level, and specific gaps were assumed to exist between the frame and infill. To simulate cracking in the wall, joint elements would be specified along the boundaries of the wall elements. The ground acceleration may be specified for one of the joints at the base of the structure. Then, to simulate an earthquake type loading, all degrees of freedom for the base of the structure would be specified to move simultaneously. Although a solution to a three story frame-infill-wall system will be demonstrated, the solution to the specific three story structure shown in Fig. 2.5 will not be done.

CHAPTER 3

MATERIAL MODEL

3.1 Introduction

The material models presented in this chapter and the physical model presented in Chapter 2 will constitute the complete inelastic nonlinear model to be used in this study. Just like the topological aspects of the model which were divided into parts representing different aspects of the structure, the material model has similar subdivisions which depend on the part of the structure being represented. The material model may be divided into four areas:

1. The frame material model.
2. The masonry material model.
3. The joint material model.
4. The gap model.

The words "material model" are used here not only in the context of stress strain relationships but also, as in the case of the frame and gap model, to signify a load displacement relationship.

3.2 Frame Material Model

The beam and column elements of the frame are assumed to have a bilinear moment rotation behavior concentrated in the nonlinear

hinges at the ends of the element. Figure 3.1 shows a typical moment rotation curve. This type of moment rotation curve is well suited for steel structures but lacks the degrading stiffness behavior found in concrete structures. Yet its simplicity will help in the understanding of the proposed model.

In the case of the frame-infill-wall, the variation of the curvature over the length of the column is, in general, nonlinear. This is due to the interaction between the frame and wall. Since the change in rotation between the ends of a beam element is the integral of the curvature over its length, the moment rotation relationship will not be bilinear as is being assumed in the material model. However, in modeling the frame-infill-wall problem, the interaction between the frame and wall requires that the columns and beams be subdivided into smaller segments. Over each of these segments the linear variation of the curvature as is used in the proposed model should be a better approximation of the real curvature.

In the case of columns no inelastic material interaction between the axial load and moment is assumed. The axial load has a simple elastoplastic model for material behavior which is independent of the moment rotation model shown in Fig. 3.1. This means that yielding in the flexural mode does not necessarily cause yielding in the axial mode and vice versa. The only interaction of the axial load and moment comes indirectly through the stability of the element. Although not in accord with the

moment-axial load interaction of columns this approach of separating the axial behavior from the moment behavior was chosen so as to simplify the interpretation of results of the overall model.

3.3 Joint Material Model

In the model proposed in Chapter 2 cracking of the masonry wall may be assumed to occur mainly along the mortar joints. Due to the relative dimensions of a typical mortar joint one may assume that only two of the six stress components are not zero.

They are taken to be:

1. Normal stress acting perpendicular to the direction of the largest dimension in the joint.
2. Shear stress acting along the direction of the largest dimension in the joint.

The joint is assumed to have linear elastic behavior up to failure. After failure only compression stresses may be carried across the joint. It is assumed that no shear stresses may be carried across the joint after failure but incremental shear stiffness relationships may exist when normal compressive stresses are present in the joint. The assumed failure surface for the joint element is shown in Fig. 3.2. This figure relates the maximum shear stress that may be carried by the joint to a specific normal stress level. This figure is based on experimental results which are presented in Ref.[41] and discussed in Appendix A.

3.4 Gap Model

A gap element is a function which measures a space. It is in relation to this function or measure that the material model may be specified. The material model of the gap element may be defined in accordance with a load displacement relationship.

The basic property of the gap element is the size of the original gap. If the material on both sides of the gap remain elastic the original size of the gap is a constant and may be used as such. This assertion is based on the fact that when all loads are removed or brought to their initial state the structure returns to its original configuration. If the material on either side of the gap is able to undergo inelastic deformations the original gap size is no longer a constant and must be updated at every step of the computation.

Once the two points across the gap come into contact the gap element problem becomes a surface contact problem. This aspect of the behavior will be discussed in the next chapter.

3.5 Wall Material Model

The wall model proposed in Chapter 2 is assumed to be homogeneous, isotropic, and linearly elastic up to failure. Although masonry is not a homogeneous material this assumption is needed to simplify the modeling of the masonry. The assumption of

linear elastic behavior is based on the experimental evidence available for masonry. This evidence seems to show that unlike concrete, masonry behaves linearly almost up to failure. The treatment of nonisotropic materials is simple to handle under the finite element formulation but the present understanding of the behavior of masonry does not warrant the use of such a model.

The assumed failure surface for masonry is shown in Fig. 3.3. The surface is drawn using the principal stresses as the system of coordinates and the assumption of a plane stress condition for the masonry. Due to the inhomogeneous character of masonry the failure surface may be assumed to depend not only on the principal stresses but also on the angle that these principal stresses make with the mortar joints. To make the failure surface dependent on the principal stresses and the angle at which these are applied the functional shape of the surface may be assumed invariant. Then the five control points F_1, F_2, F_3, F_4, and F_5 may be assumed to be functions of the angle with respect to the mortar joints at which the principal stresses act.

The control points F_1, F_2, in the tension side of the failure surface may be assumed to depend on the principal stress angle in accordance with the following equations:

$$F_1 = f_t(n \times \sin^2 \theta + \cos^2 \theta)$$
$$F_2 = f_t(\sin^2 \theta + n \times \cos^2 \theta) \qquad (3.1)$$

where

n = constant greater than 1

θ = angle with respect to the mortar joints at which the principal stresses occur

f_t = masonry tensile strength

A plot of these two equations is shown in Fig. 3.4. These equations are based on experimental results which may also be found in Ref.[41] and discussed in Appendix A.

The assumed functional dependence of the failure surface control points F_3, and F_4, on the principal stress angle is shown in Fig. 3.5. These functions are also based on experimental results. These results may be found in Ref.[22] and are also discussed in Appendix A. The failure surface control point F_5 is assumed to be equal to the maximum of F_3 or F_4 multiplied by a constant. This constant is assumed to be less than one. Based on the existence of a biaxial state of stress, confinement may be expected to make the control point F_5 greater than F_3 or F_4 rather than less as is being assumed. Due to the lack of available information it was deemed a better approach to make F_5 at most equal to the greater of F_3 or F_4.

CHAPTER 4

ANALYTICAL PROCEDURE

4.1 Introduction

In the previous three chapters a model for the frame-infill-wall system has been described. This chapter deals with the specifics of the model which include, the choosing of the finite elements to represent the structure, the development of the equations of motion, the techniques for numerical integration of these equations and the development of the computer program to implement the model.

4.2 Element Stiffness Matrix

In choosing the elements to represent the structural stiffness it is desirable to choose elements that not only meet the requirements of the previous chapters but are also as simple as the model will permit. Each element stiffness constitutes a part of the total structural stiffness. The assembly of the stiffness matrix for the whole structure based on the element stiffness presented in this section is covered in Sec. 4.3.3.

4.2.1 Column and Beam Element

The element chosen to represent the beams and columns of the structure is the one developed by Giberson. The derivation of the

incremental stiffness matrix may be found in Ref.[20] and will not be repeated here. To take into account the stability of the element a geometric stiffness is added to the stiffness matrix.

This element was chosen because of its ability to have the yield levels at each end specified independently of each other. This characteristic may be needed because beams and columns should be modeled as an assembly of shorter elements so as to guarantee compatibility with the wall not only at the ends of the columns and beams but also at intermediate points along their length.

4.2.2 Wall Element

The element chosen to represent the wall is the constant stress triangle. The derivation of the incremental stiffness matrix for this element may be found in Ref.[68] and will not be repeated here. This element was chosen for its simplicity and widespread use. Although this element is usually considered to give poor results when compared to other more sophisticated elements it was deemed that a greater accuracy, at the present time, may not be justified based on the present understanding of some of the variables and assumptions made for the proposed model.

4.2.3 Joint Element

Since most of the joint elements available in the literature were deemed too complex for the present objectives of the study,

a simple element was derived. The details of the derivation of the incremental stiffness matrix may be found in Appendix B.

The important characteristic of the joint element is that once failure occurs incremental stiffness relations may exist only when the stress across the joint is compressive. In addition only when there is compression across the joint after failure will there be an internal resistance developed across the joint. This internal resistance will be due to the normal stresses only. Incremental stiffness relations due to shear may exist after failure only when there is a compressive normal stress, while the internal resistance of the joint due to shear stresses is always assumed to be zero after failure. The joint element has the directional property of allowing joints to increase their separation but not to decrease it. Therefore the joint element is unidirectional and its incidences should be specified taking this factor into account.

4.2.4 Gap Element

The stiffness of the gap element is zero as long as the gap size is not reduced to zero. Once the gap is closed the problem changes and it becomes a surface contact problem. In this study the contact problem will be treated using an element which has a change in stiffness when the gap closes.

Contact problems may be subdivided into three distinct phases. These three phases may be denoted, "stick", "slip", and "gap

mode", respectively. The stick mode is when points across the boundary have the same increments in displacements both perpendicular and tangential to the surface. The slip mode is when the increments in displacements tangential to the surface of contact may be different while increments in displacements perpendicular to the surface are the same. The gap mode is when both normal and tangential increments in displacements across the boundary are independent.

Whenever the slip or stick mode is the controlling phase, one may derive a set of constraining equations for the increments in displacements while the stresses across the boundary become unknown. In this study this constraint is handled approximately by placing a joint element between the two points which have come into contact. By doing this the constraint may only be satisfied to within a certain order of magnitude which depends on the material constants assumed for the joint element. The whole process of gap detection and contact problem is placed under the present gap element. The joint element used is the same as the one derived in Appendix B but with the additional assumption that the element has already reached the failure criteria. Therefore the gap element is also unidirectional and its incidences must also be specified taking this factor into account.

4.3 Dynamic Analysis

The equations of motion may be expressed as the sum of the inertial forces, damping forces, structural forces, and external

loading for each degree of freedom. To evaluate the inertia, damping, structural, and external forces one must calculate the mass matrix, damping matrix, instantaneous stiffness matrix, and the external influence vector for the whole structure.

4.3.1 Mass Matrix

In this study the lumped mass matrix technique will be used exclusively. Masses may be lumped at any degree of freedom. This generates a mass matrix whose off diagonal terms are all zero. Since a mass may be lumped for any degree of freedom, rotational as well as translational inertial forces may be present. The overall structural mass matrix has the following form:

$$[M] = \begin{bmatrix} m_1 & & 0 \\ & \ddots & \\ & & m_I \end{bmatrix} \qquad (4.1)$$

where

[M] = diagonal mass matrix

m_i = lumped masses at the dynamic degrees of freedom

I = number of dynamic degrees of freedom

4.3.2 Damping Matrix

Linear viscous damping is adopted in this analysis because of its mathematical simplicity and widespread use. Therefore the damping forces are proportional to the velocities of the dynamic

degrees of freedom relative to the velocity of the boundary of the structure. It was deemed desirable to have a damping matrix which may have any or all of the following characteristics.

1. The damping ratio increases with the initial elastic frequency.
2. The damping ratio decreases with the initial elastic frequency.
3. The damping ratio may be specified arbitrarily for any or all initial elastic frequencies.

The first two conditions may be accomplished by Rayleigh type damping. The third condition may be achieved by transformation using the natural mode shapes of the structure.

Rayleigh or proportional damping is expressed in the following form:

$$[C] = a_1[M] + a_2[K'] \tag{4.2}$$

where

$[C]$ = damping matrix, same size as the mass matrix

$[M]$ = mass matrix

$[K']$ = reduced stiffness matrix

a_1, a_2 = constants to be specified

Based on the orthogonality of the mode shapes with respect to the mass and stiffness matrix the damping matrix as defined in Eq. 4.2 may be diagonalized. Using this property the following

equation is obtained:

$$c_i = a_1 \cdot m_i + a_2 \cdot k_i \tag{4.3}$$

or

$$n_i = \frac{1}{2}\frac{a_1}{p_i} + \frac{1}{2} a_2 \cdot p_i \tag{4.4}$$

where

c_i = modal damping corresponding to mode i

m_i = modal mass corresponding to mode i

k_i = modal stiffness corresponding to mode i

n_i = damping ratio corresponding to mode i

p_i = circular frequency corresponding to mode i

The constants a_1 and a_2 in Eqs. 4.3 or 4.4 may be evaluated by specifying one or two values of n_i or c_i depending on which formula one uses. Given two values of n_i then a_1 and a_2 may be determined as follows:

$$a_1 = \frac{2\, p_i p_j (n_j p_i - n_i p_j)}{p_i^2 - p_j^2} \tag{4.5}$$

$$a_2 = \frac{2(n_i p_i - n_j p_j)}{p_i^2 - p_j^2} \tag{4.6}$$

where

n_i = damping ratios specified

p_i = circular frequencies specified

Usually the damping ratios specified are those corresponding to the first and second elastic frequencies of the structure. If the damping matrix is considered proportional only to the stiffness matrix then the damping ratio will increase with frequency. If the damping matrix is considered proportional only to the mass matrix then the damping ratio will decrease with increasing frequency.

A different approach must be taken to provide an arbitrary damping ratio for each frequency. Using the mode shape matrix as an inverse transformation one may specify the damping ratios as follows:

$$[C] = \left[Q^T\right]^{-1} \begin{bmatrix} \ddots & & \\ & c_i & \\ & & \ddots \end{bmatrix} \left[Q\right] \qquad (4.7)$$

where

[C] = damping matrix

[Q] = modal matix, matrix formed by the mode shapes

c_i = damping constant for mode i

It is seen from Eq. 4.7 that only those modes shapes whose values of c_i are nonzero will be damped the rest of the modes will have no damping unless proportional damping is specified. A more detailed derivation of Eq. 4.7 may be found in Ref.[12]. The damping matrix is assumed to remain constant.

4.3.3 Stiffness Matrix

The complete incremental stiffness matrix is formulated by assembling all of the individual incremental stiffness matrices from the element level. The full incremental stiffness matrix may include both dynamic degrees of freedom and static degrees of freedom. Therefore not all of the structural degrees of freedom in the stiffness matrix may have corresponding damping and inertia forces related to them.

In the usual approach the degrees of freedom for which no masses have been specified are condensed out of the stiffness matrix. In this study the need to have the displacements of all the degrees of freedom readily available and the fact that, in this case, no great computational advantage would be gained the usual procedure of condensation was not followed. Therefore the structural stiffness is as follows:

$$[K]\ \{*d\} = \begin{bmatrix} [K_{11}] & [K_{12}] \\ [K_{21}] & [K_{22}] \end{bmatrix} \begin{bmatrix} *d_1 \\ *d_2 \end{bmatrix} \tag{4.8}$$

where

$[K_{11}]$ = submatrix size I x I

$[K_{12}]$ = submatrix size I x J

$[K_{21}]$ = submatrix size J x I

$[K_{22}]$ = submatrix size J x J

I = number of dynamic degrees of freedom

J = number of static degrees of freedom

$\{*d_1\}$ = increment in displacements of the dynamic degrees of freedom

$\{*d_2\}$ = increment in displacements of the static degrees of freedom

The instantaneous stiffness matrix may change, under inelastic conditions, at every time step. This requires both a frequent updating of the stiffness matrix and the evaluation of a residual force vector which may be induced in the structure due to the changes in the stiffness of the elements. This residual force vector will be discussed in Sec. 4.4.3.

4.3.4 Ground Influence Vector

The ground influence vector is the set of structural displacements induced in the structure when one applies a unit displacement at one boundary point with zero displacement at all other boundary points of the structure. For most structural systems this vector may be derived from a consideration of statics but in complex structures a more general approach is needed.

Taking first the stiffness matrix of the structure times the increments in displacements and setting them equal to zero yields:

$$[K]\ \{*d\} = \begin{bmatrix} [K_{11}] & [K_{12}] \\ [K_{21}] & [K_{22}] \end{bmatrix} \begin{bmatrix} *d_1 \\ *d_2 \end{bmatrix} = \begin{bmatrix} 0 \\ 0 \end{bmatrix} \qquad (4.9)$$

where

$[K_{11}]$ = submatrix corresponding to the structure degrees of freedom

$[K_{22}]$ = submatrix corresponding to the boundary degrees of freedom

$[K_{12}]$ = submatrix corresponding to the relation between boundary degrees of freedom and structure degrees of freedom

$\{*d_1\}$ = increment in displacements of the structure degrees of freedom

$\{*d_2\}$ = increment in displacements of the boundary degrees of freedom

Now applying the above definition one arrives at the following equation:

$$\{*d_1\} = -[K_{11}]^{-1}\ [K_{12}]\ \{*d_2\} \qquad (4.10)$$

This equation relates the boundary degrees of freedom to the structure degrees of freedom. In the present study only one boundary point may have a defined ground motion and Eq. 4.10 is simplified to:

$$\{*d_1\} = *d_2 \cdot \{R\} \qquad (4.11)$$

where

$\{R\}$ = ground influence vector defined as $-[K_{11}]^{-1}[K_{12}]$

The ground influence vector will permit the equations of motion to be written in terms of the relative displacements of the structure. In general the influence vector depends on the displacements of the structure as may be seen from Eq. 4.10. This implies that under inelastic conditions it should be updated at every time step. In the particular case that the ground influence vector represents a rigid body mode, the vector becomes independent of the displacements and a constant for all times. The previous derivation may also be found in Ref.[12].

4.4 Equations of Motion and Solution

4.4.1 Equations of Motion

The equations of motion are stated in the incremental form assumming that the properties of the structure are constant within each time interval:

$$\begin{bmatrix} [M] & 0 \\ 0 & 0 \end{bmatrix} \begin{bmatrix} {}^*a_1 \\ {}^*a_2 \end{bmatrix} + \begin{bmatrix} [C] & 0 \\ 0 & 0 \end{bmatrix} \begin{bmatrix} {}^*v_1 \\ {}^*v_2 \end{bmatrix} + \begin{bmatrix} K_{11} & K_{12} \\ K_{21} & K_{22} \end{bmatrix} \begin{bmatrix} {}^*d_1 \\ {}^*d_2 \end{bmatrix}$$

$$= - \begin{bmatrix} [M] & 0 \\ 0 & 0 \end{bmatrix} \begin{bmatrix} R \\ 0 \end{bmatrix} \cdot {}^*a_g \qquad (4.12)$$

where

$[M]$ = diagonal mass matrix

$[C]$ = damping matrix

$[K_{11}]$ = instantaneous structural stiffness matrix for the dynamic degrees of freedom evaluated at the end of the previous time step

$[K_{22}]$ = instantaneous structural stiffness matrix for the static degrees of freedom evaluated at the end of the previous time step

$[K_{12}]$ = instantaneous structural stiffness matrix for the coupled degrees of freedom evaluated at the end of the previous time step

$\{R\}$ = ground influence vector

$*a_1$ $*v_1$ $*d_1$ = incremental accelerations, velocities, and displacements of the dynamic degrees of freedom

$*a_2$ $*v_2$ $*d_2$ = incremental accelerations, velocities, and displacements of the static degrees of freedom

$*a_g$ = incremental boundary acceleration

4.4.2 Integration

To integrate the equations of motion the numerical scheme developed by Newmark will be used. In Ref.[68] this method was shown to be the most general second order integration scheme that may be used to integrate the equations of motion. The incremental acceleration and velocity are given as:

$$\{*a\} = \frac{1}{q(*t)^2}\{*d\} - \frac{1}{q(*t)}\{v\} - \frac{1}{2q}\{a\} \qquad (4.13)$$

$$\{*v\} = \frac{1}{2q(*t)}\{*d\} - \frac{1}{2q}\{v\} - (\frac{1}{4q} - 1)\ (*t)\ \{a\} \qquad (4.14)$$

where

*t = time interval, or integration time step

q = a constant which is usually chosen between 1/6 and 1/4 and controls the stability, convergence, and accuracy of the integration scheme

{a} = acceleration at the end of previous time step

{v} = velocity at the end of previous time step

{*a} = increment in acceleration

{*v} = increment in velocity

{*d} = increment in displacement

There are two basic ways to solve the equations of motion. One is termed the explicit method and the other the implicit method. The implicit method either assumes or calculates a value of the acceleration and then using the assumed relations between the displacements, velocities, and accelerations integrates for the velocities and displacements. The explicit method combines the assumed relations between acceleration, velocity, and displacements with the equation of motion to obtain an equation from which the increments in displacements may be calculated directly. In this study the explicit approach will be used.

Combining Eqs. 4.12, 4.13, and 4.14, the increment in displacements may be expressed as a function of the response values and stiffness properties at the end of the previous time step. This is done as follows:

$$\{*d\} = [A]^{-1} \{B\} \tag{4.15}$$

where

$$[A] = \frac{1}{q(*t)^2}[M] + \frac{1}{2q(*t)}[C] + [K] \tag{4.16}$$

$$\{B\} = [M]\left[\frac{1}{2q}\{a\} + \frac{1}{q(*t)}\{v\} - \{R\} \cdot a_g\right] + [C]\left[\left(\frac{1}{4q} - 1\right)(*t)\{a\} + \frac{1}{2q}\{v\}\right] \tag{4.17}$$

This approach has the advantage that if the stiffness properties do not change over several time steps the inversion of matrix [A] has to be done only once. In this study the value of "q" will be taken as 1/4. This makes the solution scheme unconditionally stable.

4.4.3 Correction

Since the conditions used to establish Eq. 4.15 are those existing at the end of the previous time step, any change in the properties of the structure during the present time interval are not included in the equation. This implies that an iterative solution process would be needed to arrive at the values of the acceleration, velocity, and displacements. This approach may be costly for the proposed model as Eq. 4.15 would have to be solved several times in every time step. Therefore the iterative approach will not be used in this study. Yet without an iteration process errors can be shown to accumulate and considerably alter the solution of the problem. Therefore some correction should be applied to the response.

In this study the following correction is used: at the end of each time step a total equilibrium equation is established. The total inertial force must be in equilibrium with the total damping force, total internal resistance of the structure, and the total external force. If any changes in the structural properties have occurred during the time interval this equilibrium equation would not be satisfied. This creates a residual force which is added as an external load in the next time interval. The residual load is formulated as follows:

$$\{res\} = \{TIF\} + \{TDF\} + \{TIR\} + \{TEF\} \qquad (4.18)$$

where

{res} = total residual force vector of the structure

{TIF} = total inertial force vector of the structure

{TDF} = total damping force vector of the structure

{TEF} = total external force vector of the structure

{TIR} = total internal force vector of the structure

The method just outlined has the advantage of making the updating of the structural stiffness matrix independent of the corrections which must be carried out at each time step. This is accomplished by the use of the internal force vector which may be calculated from the material models being used for the structure.

4.5 Computer Implementation

The model proposed in the previous sections was implemented using a computer program called AWALL. The program AWALL is a finite element program with the following capabilities.

The program has a main storage block where most of the data is stored column-wise and in sequence by the use of pointers. All computations are done through subroutines. The dynamic stiffness matrix is stored in banded form with only half the band width plus the diagonal being stored. At each joint three global degrees of freedom are specified, two perpendicular translations, and one rotation. The solution is in the plane of the structure and no out-of-plane degrees of freedom may be specified. One may specify a concentrated mass at each degree of freedom. The solution has two time sequences which may be specified: the time sequence over which the ground motion is applied and the free vibration sequence. Each may be specified independently. The number of times the stiffness matrix is updated may be specified. If the number of time steps to update the stiffness matrix is greater than the total number of time steps available for the solution then the structure is assumed to be elastic.

The structure is assumed to be initially unconstrained when one specifies the joint coordinates and element incidences. One may specify two types of constraints, absolute and relative. The absolute constraints are those for which the degree of freedom is either always zero or does not apply to the specific joint. The

relative constraints are those that force two or more degrees of freedom to have the same response. If any of the degrees of freedom in a relative constraint is in fact a degree of freedom with an absolute constraint then all degrees of freedom with said relative constraint will have an absolute constraint.

The program may generate three different types of ground motions or it may read a specified input ground motion. The three types of ground motions which the program generates may be separated into two consecutive pulses with different scaling factors for time and acceleration in each pulse Ref.[65]. The basic pulse for each of the three ground motions it generates are sinusoidal, linear, or quadratic. If a specific the ground motion is read a linear interpolation is assumed between the points. This condition may also be scaled in both time and acceleration. The ground motion to be used may be specified for any degree of freedom in the structure but only one degree of freedom may be specified. At the present time the acceleration is generated and stored before it is used and therefore this may require a large amount of storage if the integration time step is small.

Based on the degree of freedom specified for the ground motion the program generates a ground acceleration influence vector for the masses of the structure. This vector is assumed constant throughout the computation. In general, this will not effect the results if said vector corresponds to a rigid body mode. Static loads may be specified at any degree of freedom. No element loads

may be specified. The dynamic response is computed from the equilibrium position generated by the static loads. All material stress computations are based on the total displacements which may include the static condition if static loads are present.

The program calculates all elastic frequencies and mode shapes for the system but prints only the first ten. Damping may be specified in two ways: Rayleigh damping and damping for a specific mode shape. For Rayleigh damping one may specify the mode shapes to determine the constants of proportionality. For arbitrary damping of a specific mode shape one must specify a damping ratio for each mass degree of freedom. Both types of damping may be specified in a given problem and they will be additive. The dimensions of the data provided must be consistent as the program does not provide any transformations.

CHAPTER 5

COMPUTATIONS AND RESULTS

5.1 Introduction

The objective of this chapter is to assess the model proposed in the previous four chapters. The first obstacle encountered is the lack of experimental data to compare the results of any computations that might be proposed. Only a limited number of experiments under dynamic loading have been carried out and although the results of these are very instructive in their overall content they lack sufficient data to make a meaningful comparison with the proposed analytical model. This lack of data coupled with the nonlinearities of the problem suggest the need to study the model on a simple frame wall system whose overall behavior is sufficiently well understood. Under these conditions the ground motion should also be simple so as to provide a spectrum which is relatively smooth. This should permit an easier interpretation of the results as nonlinearities will already make the interpretation difficult.

5.2 Proposed Computations

In order to assess the proposed model four basic structures are studied. The first is a one bay, one story frame which will be used as a bench mark for the other three structures. The

second through fourth structure consists of the same frame as the first structure to which a masonry infill wall is added. The second structure will assume initial continuity between the frame and wall, but the third and fourth structures have a specified gap at the frame wall boundary. The third and fourth structures will have different failure capacities specified for the masonry wall.

In comparing these four structures the capabilities of the model and the difference in behavior between the open frame and the frame-infill-wall system should become clear. In addition the effect of continuity at the frame wall boundary may be studied by comparing the results of the second structure for which continuity has been specified to the results of the third and fourth structure for which a gap is specified.

In addition to the four basic structures a three story one bay frame-infill-wall will be studied. The first story of the structure will be essentially the same as the previous four structures. The second and third stories will have a simpler discretization as follows. The wall for the second and third stories will be subdivided into only four elements while the columns and beams will be made up of only one element and not two elements as shown in Fig. 5.1. This structure will have a specified gap size of zero but will not be assumed continuous with the main frame. In addition the structure will be subjected to a different ground motion than the previous four structures.

5.2.1 Input Data

The overall dimensions of the frame wall system to be used for the first four structures is shown in Fig. 5.1. The span to height ratio of the frame was taken as 2. This is an average value for typical frames whose span to height ratio vary between 1.5 to 2.5. The height of the column, taken as 3.5 m, is also believed to be typical. The size of the gap at the frame wall boundary was taken as 5 mm. The space between the wall and the ground shown in the figure is not a gap but signifies that the wall may become discontinuous with the base during the loading cycle. The masses have been specified at the three joints in the beam with only the horizontal degree of freedom being active. They are tied by a rigid link providing only one dynamic degree of freedom in the horizontal direction. The value of the mass was specified as 50 Mg making the total mass in the story 150 Mg. This value was chosen based on the response spectrum of the ground motion to be used for the first four structures. The overall viscous damping was taken as 2.0 percent of critical. The modulus of elasticity for the frame was taken as 25 GPa. The area of the column was taken as 123×10^3 mm^2 and the moment of inertia was taken as 1.25×10^9 mm^4. The area of the beam was taken as 245×10^3 mm^2 and the moment of inertia was taken as 5 x 109 mm^4. The yield moment was taken as 214.0 kN-m for both the beam and column. The slope of the yield branch in the moment rotation relationship was taken as 1.0 percent of the original stiffness for both the beam and column. The dead load was

concentrated at the corner masses. It was specified as 245 kN each. The data for the frame is summarized in Table 5.1.

The wall was divided into 16 elements as this is the smallest number of elements that may reflect the bracing effect on the surrounding columns. The modulus of elasticity of the masonry was taken as 14 GPa. The equivalent thickness is based on an ungrouted 200 mm brick and was taken as 100 mm. Poisson's ratio was taken as 0.25. The masonry uniaxial compressive strength was taken as 24.0 MPa for the third structure and 34.0 MPa for the fourth structure; the masonry uniaxial tensile strength was taken as 2.4 MPa for the third structure and 3.4 MPa for the fourth structure. The dead load was distributed in proportion to the area of the wall. It was specified as 1.25 kN at each independent node in the wall. The data for the wall is summarized in Table 5.2.

A joint was specified at the boundaries of the wall elements and at the base of the wall. Joint elements were specified at the frame wall boundary for the structure where initial continuity was assumed to exist between the wall and the frame. The modulus of elasticity was taken as 7 GPa. The thickness of the joint was taken as 10 mm and Poisson's ratio was taken as 0.15. The area of the joint depends on its location and varied from 87.5×10^3 mm^2 to 175×10^3 mm^2. The data for the joint element is summarized in Table 5.3.

The control points for the different failure surfaces were specified as follows. In Fig. 3.2 the value of s_1 and n_1 were given as 1360 kPa and 340 kPa, respectively and the two slopes "n" and "m" were specified as 2 and 1, respectively. In Fig. 3.4, part of the control points for Fig. 3.3, the value of "n" was assumed as 1.5; in Fig. 3.5 the value of "n" was assumed as 0.42. These values are summarized in Table 5.4.

For the first four structures Fig. 5.2 shows the joint numbering corresponding to Fig. 5.1; Figs. 5.3 and 5.4 show the element numbering for the same figure. The time step used for integration of the equations of motion was taken as *t=0.005 sec.

The data for the three story structure is essentially the same as the data for the previous four structures with the notable exception of the mass specified at each story. The mass for the three story structure was taken as 30 Mg for each story. This value is also presented in Table 5.1.

5.2.2 Base Acceleration and Spectrum

The input base acceleration used for the first four structures was taken as a sine wave with a period of 0.5 sec. The total duration of the base motion was taken as 1.0 sec. This gives a sinusoidal motion which has two complete sine waves. The peak acceleration for the ground motion was taken as 0.4g. The spectrum for this base motion at 2 and 20 percent of critical

damping is shown in Fig. 5.5. As would be expected the spectrum has a peak value at approximately 2 Hz (0.5 sec); a second maximum occurs at about 0.5 Hz (2.0 sec). At very high and low frequencies the spectrum tends to the maximum ground acceleration of 0.4g and the maximum ground displacement of 312 mm, respectively.

The input base acceleration used for the three story structure consisted of the first ten seconds of the South-East component of the Imperial Valley earthquake recorded at El Centro California on May 18, 1940. The ground acceleration was scaled such that the maximum acceleration was 0.4g. In addition a 2 sec prefixed pulse was added at the beginning of the ground motion. The complete ground motion is shown in Fig. 5.51. The elastic spectrum for the ground motion at 2 and 20 percent damping is shown in Fig. 5.52.

5.3 Results

The results of the computations are presented in three different forms. The first is a time history response of the system, which will include plots of the relative displacement, relative velocity, and absolute acceleration of the mass of the system. Time history plots of the moment shear and axial load of the columns will be presented for comparison between the different structures. In addition, a time history plot of the relative displacement, total resistance, and base acceleration will be included. The second method for presenting the results is in the form of a load displacement plot for the mass of the

system. The third method of presenting the results will be in the form of sketches of damage sequences for the structure. This last method will only be presented for the frame-infill-wall model and not for the open frame.

5.3.1 Open Frame

The results of the computations for the open frame are presented in Figs. 5.6 through 5.12. Figures 5.6 through 5.11 are time history plots and Fig. 5.12 is the load displacement curve for the time history response. A brief summary of the key events that occurred during the response is presented in Table 5.5.

The elastic fundamental frequency of the open frame is 1.53 Hz. Looking at the spectrum for the base acceleration in Fig. 5.5 this sets the open frame just to the left of the maximum response at 2.0 Hz. As the frame yields the equivalent frequency should decrease while the equivalent damping increases forcing the response to move away from the maximum value at 2.0 Hz. This observation with respect to the open frame is important in interpreting some of the overall results for the frame wall system. The relative position of the initial frequency with respect to the peak value of the spectrum at 2.0 Hz may serve as an approximate guide for this comparison.

Figure 5.6 shows the time history plots of the relative displacement, the relative velocity and absolute acceleration. As expected for a bilinear system, the total acceleration reaches a

maximum value in accordance with the yield resistance of the frame. The relative displacement has a maximum value of 77.3 mm and the total acceleration has a maximum value of 0.188g. Figure 5.7 shows the time histories for the relative displacement total force and ground acceleration.

Figures 5.8 through 5.11 correspond to the time history response of the columns. The shear and moment presented in Fig. 5.8 correspond to the base of the left column while the shear and moment in Fig. 5.9 correspond to the top of the same column. The shear and moment presented in Fig. 5.10 correspond to the top of the right column and the moment and shear presented in Fig. 5.11 correspond to the bottom of the same column. The time history response of the axial behavior for each column is presented in each figure, respectively.

Figure 5.12 shows the load displacement response for the open frame. The response has three branches: the first branch is the elastic behavior. The second branch corresponds to yielding at the bottom of the columns while the third branch corresponds to full yielding in the frame at the top and bottom of the columns as well as yielding in the beams. Figure 5.12 shows some erratic behavior in the vicinity of the yield point. This is due mainly to the fact that the force that is plotted is the one at the end of the time step to which no corrections for yielding have been added. When a typical overshoot of the yield point occurs this value is corrected in the next time step since no iteration is used to correct the error in the same time step.

Figures 5.6 through 5.12 show, as should be expected, a response which approximates the behavior of a typical one story ductile frame. These results will serve as a basis for comparison with the three frame wall solutions to be presented in the following sections.

5.3.2 Frame Wall

The response of the frame wall system for which no gaps have been specified is shown in Figs. 5.13 through 5.25. Figures 5.13 through 5.19 have a correspondence with Figs. 5.6 through 5.12 of the open frame. Figures 5.20 through 5.25 represent the cracking pattern for the frame wall. A brief summary of the key events that occurred during the response is presented in Table 5.6.

Two types of comparisons will be made. The first will be a qualitative comparison of the time history responses of the frame wall to those of the open frame; and of the corresponding load displacement curves. The second will be a qualitative correlation of the time history responses with both the cracking pattern shown in Figs. 5.20 through 5.25 and the load displacement curve of Fig. 5.19.

The elastic fundamental frequency of the frame wall system is approximately 13 Hz. The elastic fundamental frequency of the open frame was 1.53 Hz which gives a ratio of frequencies of the wall to the frame of 8.6. Since the total mass is unchanged the

stiffness must change in proportion to the square of the frequency ratio. Therefore the frame wall structure is 74 times stiffer than the open frame. This very large increase in stiffness is in accord with what has been observed experimentally. As long as the frame is in full contact with the wall large increases in the stiffness may be expected.

Looking at the spectrum in Fig. 5.5 it may be seen that the frequency of the frame wall system, 13 Hz, falls considerably to the right of the maximum response which occurs at 2 Hz. This shift in frequency results, in this case, in a reduction of the maximum response quantities. As the equivalent frequency decreases with the damage suffered, the system should tend to move towards the maximum response but at a higher damping ratio as the equivalent damping should increase with the damage.

Looking at the time history of the relative displacement shown in Fig. 5.6 for the frame and Fig. 5.13 for the frame wall two basic differences may be noticed. The open frame tends to vibrate around a permanent displacement of about 50 to 55 mm in the forced vibration part of the response. This is very typical of bilinear systems. No permanent set is detected in the frame wall response as the frame is not allowed to reach its yield displacement. Yet, as will be seen, considerable inelastic response has taken place. The second difference lies in the free vibration response. While the open frame vibrates around a permanent displacement of about 3 mm the frame wall shows a

heavily damped response, decreasing almost linearly to zero. This type of response is similar to that encountered in friction type damping. In the same figures one may compare the absolute acceleration of both systems. While the open frame shows the distinctive upper limit to the absolute acceleration due to the yielding of the frame, the frame wall system shows no yielding at all and the maximum acceleration is approximately 2.7 times greater than that of the open frame. Comparing the total resistance of both systems Fig. 5.7 and Fig. 5.14 show that the open frame has a maximum resistance of 245 kN while the response of the frame wall reaches a maximum of about 680 kN.

It seems apparent that a fundamental change in the behavior of the frame has come about. This change in the overall response quantaties may not be solely justified on the basis of a large change in the fundamental frequency due to the presence of the wall. Further evidence of this fact may be seen in Figs. 5.15 through 5.18 which show the response of the moment, shear and axial load for the infilled frame. From these figures one may conclude that the load carried by the system may not be assigned as if the wall and frame were acting in parallel. Figures 5.15 through 5.18 show time histories for these columns which are radically different from the time histories of a frame that has not yielded. Additional evidence that the behavior of the open frame has been altered is shown in Fig. 5.19. This figure shows a load displacement curve that reflects neither an open frame type behavior nor that of a frame and wall acting strictly in

parallel. Since the frame has not yielded, the inelastic behavior shown in Fig. 5.19 must be due solely to the interaction between the frame and wall and to cracking within the wall.

In order to understand the behavior of the frame-infill-wall system one should take a closer look at Figs. 5.13 through 5.25. Figures 5.20 through 5.25 represent the sequence of cracking in the wall as well as the crack pattern. They are divided in the following manner. Figure 5.20 represents the summary of crack patterns from time t=0.0 to 0.155 sec. The numbering sequence indicates at which time step the specific portion of the crack occurred. Figures 5.21 through 5.24 are based on Fig. 5.20. This set of figures represent the existing crack pattern at the time specified in each figure. In doing this a better picture of the sequence of cracking may be observed and studied. Figure 5.25 is similar to Fig. 5.20, but is presented for the time interval from t=0.275 to 0.555 sec.

The load displacement curve shown in Fig. 5.19 depicts a change in behavior of the frame wall system from linear to nonlinear at a displacement of about 0.4 mm. This displacement corresponds approximately to a time t=0.045 sec. At this time the displacement time history shown in Fig. 5.13 shows a change in the response.

Up to this point the wall and frame act as a monolithic unit to carry the horizontal force of 410 kN which has been developed. In this interaction the system tends to behave as the cross

section of a beam with the columns tending to act as flanges and the wall tending to act as a web. This may be verified by looking at the response of the columns shown in Figs. 5.15 through 5.18. In these figures one may see that frame action as represented by the shears and moments in the columns may be considered small in comparison to the axial behavior of these same elements. The axial response of the elements shown in Figs. 5.15 and 5.18 correspond to about 100 kN in tension and compression, respectively. This seems to indicate that the columns tend to act as axial elements in the interaction with the wall, much like the flanges of a beam.

The above interpretation is partially based on the compatibility between the frame and wall and the compatibility between the ground and the base of the wall. Figure 5.21 represents the cracking pattern at time t=0.045 sec. This figure shows that cracks have already developed between the frame and wall. Since there is no detectable change in the stiffness, as may be seen in the load displacement response of Fig. 5.19, it seems that full compatibility between columns and wall is not necessary as long as a certain amount of shear can be transmitted between the column and wall.

This condition does not seem to hold true for the compatibility between the wall and ground where the stresses to be transmitted across the crack are normal tensile stresses. This may be seen in Fig. 5.20 at time t=0.05 sec where a crack has

developed at the base of the wall producing a radical change in both the stiffness and behavior of the frame wall system. This is depicted in the load displacement response of Fig. 5.19 as a drop in the load at a displacement of about 0.5 mm.

Figure 5.22 shows the crack pattern at time t=0.060 sec. As may be seen a continuous crack has developed between the right column and the wall in addition to the crack which has developed between the wall and its boundary on the lower left side of the wall. The cracks along the boundary alter the behavior of the frame wall system from a shear wall to a frame that is braced across its diagonal.

The load displacement curve in Fig. 5.19 seems to indicate that the change in behavior is marked by a transition which transition begins at time t=0.05 sec with a displacement of 0.5 mm and continues up to time t=0.125 sec at a displacement of about 2.3 mm. In this transition two different phases may be identified. The first occurs at a displacement of about 0.75 mm and the second occurs at a displacement of about 2.0 mm. Both phases are related to additional cracking in the wall both inside and at its boundary.

Figure 5.23 represents the crack pattern at time t=0.075 sec. This crack pattern corresponds to the end of the first phase of the transition at a displacement of about 0.75 mm. Figure 5.23 seems to indicate that the reduction in load shown in Fig. 5.19 may be due mainly to extensive cracking inside the wall.

Especially noticeable is the horizontal crack on the right side of the wall at midheight.

Figure 5.24 represents the crack pattern at time t=0.110 sec. As may be seen, additional cracking has occurred along the diagonal of the wall. This crack pattern corresponds to a displacement of about 1 mm in the load displacement response of Fig. 5.19. The response shows an increase in load from time t=0.075 sec. This fact shows the importance of the development of a horizontal crack in the transition phase between shear wall and braced frame behavior.

The second phase of the transition occurs at time t=0.125 sec and a displacement of 2 mm. The crack pattern in Fig. 5.20 indicates that this mainly corresponds to additional cracking along the base of the wall. The load displacement curve in Fig. 5.19 shows a drop in the load as the wall moves into its final condition of acting as a bracing element across the diagonal of the frame.

It may be seen from Fig. 5.19 that the change in behavior brings about a greater energy dissipation in the system without any yielding having occurred in the frame.

Figure 5.25 shows the additional cracking corresponding to the first load reversal in Fig. 5.19. As the load is reversed some cracks that were opened in the first cycle are now closed. These cracks are not shown in Fig. 5.25 but the load displacement curve

shows that as the load is reversed the frame becomes braced across the alternate diagonal.

That a full transition to a braced frame has occurred may be seen in the time histories of the columns shown in Figs. 5.15 through 5.18. After time t=0.130 sec, the moments and shears are no longer small, and the axial loads in the columns alternate from tension to compression as would be expected in a braced frame under reversed loading.

5.3.3 Frame Wall with Gaps(I)

The response of the frame wall system for which 5 mm gaps have been specified is shown in Figs. 5.26 through 5.38. These figures represent the same group of response quantities presented for the frame wall without gaps. The masonry's ultimate compressive strength was taken as 24 MPa and the ultimate tensile strength was taken as 2.4 MPa. A brief summary of the key events that occurred during the response is presented in Table 5.7.

The elastic fundamental frequency of the structure is the same as that of the open frame since the wall is not in contact with the frame and therefore does not contribute to the stiffness under small displacement theory. The elastic fundamental frequency of 1.53 Hz for this frame wall system, like the open frame, is thus just to the left maximum response point on the spectrum, Fig. 5.5.

The time histories of the relative displacement and absolute acceleration shown in Fig. 5.26 seems to show that the behavior of the frame wall with a gap is in this case essentially elastoplastic. The absolute acceleration shows, with the exception of the two spikes, the typical flat response at a maximum value which is characteristic of an elastoplastic frame. The maximum value of the absolute acceleration, again ignoring the two spikes, is about 0.25g, that is, about 30 percent greater than the open frame. This increase is directly related to the two spikes which represent, as will be seen, a change in the behavior of the frame. The relative displacement also shown in the same figure shows that the maximum relative displacement is 52 mm which is about 40 percent less than that corresponding to the open frame. Also, the relative displacement tends to vibrate about a permanent displacement as may be seen in the free vibration phase of the response. This again is characteristic of elastoplastic systems.

Although the behavior reflected in these response quantities is approximately elastoplastic, there are certain discrepancies which distinguish it from the open frame. The first are the obvious spikes which are due to the failure of the upper corners of the wall. The second is the greater yield load. Since the wall has no elastoplastic behavior and the open frame has a lower yield load, the increase in the load at which the yield plateau is reached can only be due to a change in the behavior of the

frame due to the presence of the wall. The third discrepancy may be seen at time t=0.8 and 1.05 sec in Fig. 5.26 where an increase in the accelerations above the yield plateau implies again a change in the behavior in this case away from the preceding elastoplastic mode. These differences are due to the presence of the wall and its bracing effect on the frame. These changes in behavior may be studied by looking at the load displacement curve in Fig. 5.32 and relating its changes to the time histories and cracking patterns.

The cracking, yield, and failure pattern up to time t=0.315 sec is presented in Fig. 5.33. This figure indicates that the 5 mm gap closes at time t=0.09 sec. Up until that time the frame is free to deform. This is reflected in a change in stiffness in the load displacement curve at a displacement of 5 mm. At time t=0.095 sec the center of the wall, due to tensile stresses, develops a horizontal crack at midheight on its left side; this may be seen in the crack pattern in Fig. 5.34. This figure also shows horizontal cracking along the wall base. This cracking is also reflected in a slight change in stiffness in the load displacement curve before the maximum load is reached.

At time t=0.1 sec the frame wall system reaches its maximum capacity and the upper left corner of the wall begins to fail. This may be seen in Fig. 5.35 where the wall has cracked along the horizontal plane at midheight in addition to extensive cracking in the lower half of the wall. The condition of the wall

and frame at time t=0.110 sec is shown in Fig. 5.36. It may be seen that the upper left corner of the wall has failed. This condition corresponds in the load displacement curve of Fig. 5.32 to the right side of the bottom part of the spike. The system should again behave as an open frame; and this may be verified in Fig. 5.32 by the fact that the stiffness of the system after the failure of the wall is approximately the same as the original stiffness.

From time t=0.11 to 0.125 sec the frame deforms with little interference from the wall, but at time t=0.125 sec the frame comes into contact with the wall at midheight. This is depicted in Fig. 5.33. This contact induces a change in stiffness in the structure which may be seen in the load displacement curve of Fig. 5.32 at a displacement of about 12 mm. At this point the left column becomes braced inducing a change in the moment and shear. This may be detected in Figs. 5.28 and 5.29. Here, as expected, the shear and moment in the lower half of the column, Fig. 5.28, are reduced while these same quantities increase in the upper half of the column, Fig. 5.29. No such behavior is seen in the right column, Figs. 5.30 and 5.31, as this column deforms without any constraints.

At time t=0.145 sec part of the frame yields. This is depicted in Fig. 5.32 by the reduction in stiffness at a displacement of about 16 mm. The yielding in the frame occurs in the top part of the left column including the beam and at the base of the right

column. This may be seen in the column response shown in Figs. 5.29 and 5.31 where the moment has reached its yield value. Figure 5.29 shows that the shear, induced by the short column effect, has not yet reached its maximum value. Therefore between time t=0.145 and 0.180 sec the shear in the column increases to a value greater than that of the open frame.

At time t=0.180 sec, the frame again yields. This time at the center of the left column and the top of the right column forming a yield mechanism. This is depicted in Fig. 5.37 where both time steps t=0.145 and 0.180 sec are shown. This step is depicted in the load displacement curve at about 25 mm where the yield plateau is reached. Also at this time the shear and moment at the center and base of the left column reaches a plateau as may be seen in Figs. 5.28 and 5.29.

At time t=0.20 sec, the wall becomes fully cracked along its base. The only change that occurs is in the behavior of the lower left column shown in Fig. 5.28. As the wall, still bracing the column at midheight, moves to the right, the base moment of the left column increases up to yield at time t=0.305 sec. At time t=0.315 sec. the gap at the lower right side of the wall closes.

At time t=0.305 sec, the maximum displacement is reached and the system begins to unload. As the frame wall begins to unload the frame remains braced and therefore the system unloads with a higher stiffness than the open frame. This may be seen in Fig. 5.32 at a displacement of 52 mm. Once the center of the left

column moves away from the wall, the system returns to its original open frame stiffness. This occurs at a displacement of about 45 mm. Figure 5.28 shows that the bottom of the braced column on the left side of the frame does not unload until the frame loses contact with the wall at time t=0.35 sec. At this time the shear drops to reflect the fact that the wall no longer carries any shear, then it reloads. This jump in the shear is due to the fact that no iteration within a time step is carried out and therefore no redistribution of the unbalanced forces may be accomplished within a given time step.

The load displacement curve in Fig. 5.32 shows that between the displacement of about 42 mm and 20 mm the frame, which is free to deform, behaves elastically. At time t=0.425 sec the upper part of the left column and the base of the right column yield. This depicted in the load displacement response as a change in stiffness at a displacment of 18 mm. At time t=0.45 sec the frame yields at the base of the left column and at the top of the right column. This sequence corresponds in Fig. 5.32 to the yield plateau that occurs at a displacement of about 5 mm. This whole sequence is presented in Fig. 5.38.

At time t=0.46 sec, the frame comes into contact with the wall. The load displacement curve in Fig. 5.32 shows that this contact does not occur at a zero displacement but at a displacement of about 1 mm. This is due to the fact that the wall, which has cracked at midheight, has been displaced slightly

more to the right than its base whose total movement is restricted to 10 mm. During the time interval t=0.46 to 0.465 sec the interaction with the wall increases the resistance of the structure by more than 4 times the open frame value. This is seen in Fig. 5.32 as the spike in the lower half of the plot.

At time t=0.465 sec the upper right corner of the wall fails. At the same time part of the lower right corner also fails. This is depicted in Fig. 5.38 at time t=0.465 sec and seen as a reduction in the load in Fig. 5.32. The load displacement curve of Fig. 5.32 shows that the load does not reduce to the yield plateau that existed at a displacement of 1 mm. This is due to the bracing effect of the wall on the right column. This is shown in the column response of Fig. 5.30 as an increase in the shear in the upper half of the column at time t=0.47 sec. From time t=0.465 to 0.5 sec, the shear at the top of the column increases until the column yields at its midsection. It should be noted, as seen in Fig. 5.31, that the moment at the base of the right column has dropped below its yield value just as the moment at the center of the column increases due to the bracing effect.

Figure 5.32 shows that the system undergoes two additional cycles of loading. The principal difference between these two additional cycles and the two previous ones is that the frame yields before it comes into contact with the wall at midheight. Once the wall and frame come into contact, the shear starts to increase again but this time in a nonlinear fashion due to the

fact that the wall may slide along its base. This is depicted in the column behavior of Figs. 5.28 through 5.31 as an increase or decrease in the shear at times t=0.8 and 1.05 sec. The load displacement curve of Fig. 5.32 also shows this change at a load level of 245 kN and a displacement of about 25 mm for the third cycle and a load level of 245 kN and a displacement of about -25 mm for the fourth cycle.

The fundamental difference in behavior between the frame wall with no gaps and the present structure is the fact that no diagonal compressive behavior has been observed. Although the wall alters the behavior of the frame by bracing the columns, the behavior is still that of a frame. This may be seen in the axial load behavior of the columns in this structure. The behavior of the columns in this structure is similar to the columns of an open frame. Their behavior lacks any of the large axial load changes encountered in the previous structure changes which were mainly due to the diagonal bracing effect of the wall.

5.3.4 Frame Wall with Gaps(II)

In this frame wall structure the ultimate compressive strength for the masonry was increased to 34 MPa and the tensile strength to 3.4 MPa. A gap of 5 mm was specified between the wall and the frame just as in the previous structure. The response of the system is shown in Figs. 5.39 through 5.50. They represent the same response quantities as the previous structures. A brief summary of the key events that occurred during the response is presented in Table 5.8.

As with the previous structure, the wall is not in contact with the frame and does not contribute to its stiffness under the small displacement theory therefore its fundamental frequency of 1.53 Hz coincides with that of the open frame. This again sets the frame wall system just to the left of the spectrum's maximum response.

The time histories of the relative displacement and absolute acceleration are shown in Fig. 5.39. Unlike the previous test this response shows no elastoplastic behavior. The relative displacement response shows no permanent deformation and the free vibration response seems to be that of an open frame. The maximum displacement is about 19 mm which is about 2.7 times less than the previous structure and 4 times less than the open frame. The limitation on the maximum displacement is due, as will be seen, to the development of the wall as a diagonal element across the frame and not, as in the previous structure, to the effective shortening of the column caused by the bracing effect of the wall when its upper half failed.

The load displacement curve is shown in Fig. 5.45; in which a sharp change in stiffness is seen at a displacement of about 5 mm as the frame comes into contact with the wall. This condition is depicted in Fig. 5.39 as a sharp rise in the absolute acceleration at a time t=0.1 sec. The closing of the gap is depicted in Fig. 5.46 at time t=0.09 sec.

The first change in stiffness comes at time t=0.095 sec due to cracking in the wall. This is seen in the load displacement plot of Fig. 5.45 and in the absolute acceleration of Fig. 5.39. The crack pattern for time t=0.095 sec is shown in Fig. 5.47. The second change in stiffness is seen in Fig. 5.45 at a displacement of about 7 mm. This corresponds to a time t=0.105 sec in Fig. 5.48; a full horizontal crack develops at the midheight of the wall and almost a full crack at the base of the wall in addition to some diagonal cracking.

The third change in stiffness in Fig. 5.45 takes place at about 11 mm and is the most important of the three that occur. At this point the wall has failed along its base as may be seen in Fig. 5.49 at time t=0.145 sec. The wall may now slide along its base and, as expected, the load level declines as seen in the load displacement response, Fig. 5.45. This decline begins at a displacement of 11 mm and ends, as expected, at a displacement of 16 mm when the wall comes into contact with the right column at its lower right corner. This is depicted in Fig. 5.46 at time t=0.185 sec.

In the load displacement curve the load begins to increase again at a displacement of 16 mm. But the increase is small as the base acceleration has already begun to decline. The base of the columns yields at time t=0.190 sec this may be seen in Figs. 5.41 and 5.44. At this time no appreciable change has occurred in

the axial behavior of the columns indicating that the wall is not yet acting as a diagonal element. This is due to the fact that no contact has occurred between the beam and wall, an apparent requisite for this type of behavior.

Once unloading occurs, Fig. 5.45 shows that the structure returns to the stiffness of the open frame. This unloading begins at a displacement of about 17 mm and remains unchanged up to a displacement of 5 mm. This is to be expected as the wall is now 5 mm to the right of its original position. The crack pattern in Fig. 5.50 depicts the behavior of the system during the load reversal.

At time t=0.29 sec the frame comes into contact with the wall at midheight. Since the wall has had a greater relative displacement in its upper half only the gap elements at midheight which correspond to this condition are closed. This contact as well as the one that occurs at time t=0.32 sec seems to have little effect on the stiffness of the system. This may be verified by looking at the absolute acceleration in Fig. 5.39 and load displacement curve in Fig. 5.45.

At time t=0.335 sec the frame comes into contact with the wall at the upper right corner. This corresponds in the load displacement curve with the increase in the stiffness at a displacement of 5 mm in the lower right quadrant. The increase in stiffness is less than in the first loading cycle as the wall may slide along its midheight as well as along its base. The change

in stiffness at 4 mm is due to the sliding effect. This condition lasts, while the load is increasing, until a displacement of -4 mm.

At this point a drop in the load occurs. This corresponds to the failure of part of the wall at time t=0.37 sec as depicted in Fig. 5.50. In this same figure in the next time step, the beam comes into contact with the wall, setting the condition for the wall to behave as a diagonal element. From a displacement of -4 mm which occurs at time t=0.37 sec to a displacement of -12 mm, at t=0.405 sec, no appreciable increase in load is detected.

At time t=0.405 sec the wall comes into contact with the base of the left column and begins to behave as a diagonal element. In addition the frame yields at the base of both columns. The load increases as the behavior of the system is altered from an open frame behavior to a braced frame behavior. The right column is put in tension as may be seen in the column response histories shown in Figs. 5.43 and 5.44; confirming the fact that a large compressive force is being carried across the diagonal of the frame. This bracing of the frame across its diagonal is repeated in the next two cycles of loading as may be seen by looking at Figs. 5.41 through 5.45.

An important factor that differentiates this response from that of the frame wall system which had no gaps is the level of the moments and shears when the system is acting as a braced frame. In the present case, the moments and shears are larger

than the ones developed in the frame wall system for which initial continuity was assumed.

5.3.5 Three Story Frame Wall

The response of the three story structure is shown in Figs. 5.51 through 5.69. Figure 5.51 is the ground motion and Fig. 5.52 is the elastic spectrum for the ground motion. Figures 5.53 through 5.69 represent the same response quantaties as the previous structures. A brief summary of the key events that occurred during the response of each story is presented in Tables 5.10 through 5.12. The first three seconds of the motion are not included in Figs. 5.53 through 5.69 because the response is undetectable when compared to the rest of the time history.

The size of the gap for all three stories was taken as zero but the wall was not assumed continuous with the frame as in the case of the frame wall of Sec. 5.3.2. Under the small displacement theory this gives a set of frequencies which correspond to the open frame. In order to assess the difference between specifying a gap size of zero and a continuous system two sets of frequencies were calculated; these are shown in Table 5.9. Again the great difference in the frequencies between the open frame, as represented by the gap size of zero, and the frame wall is evident. Although the fundamental elastic frequency of the three story frame wall is 1.33 Hz the response should correspond to a frequency of about 10.0 Hz due to the gap size of zero.

Due to the complexity of the ground motion a detailed discussion as provided for the previous structures will not be presented. However, there are some changes in behavior that are due to the occurrence of a very specific event.

In the first story there are three very specific changes in behavior as may be seen in the load displacement curve, Fig. 5.55. At first the frame acts monolithically with the wall giving the first story a relatively high stiffness. This condition lasts for the first 3.5 sec providing for small displacements, shears and moments while giving large changes in the axial loads of the columns. Between t=3.5 and 4.1 sec considerable cracking is developed within the wall until a complete crack across the diagonal of the wall is developed and a large change in stiffness occurs; Fig. 5.55. The third major change in the behavior of the first story occurs at t=6.37 sec when the frame yields at the base of the columns. This condition is depicted in Fig. 5.55 as two large loops which provide the maximum load developed in the story.

In the third story up to t=3.5 sec the system behaves as a monolithic unit with the same consequences as the first story of having small displacements, shears and moments with a relatively high stiffness. The first change in behavior occurs at t=4.66 sec with a slight reduction in the stiffness due to some cracking within the wall, this may be seen in Fig. 5.61. The second and

largest change in behavior occurs at t=5.32 sec. At this time a full crack across the diagonal of the wall is developed. The development of this crack results in a sharp reduction in the stiffness of the story, as shown in Fig. 5.61. After this time the displacements, moments and shears are no longer small.

In the second story the most interesting event occurs at t=4.1 sec. At this point the interstory drift, Fig. 5.57, has a radical change in behavior where the response frequency of the story is altered. The story then vibrates at a frequency of about 30 Hz but its base motion slowly fluctuates. Since any one of the three stories has a frequency, if treated as a single degree of freedom, of about 30 Hz the second story then behaves as a relatively stiff system which sits on a more flexible one. Something similar is reflected in the third story response, Fig. 5.60, up to t=5.32 sec at which point the wall becomes fully cracked across its diagonal. Little or no change in stiffness occurs for the second story throughout the ground motion as may be seen in Fig. 5.58.

5.4 Discussion of Results and Design Implications

The most important result that may be deduced from the previous studies is the tremendous influence that the initial conditions of strength and gap size have on the behavior of the system. The radical change in behavior between the second, third, and fourth structure is a case in point.

The second structure consisted of a frame with an infill masonry wall but the wall was assumed continuous with the frame at the beginning of the ground motion. The third structure differed from the second one in that a gap was specified at the frame wall boundary. The size of this gap was taken as 5 mm. The significant difference in the results of these two structures has already been shown. The fourth structure differed from the third structure only in the compressive strength assumed for the masonry. Again the difference in behavior between the fourth structure and the second and third structures was evident.

The differences in behavior between the second and third structures may be in part explained by looking at the spectrum for the base acceleration shown in Fig. 5.5. The gap specified for the third structure causes the initial frequency of that system to be the same as that of the open frame, 1.53 Hz. This places the third structure close to the maximum response of the spectrum at a frequency of 2 Hz. The second structure has an initial frequency of 13 Hz due to the continuity with the wall. This places the second structure at the right side of the spectrum at a much lower response than the third structure. The spectrum indicates that if these two systems remain at their original frequencies they will reach different maximums. One is in fact looking at two different structures. In the normal design process this is not evident.

Although the location of the initial natural frequency is important, this condition is not wholly satisfactory in explaining the great change in behavior that a 5 mm gap may induce. This is due to the fact that: (1) neither system retains its original natural frequency; and (2) the spectrum in Fig. 5.5 provides no information about the time domain.

If the specified gap of 5 mm were reduced, one may reasonably assume that the response of the third structure would tend towards the response of the second structure. This fact would be independent of the original frequency of the system as this frequency would remain at 1.53 Hz until the gap size was reduced to zero. This argument is supported by the results of the three story structure where a gap of size zero was specified. This structure in fact behaved initially at the higher frequency of 10.0 Hz rather than at 1.33 Hz, the frequency of the open frame.

This fact coupled with the two previous observations points to the size of the gap as the key factor that determines the behavior of the frame-infill-wall system. If the gap is small enough, the frame-infill-wall will tend to behave as if the system were originally continuous. In the present case, the system with the frequency of 13 Hz. would approximately determine the response of the third structure. This is in spite of the fact that the initial frequency of this system would be 1.53 Hz. If the gap is not small enough, then the behavior of the system

depends not only on the gap size but also on the strength of the wall and on the location of the initial frequency with respect to the response spectrum. This last observation is based on the results of the third and fourth structures.

In order for the wall to fail as it did in the third structure, the frame must develop sufficient momentum such that the wall cannot resist the load being applied. In order to develop this momentum, the gap size must not only be sufficiently large, but the response of the frame to the ground motion must be such that it can develop the momentum necessary to make the wall fail.

The spectrum in Fig. 5.5 gives the maximum response for a given frequency but says nothing about the time response of the system. In spite of this, the maximum response of the open frame may serve as an indication of whether sufficient momentum can be developed to make the wall fail. In this case a 5 mm gap with the present ground motion is sufficient to fail the wall in the third structure but not enough for the fourth structure.

The difference in behavior between the third and fourth structures point to the fact that contact between the beam and wall is a necessary condition to develop bracing across the diagonal of the frame. The fourth structure shows that unless the contact between the beam and wall occur, no significant changes in the axial behavior of the columns will result. This condition is important since many structures have a large space

between the top of the wall and the beam. Hence, there are structures which may only be able to shorten the effective length of the surrounding columns, as in the third structure, but never diagonally brace the frame, as in the fourth structure.

Although specific design recommendations must await further research, several observations may be made:

1. Most of the frames infilled by masonry walls do have specific separation between the columns and wall placing them in the same category as the third and fourth structures. This is supported by the type of damage observed for these systems under earthquake loadings.
2. This research indicates that for the study of the frame masonry wall system, the use of a cracking mechanism as well as the ability to model the gaps between the frame and wall may be indispensable.
3. The use of the Equivalent Strut Method to represent these walls in a design process requires judgment, experience and an understanding of the behavior of the system. A case in point is the marked difference in behavior between the second and third structures. In the second structure the straightforward use of this method should yield good results. The use of this method in the third structure is not as evident and its use would require a clear understanding of the limitations of the method as well as good engineering judgment.

4. Contact between the beam and wall is indespensable to develop a diagonal bracing across the frame. If contact between the beam and wall cannot occur, as in the case of walls which are much shorter than the columns, diagonal bracing will not occur.
5. The difference in behavior of the structures that were studied points to the inadequacy of using the open frame frequency in designing frames to which infill walls have been added.

CHAPTER 6

SUMMARY AND CONCLUSIONS

6.1 Summary

A nonlinear dynamic model to study the behavior of frames infilled by masonry walls has been presented. The nonlinearities of the model include the interaction between the frame and wall, cracking and failure of the wall, the bracing effect that the wall has on the frame, the discontinuities between the frame and wall, and the inelastic behavior of the frame.

The fundamental concept for modeling the masonry wall was based on the premise that the cracking mechanism in the wall may be separated from the material model assumed for the masonry. This premise was based on the fact that masonry tends to have preferred planes of failure along its mortar joints. The separation of the cracking mechanism not only simplified the modeling of the masonry but in the end seemed to be indispensable in predicting the different modes of behavior of the frame-infill-wall system.

Each part of the proposed model was represented by elements which were as simple as the assumptions would permit. This was done to better determine the capabilities of the model.

The model was used to study three one story, one bay frame-infill-wall systems for which different initial properties were specified and to which a sinusoidal ground motion was applied. In addition the model was used to study a three story, one bay frame-infill-wall to which an earthquake ground motion was applied.

The analytical model showed the ability to represent the different facets of behavior that have been observed experimentally. Specifically, the wall was able to alter its behavior in accord with the boundary conditions imposed by the frame. The model was also able to effectively represent the cracking pattern both inside and at the boundary of the wall. It also showed the ability to brace the frame both diagonally and as a short column.

Discrepancies that showed up in the computations were mainly due to the very simple material and element models used. Specifically, the material model for masonry after failure created the greatest discrepancies.

The studies that were done pointed to the inadequacy of some of the most common assumptions made with regard to a frame-infill-wall system. The size of the initial separation between the frame and wall may be the principal factor in determining the behavior of the system while a combination of the initial frequency, gap size, and wall strength may be the second most important condition.

6.2 Conclusions

The following conclusions are based on the development and use of the proposed model.

1. The crack mechanism proposed or some equivalent system which allows the masonry wall to become discontinuous seems to be indispensable in modeling the frame-infill-wall system. The Equivalent Strut Method seems to be extremely limited in this respect while full discretization through the Finite Element Method would seem too expensive at the present time.
2. The proposed model seems to be able to represent the different modes of behavior observed experimentally.
3. The behavior of the frame-infill-wall system is strongly depedent on the gap size specified. Any attempt at modeling this system must include the ability to specify gaps at the frame wall boundary.
4. The three most important variables in this system are the gap size, the strength of the infill wall, and the time of the maximum response of the open frame. The last condition may be measured by the initial frequency and the response spectrum leaving only the time of occurrence as a variable.
5. Diagonal bracing of the frame by the wall depends upon the wall coming into contact with the beam at opposite diagonal corners.

6. The fundamental elastic frequency of the open frame is not an adequate measure of the frequency or behavior of the frame-infill-wall system.
7. Further research is necessary to better understand the behavior of the frame-infill-wall system and develop adequate design recommendations.

TABLES

Table 5.1 Frame Data

Modulus of Elasticity	25 GPa
Beam Cross Section Area	245 x 10^3 mm^2
Beam Moment of Inertia	5 x 10^9 mm^4
Column Cross Section Area	123 x 10^3 mm^2
Column Moment of Inertia	1.25 x 10^9 mm^4
Yield Moment	214.0 kN-m
Total Mass	150 Mg
Total Dead Load	490 kN
Damping Ratio	2%
Mass Three Story Frame	30 Mg (per story)

Table 5.2 Wall Data

Modulus of Elasticity	14 GPa
Wall Thickness	100 mm
Poisson's Ratio	0.25
Masonry Compressive Strength	24 to 34 MPa
Masonry Tensile Strength	2.4 to 3.4 MPa
Total Dead Load	60 kN

Table 5.3 Joint Data

Modulus of Elasticity	7 GPa
Joint Thickness	10 mm
Poisson's Ratio	0.15
Cross Sectional Area	87.5-175 x 10^3 mm^2

Table 5.4 Failure Surface Data

Joint Failure Surface (Fig. 3.2)

Shear Stress Control Point..... 1360 kPa

Normal Stress Control Point..... 340 kPa

Slope Tension Branch..... 2

Slope Compression Branch..... 1

Masonry Failure Surface

Ratio of Tensile Strengths..... 1.5 (Fig. 3.4)

Ratio of Compressive Strengths.... 0.42 (Fig. 3.5)

Table 5.5 Key Response Quantities and Events: Open Frame

Freq. (Hz)	Max. Dis. (mm)	Max. Vel. (mm/sec)	Max. Abs. Acc. (g)	Max. Res. (kN)	Max. Double Amp. (mm)
1.53	77.3	-445.6	0.188	245.0	83.0

Col.	Max. Base Mom. (kN-m)	Max. Base Shear (kN)	Max. Center Mom. (kN-m)	Max. Top Shear (kN)	Max. Top Mom. (kN-m)	Min. Axial Load (kN)+	Axial Dead Load (kN)	Max. Axial Load (kN)
Left	215.0	126.0	-	123.0	215.0	180.0	245.0	310.0
Right	215.0	126.0	-	123.0	215.0	182.0	245.0	308.0

+Axial response for bottom section of column.

Table 5.6 Key Response Quantities and Events: Frame Wall

Freq. (Hz)	Max. Dis. (mm)	Max. Vel. (mm/sec)	Max. Abs. Acc. (g)	Max. Res. (kN)	Max. Double Amp. (mm)
13.0	3.5	-43.2	0.462	680.0	6.8

Col.	Max. Base Mom. (kN-m)	Max. Base Shear (kN)	Max. Center Mom. (kN-m)	Max. Top Shear (kN)	Max. Top Mom. (kN-m)	Min. Axial Load (kN)+	Axial Dead Load (kN)	Max. Axial Load (kN)
Left	110.8	100.0	64.0	-	69.0	-29.0	130.0	219.0
Right	118.0	-	68.4	59.0	63.5	-24.0	130.0	282.0

Summary of Key Events

Time (sec)	Disp. (mm)	Event	See Fig.
0.45	0.04	Change in response from linear to nonlinear.	5.19
0.075	0.75	Partial transition to braced frame; horizontal crack at midheight and boundary of wall.	5.23
0.125	2.0	Full transition to braced frame; crack at midheight of wall; almost full crack along base and left side of wall.	5.20

+Axial response for bottom section of column.

Table 5.7 Key Response Quantities and Events: Frame Wall-Gaps(I)

Freq. (Hz)	Max. Dis. (mm)	Max. Vel. (mm/sec)	Max. Abs. Acc. (g)	Max. Res. (kN)	Max. Double Amp. (mm)
1.53	52.1	-522.2	0.272 (0.767)++	400.0 (1100)++	99.0

Col.	Max. Base Mom. (kN-m)	Max. Base Shear (kN)	Max. Center Mom. (kN-m)	Max. Top Shear (kN)	Max. Top Mom. (kN-m)	Min. Axial Load (kN)+	Axial Dead Load (kN)	Max. Axial Load (kN)
Left	215.0	124.0	215.0	245.0	215.0	176.0 (95.2)++	245.0	308.0
Right	215.0	126.0	215.0	245.0	215.0	176.0 (-112)++	245.0	307.0

Summary of Key Events

Time (sec)	Disp. (mm)	Event	See Fig.
0.090	5	Upper left corner gap closes; wall and frame interact; large change in stiffness.	5.33
0.110	9	Upper left corner of wall fails.	5.36
0.125	12	Column braced at midheight.	5.33
0.145	16	Partial yielding of frame; bottom right column, top left column and beam.	5.37
0.180	25	Full yielding of braced frame top right column and beam, center left column.	5.37
0.305	52	Wall slides along base; gap closes at bottom of right column; maximum displacement reached.	5.33

+Axial response for bottom section of column.

++Values at spike.

Table 5.8 Key Response Quantities and Events: Frame Wall-Gaps (II)

Freq. (Hz)	Max. Dis. (mm)	Max. Vel. (mm/sec)	Max. Abs. Acc. (g)	Max. Res. (kN)	Max. Double Amp. (mm)
1.53	19.0	-287.0	0.841	1260.0	36.0

Col.	Max. Base Mom. (kN-m)	Max. Base Shear (kN)	Max. Center Mom. (kN-m)	Max. Top Shear (kN)	Max. Top Mom. (kN-m)	Min. Axial Load (kN)+	Axial Dead Load (kN)	Max. Axial Load (kN)
Left	214.0	118.0	-	130.0	207.0	-210.0	245.0	300.0
Right	214.0	149.0	-	119.0	200.0	-250.0	245.0	303.0

Summary of Key Events

Time (sec)	Disp. (mm)	Event	See Fig.
0.090	5	Upper left corner gap closes; wall and frame interact; large change in stiffness.	5.46
0.145	11	Full crack developed at midheight and at base; large reduction in load and stiffness.	5.49
0.185	16	Lower right corner gap closes; load increases; no change in column load yet.	5.46
0.335	5	Upper right corner gap closes; wall and frame interact; large change in stiffness; wall displaced 5 mm from original position.	5.50
0.405	12	Lower left corner gap closes; upper right corner gap between beam and wall closes; frame becomes braced; large change in axial load of column.	5.50

+Axial response for bottom section of column.

Table 5.9 Frequencies - Mode Shapes: Three Story Structure

	Continuous			Gap Specified[+]		
	Mode No.			Mode No.		
	1	2	3	1	2	3
Nat. Freq. (Hz)	9.92	32.2	54.2	1.33	4.07	6.60
Participation Factor [++]	8.71	3.62	-1.04	8.89	3.01	-1.41
Mode Shapes[+++]						
Story 3	0.1473	-0.0937	-0.1138	0.1398	-0.1050	-0.0527
Story 2	0.0981	0.0787	0.1324	0.1062	0.0779	0.1264
Story 1	0.0449	0.1355	-0.0534	0.0503	0.1274	-0.1207

[+] Gap size = 0.

[++] Participation Factor = $\dfrac{\{q_i\}^T [M] \{R\}}{\{q_i\}^T [M] \{q_i\}}$.

[+++] Mode shapes normalized to $\{q_i\}^T [M] \{q_i\} = 1$. $\{q_i\}$ = mode shape.

Table 5.10 Key Response Quantities and Events: First Story

Max. Dis. (mm)	Max. Vel. (mm/sec)	Max. Abs. Acc. (g)	Max. Res. (kN)	Max. Interstory Drift (mm)	Max. Story Acc. (g)
-36.2	-327.0	-2.75	478.0	-36.2	-2.82

Col.	Max. Base Mom. (kN-m)	Max. Base Shear (kN)	Max. Center Mom. (kN-m)	Max. Top Shear (kN)	Max. Top Mom. (kN-m)	Min. Axial Load (kN)+	Max. Axial Load (kN)+
Left	214.5	123.0	25.3	123.1	214.3	267.0	778.0
Right	214.5	123.0	69.5	162.1	214.4	233.0	794.0

Summary of Key Events

Time (sec)	Drift (mm)	Event	See Fig.
3.5	0.-0.5	Frame and wall act as a unit; large changes in axial force; small moments and shears.	5.62
4.1	0.-0.5	Full crack across diagonal of wall from top right to bottom left; large change in stiffness; moment and shears no longer small.	5.55
6.37	17.0	Frame yields at base of columns; larger loops in load displacement curve.	5.55
7.2	36.0	Max. displacement; permanent set of 20 mm.	5.54

+Axial response for bottom section of column.

Table 5.11 Key Response Quantities and Events: Second Story

Max. Dis. (mm)	Max. Vel. (mm/sec)	Max. Abs. Acc. (g)	Max. Res. (kN)	Max. Interstory Drift (mm)	Max. Story Acc. (g)
-36.6	-350.0	3.22	765.0	-1.39	3.62

Col.	Max. Base Mom. (kN-m)	Max. Base Shear (kN)	Min. Axial Load (kN)	Max. Axial Load (kN)
Left	76.3	38.9	70	324
Right	75.0	37.2	60	319

Summary of Key Events

Time (Sec)	Drift (mm)	Event	See Fig.
4.1	0.5	Full crack in first story detected as a change in response.	5.57
4.7	1.4	Story is very stiff compared to first story; story vibrates at a much higher frequency fluctuating about displacement of first story; frequency ~30 Hz.	5.57

Table 5.12 Key Response Quantities and Events: Third Story

Max. Dis. (mm)	Max. Vel. (mm/sec)	Max. Abs. Acc. (g)	Max. Res. (kN)	Max. Interstory Drift (mm)	Max. Story Acc. (g)
-46.0	-497.0	-1.96	579.0	-14.8	-1.99

Col.	Max. Base Mom. (kN-m)	Max. Base Shear (kN)	Min. Axial Load (kN)	Max. Axial Load (kN)
Left	158.0	88.0	8	162
Right	162.0	90.0	-20	171

Summary of Key Events

Time (sec)	Drift (mm)	Event	See Fig.
3.5	0.3	Frame and wall act as a unit; small moments and shears; large stiffness.	5.61
4.66	1.0	Some cracking across diagonal; some change in stiffness.	5.61
5.32	1.2	Full crack across diagonal; major change in stiffness.	5.61

Table 5.13 Response Quantities I: One Story Structure

Case	Gap (mm)	Freq. (Hz)	Max. Dis. (mm)	Max. Abs. Acc. (g)	Permanent Set (mm)	Max. Res. (kN)	Comments on Behavior
A	N.A.	1.53	77.3	0.188	4.0	245.0	Ductile frame; yield at base and top of columns; yield in beam.
B	N.G.	13.0	3.5	0.462	0.	680.0	Initial monolithic; columns as flanges, wall as web; change to bracing across diagonal of frame.
C	5	1.53	52.1	0.272 (0.767)+	30.0	400.0 (1100)+	Top left and right corner of wall fail; bracing and yielding of columns at midheight.
D	5	1.53	19.0	0.841	0.	1260.0	Failure of joint at base of wall; shift in wall; bracing across diagonal of frame.
Fig. 5.5	-	1.53	128.0	1.21	N.A.	1780.0	
	-	13.0	0.70	0.48	N.A.	706.0	

+Value at spike

Notes: A - Open Frame
B - Frame Wall
C - Frame Wall-Gaps(I)
D - Frame Wall-Gaps(II)

N.A. - Not Applicable
N.G. - No Gaps

Table 5.14 Response Quantities II: One Story Structure

	Left Column				Right Column				
	Case				Case				
	A	B	C	D	A	B	C	D	Comments
Max. Base Mom. (kN-m)	215.0	110.8	215.0	214.0	215.0	118.0	215.0	214.0	
Max. Base Shear (kN)	126.0	100.0	124.0	118.0	126.0	-	126.0	149.0	
Max. Center Mom. (kN-m)	-	64.0	215.0	-	-	68.4	215.0	-	Yielding in Case C due to bracing of column.
Max. Top Shear (kN)	123.0	-	245.0	130.0	123.0	59.0	245.0	119.0	Difference between Case A and Case C due to bracing of column.
Max. Top Mom. (kN-m)	215.0	69.0	215.0	207.0	215.0	63.5	215.0	200.0	
Min. Axial+ Load (kN)	180.0	-29.0	176.0 (95.2)++	-210.0	182.0	-24.0	176.0 (-112)++	-250.0	Maximum differences in axial response exhibited by frames which became braced across their diagonals.
Axial Dead Load (kN)	245.0	130.0	245.0	245.0	245.0	130.0	245.0	245.0	
Max. Axial Load (kN)	310.0	219.0	308.0	300.0	308.0	282.0	307.0	303.0	

+ Axial response for bottom section of column.

++ Value at spike

Notes: A - Open Frame
B - Frame Wall
C - Frame Wall-Gaps(I)
D - Frame Wall-Gaps(II)

FIGURES

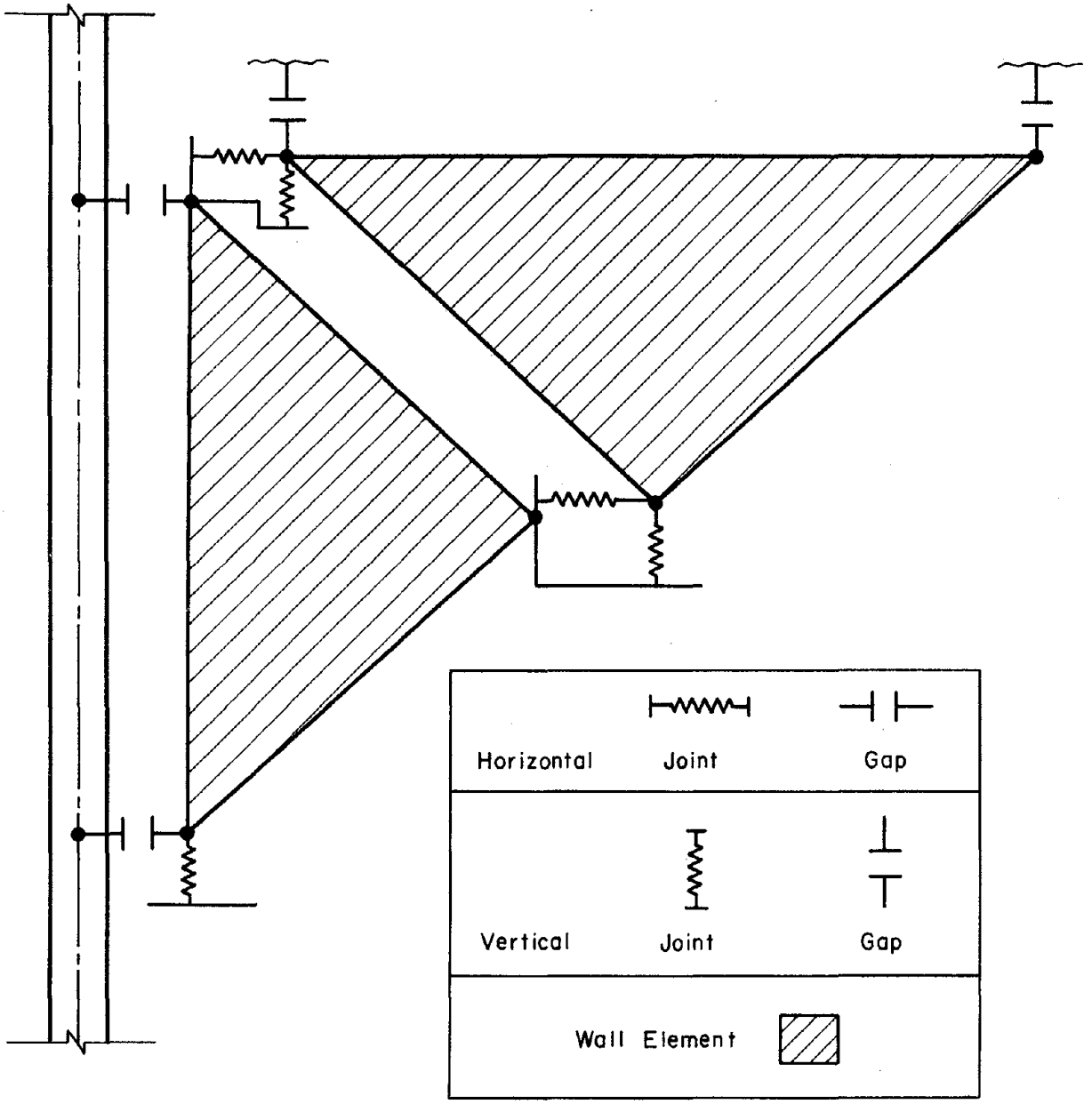

Figure 2.1 Schematic Representation of the Wall Model

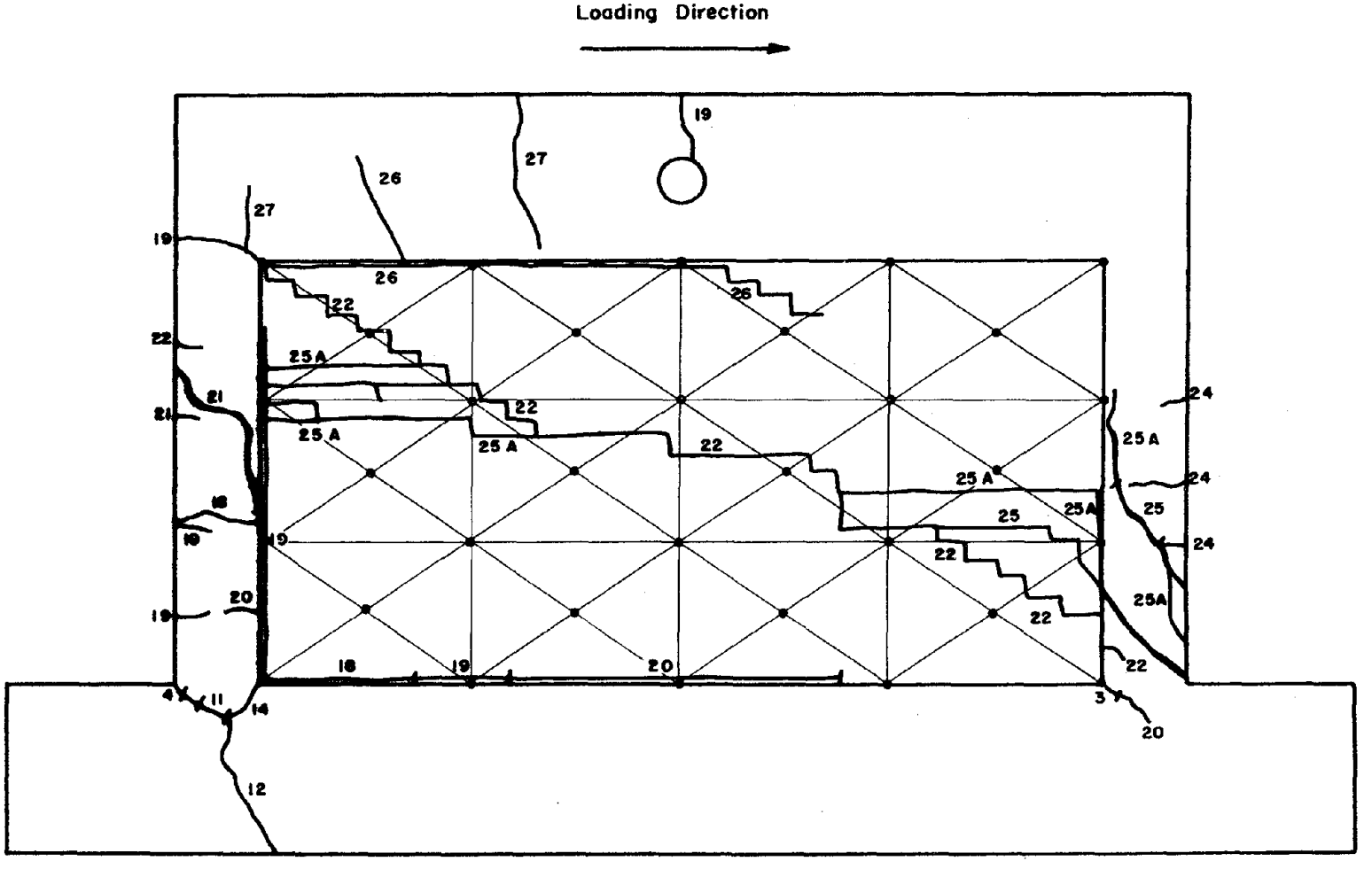

Figure 2.2 Infilled Frame Specimen, Analytical Model Superimposed (after Fiorato, Sozen, and Gamble, Ref. [18])

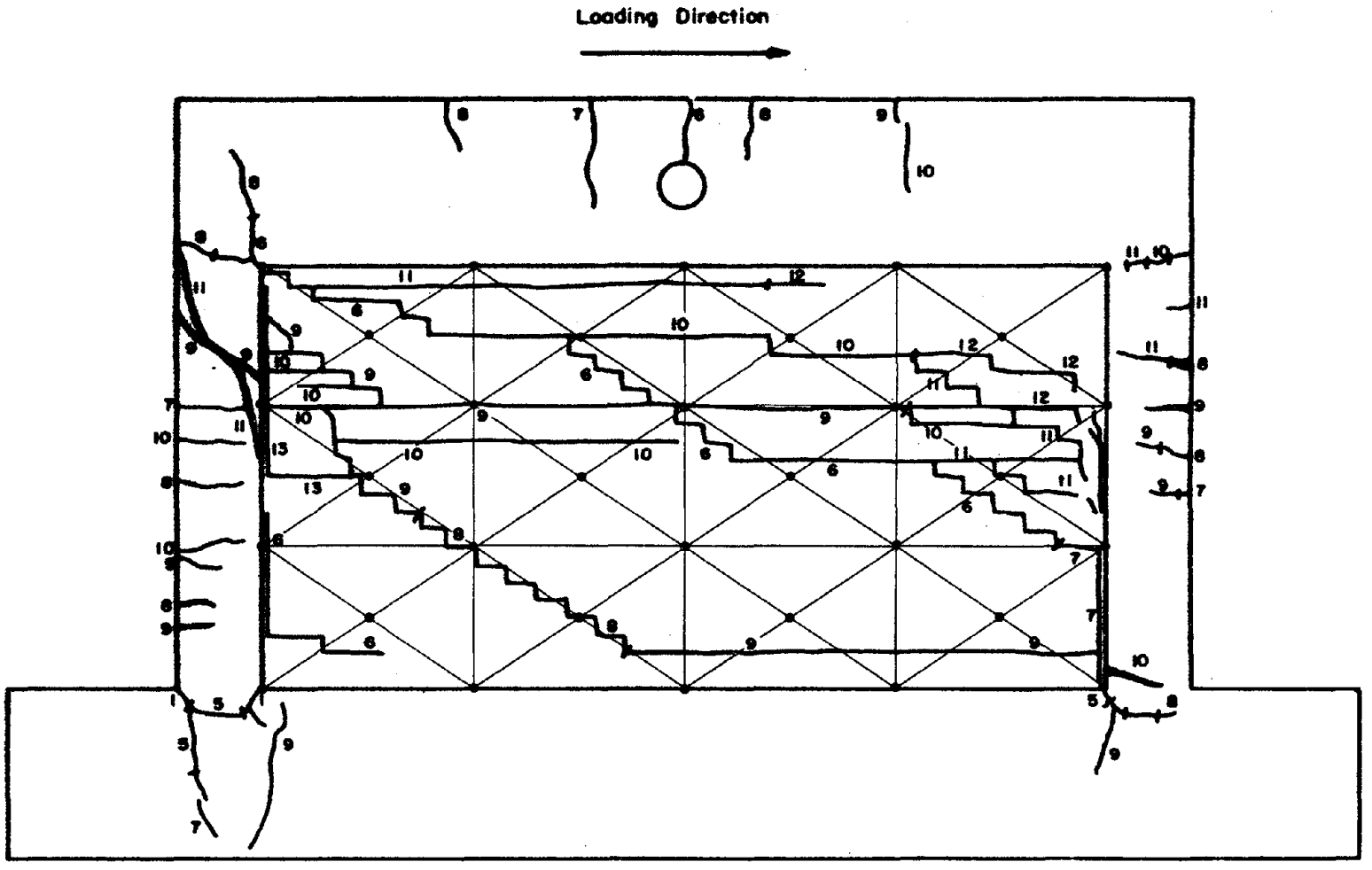

Figure 2.3 Infilled Frame Specimen, Analytical Model Superimposed (after Fiorato, Sozen, and Gamble, Ref. [18])

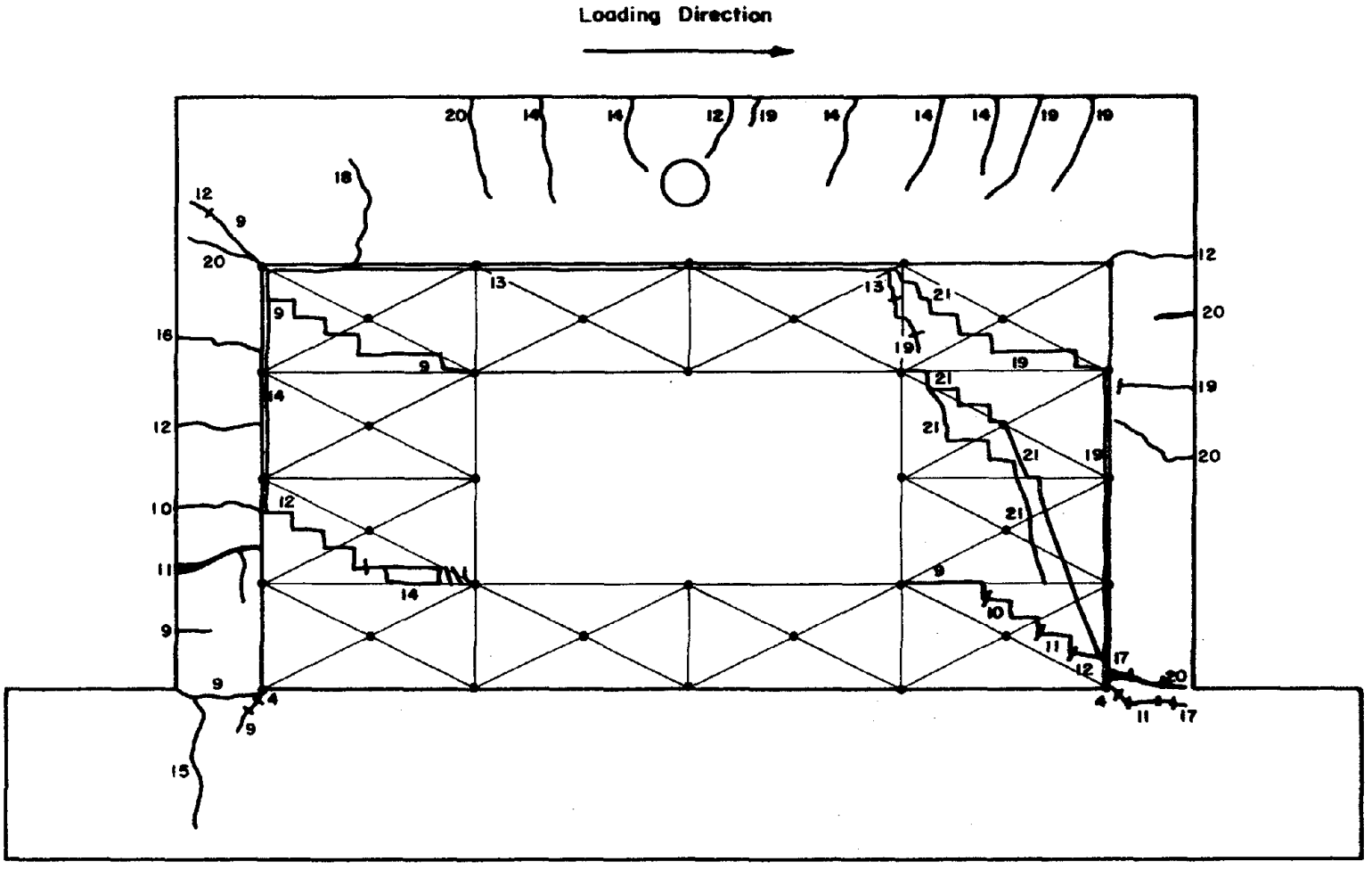

Figure 2.4 Infilled Frame Specimen with Opening, Analytical Model Superimposed (after Fiorato, Sozen, and Gamble, Ref. [18])

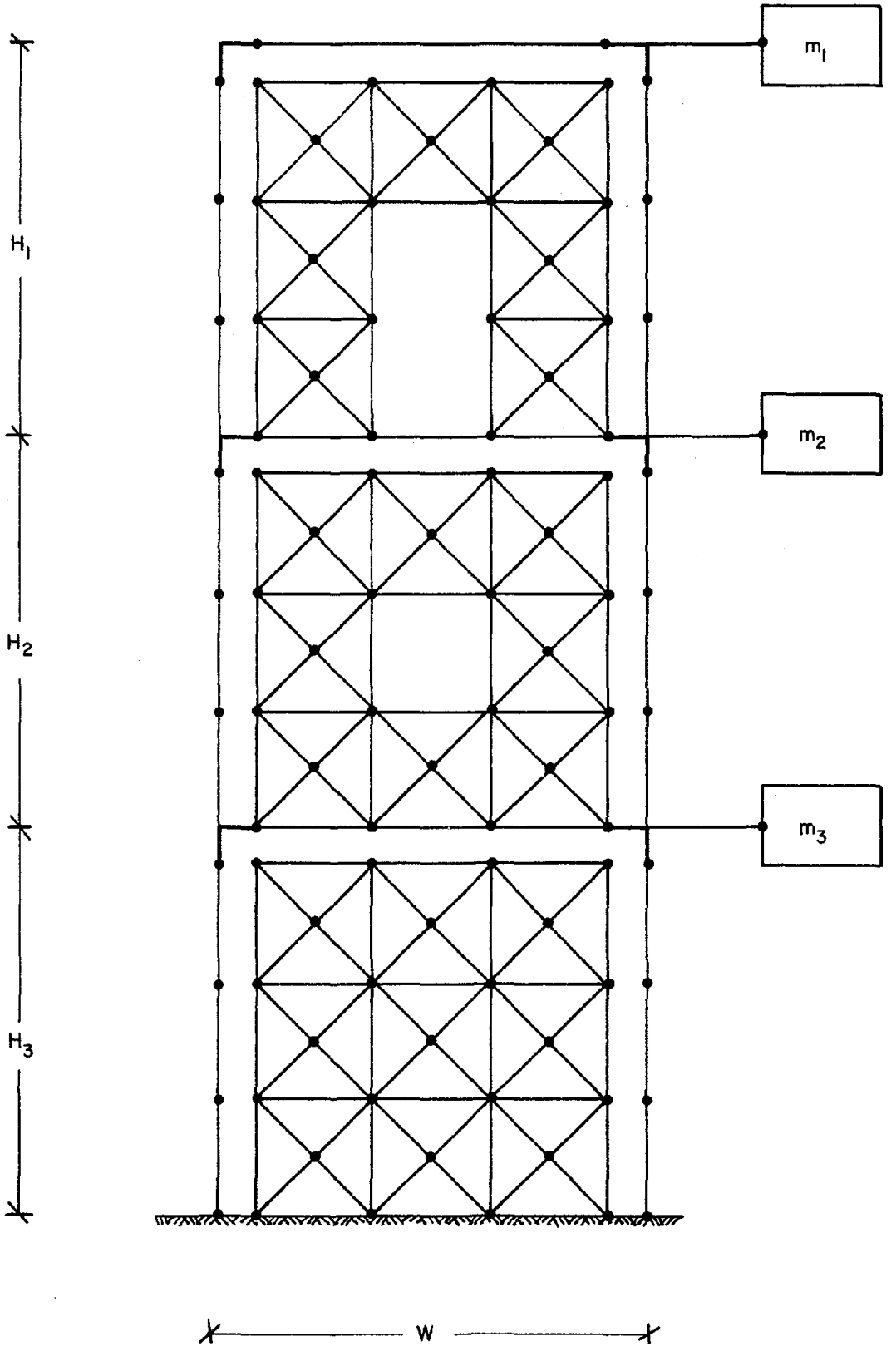

Figure 2.5 Idealization of a Three Story Frame Infill Wall

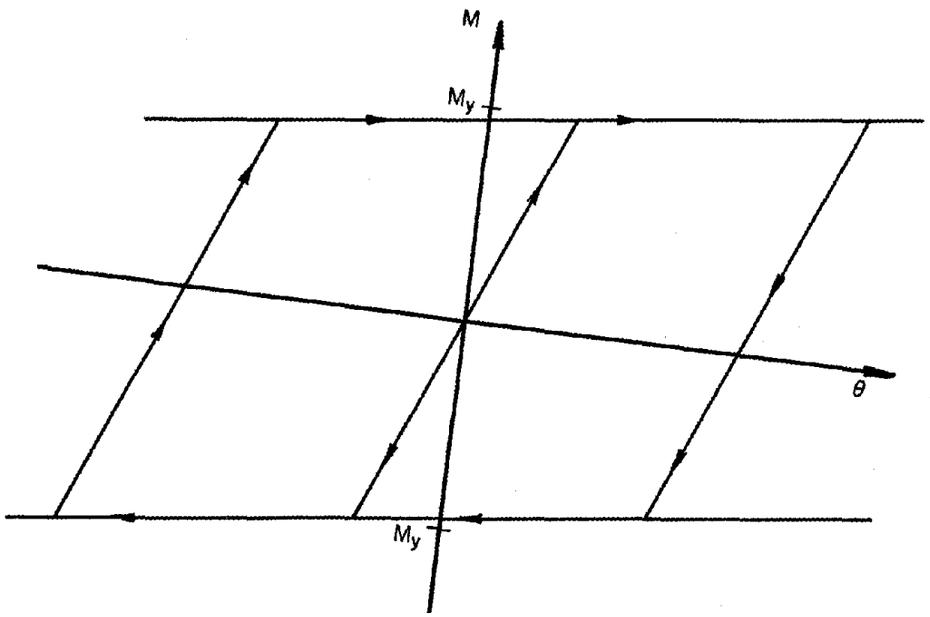

M = Moment
θ = Rotation
My = Yield Moment

Figure 3.1 Bilinear Moment Rotation Relation for the Columns and Beams

σ_n = Normal Stress
λ_s = Shear Stress
N_1 ; S_1 ; n ; m = Control Points For The Failure

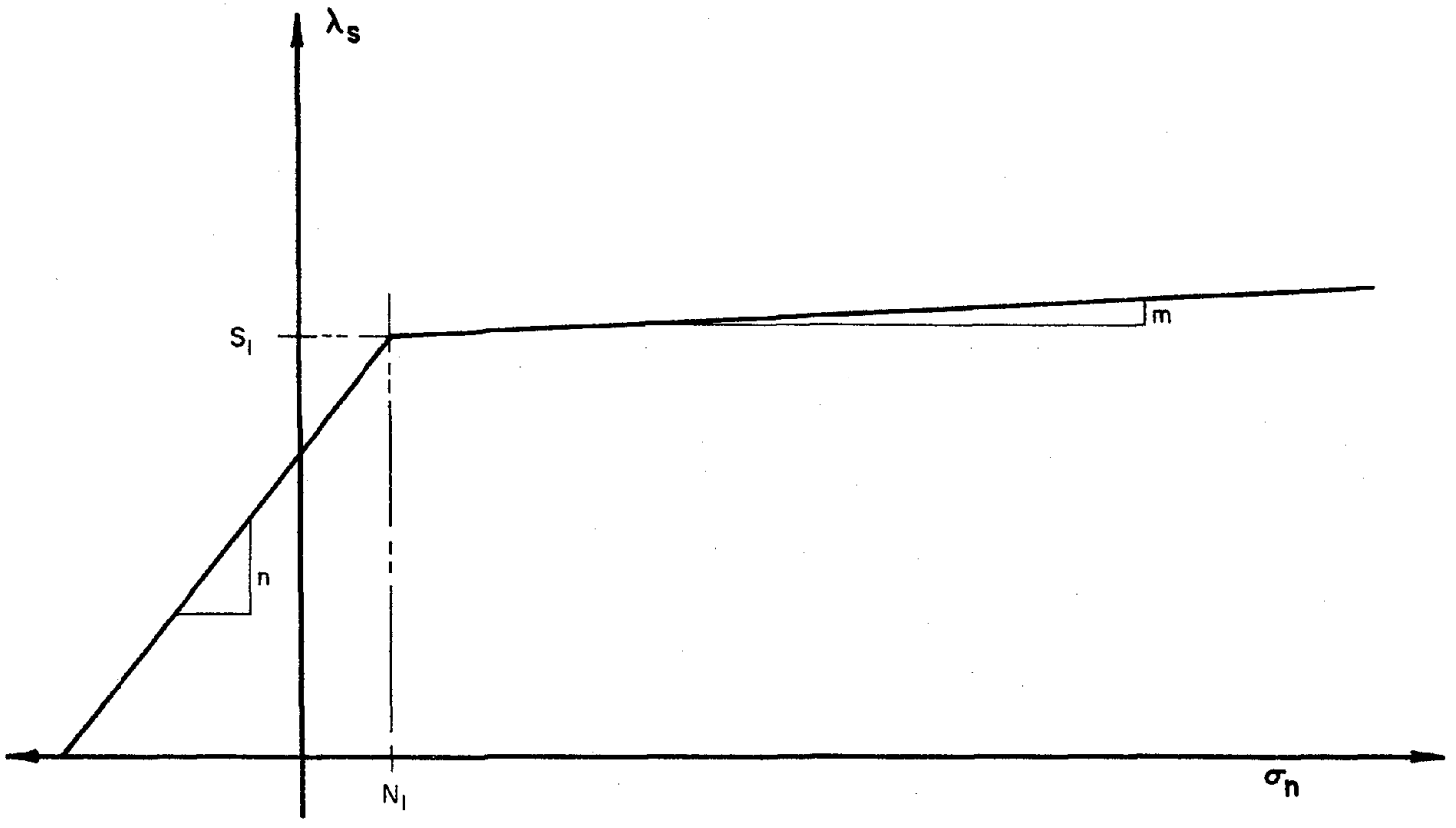

Figure 3.2 Joint Element Failure Surface

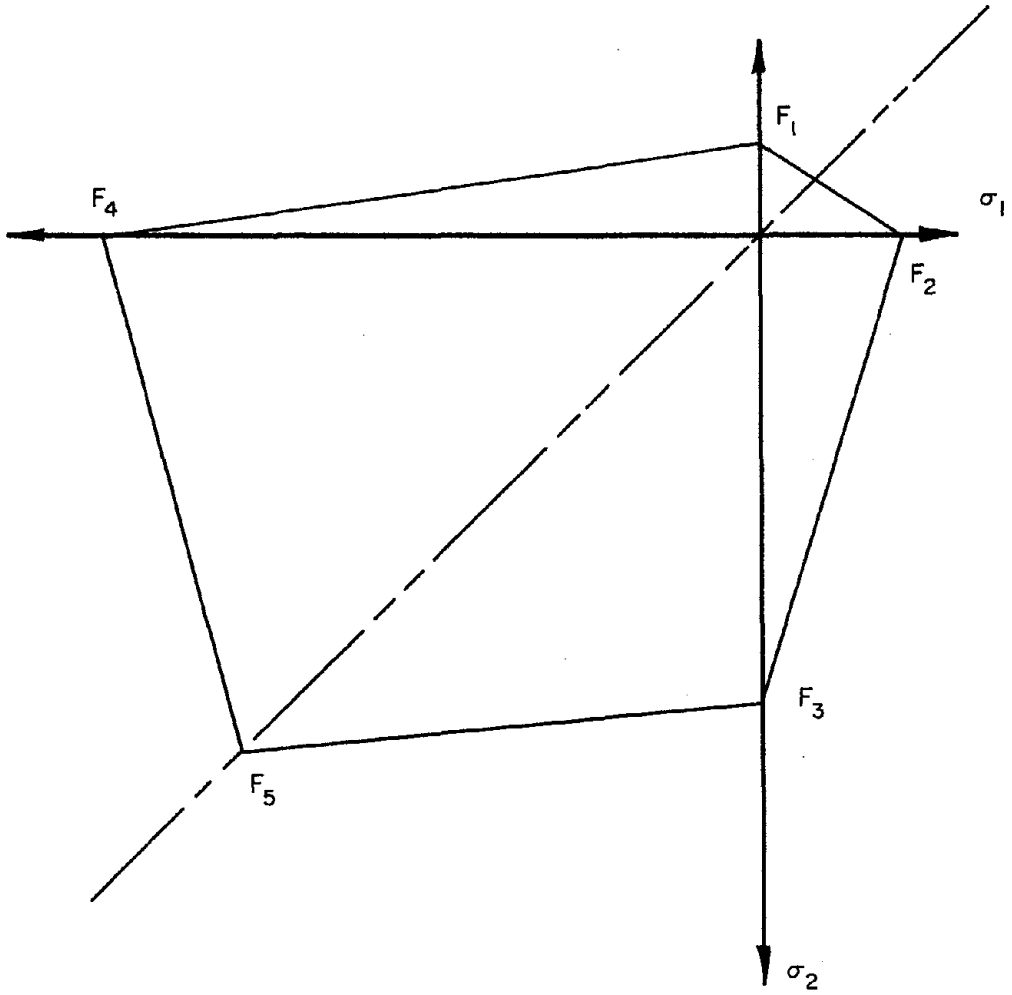

σ_1 ; σ_2 = Principal Stresses

F_1 ; F_2 ; F_3 ; F_4 ; F_5 = Control Points For The Failure Surface

F_5 = Max (F_3 ; F_4)

Figure 3.3 Masonry Wall Failure Surface in Principal Stresses

θ - Angle of Principal Stress with Respect to Mortar Joints

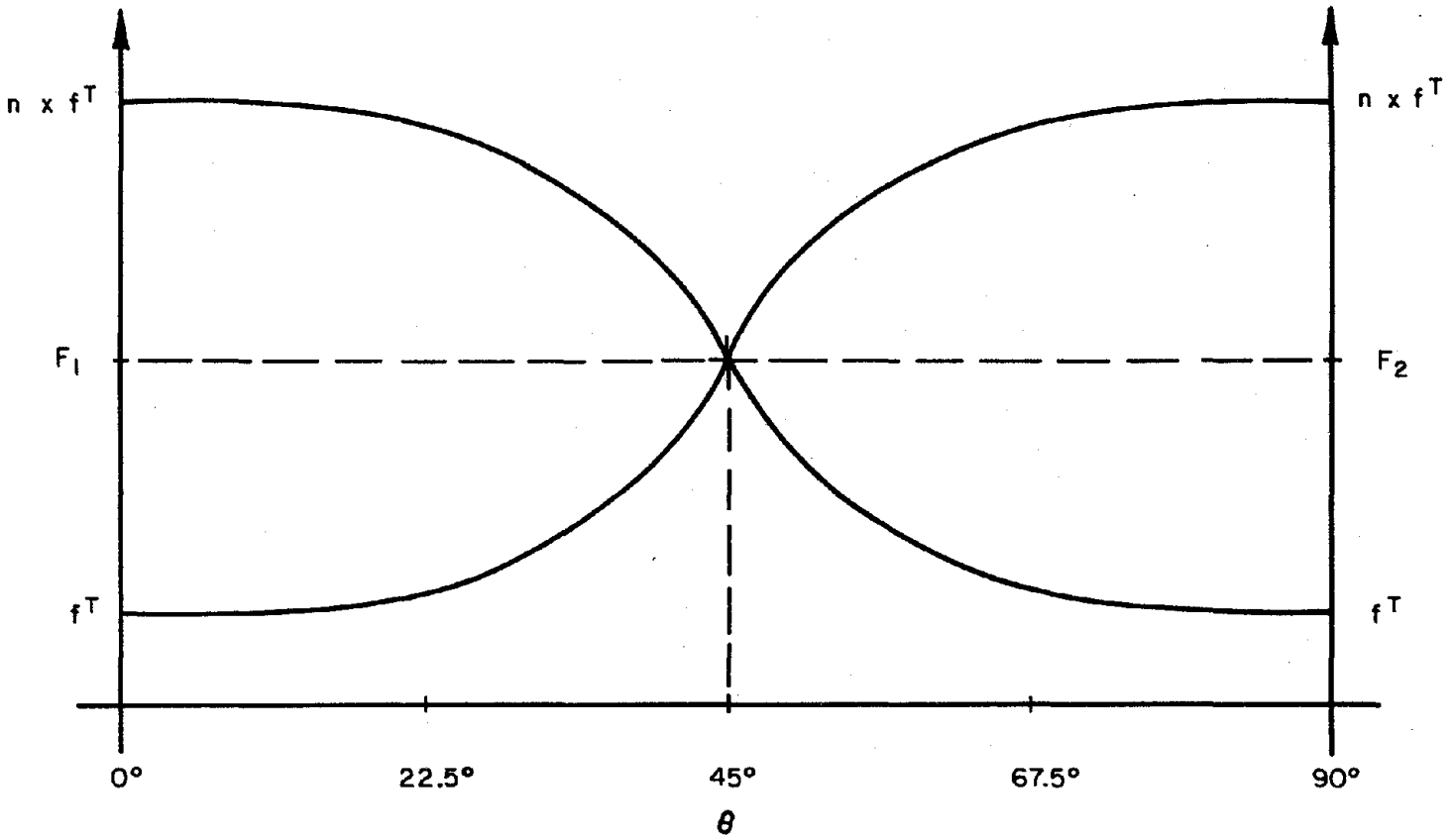

Figure 3.4 Uniaxial Tensile Strength of Masonry vs Angle of Principal Stress with Respect to the Mortar Joints

θ – Angle of Principal Stress with Respect to Mortar Joints

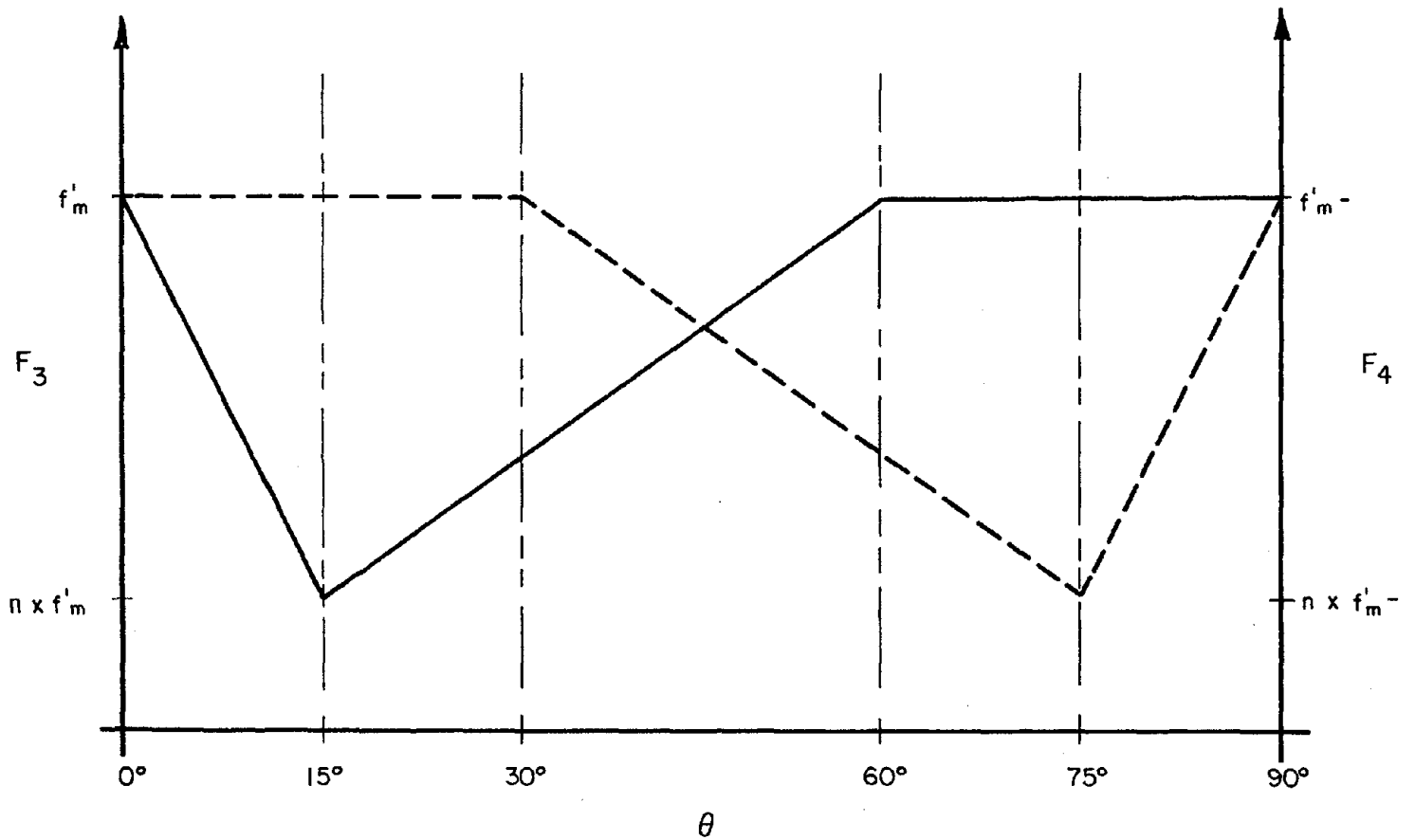

Figure 3.5 Uniaxial Compressive Strength of Masonry vs Angle of Principal Stress with Respect to the Mortar Joints

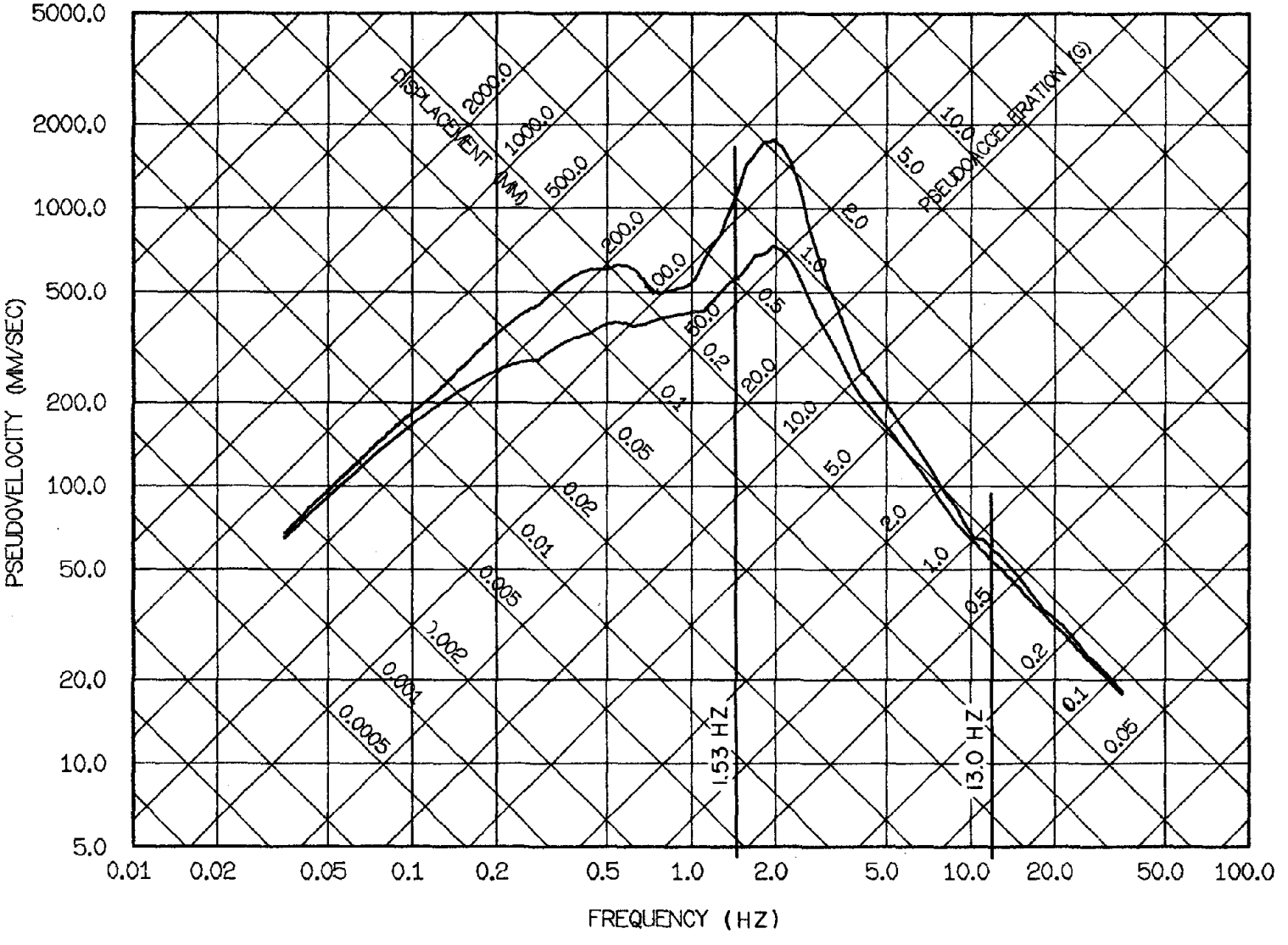

Figure 5.5 Elastic Spectrum for Sinusoidal Base Motion, 1 sec Duration, at 2% and 20% Damping

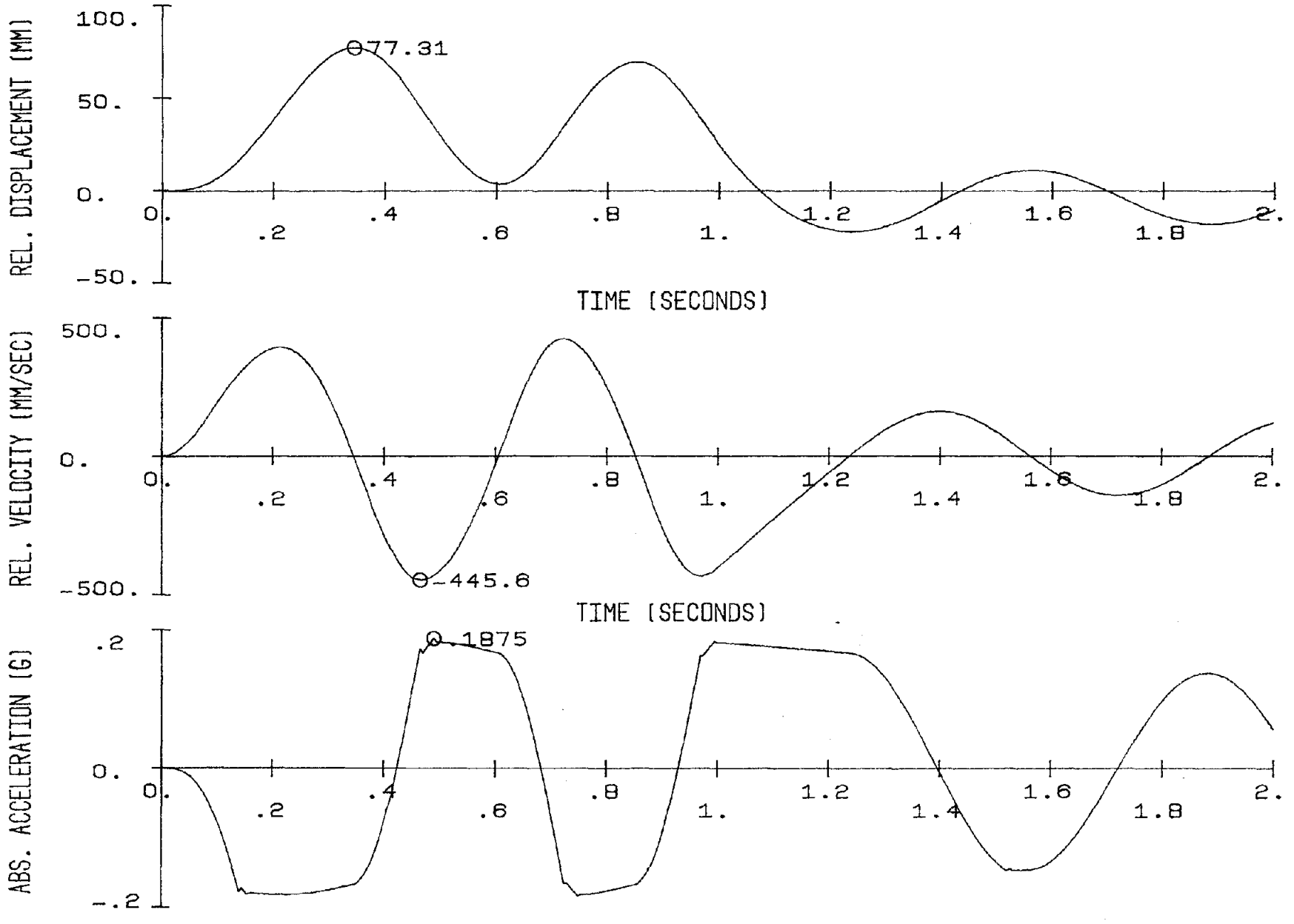

Figure 5.6 Relative Displacement, Velocity, and Absolute Acceleration of the Open Frame

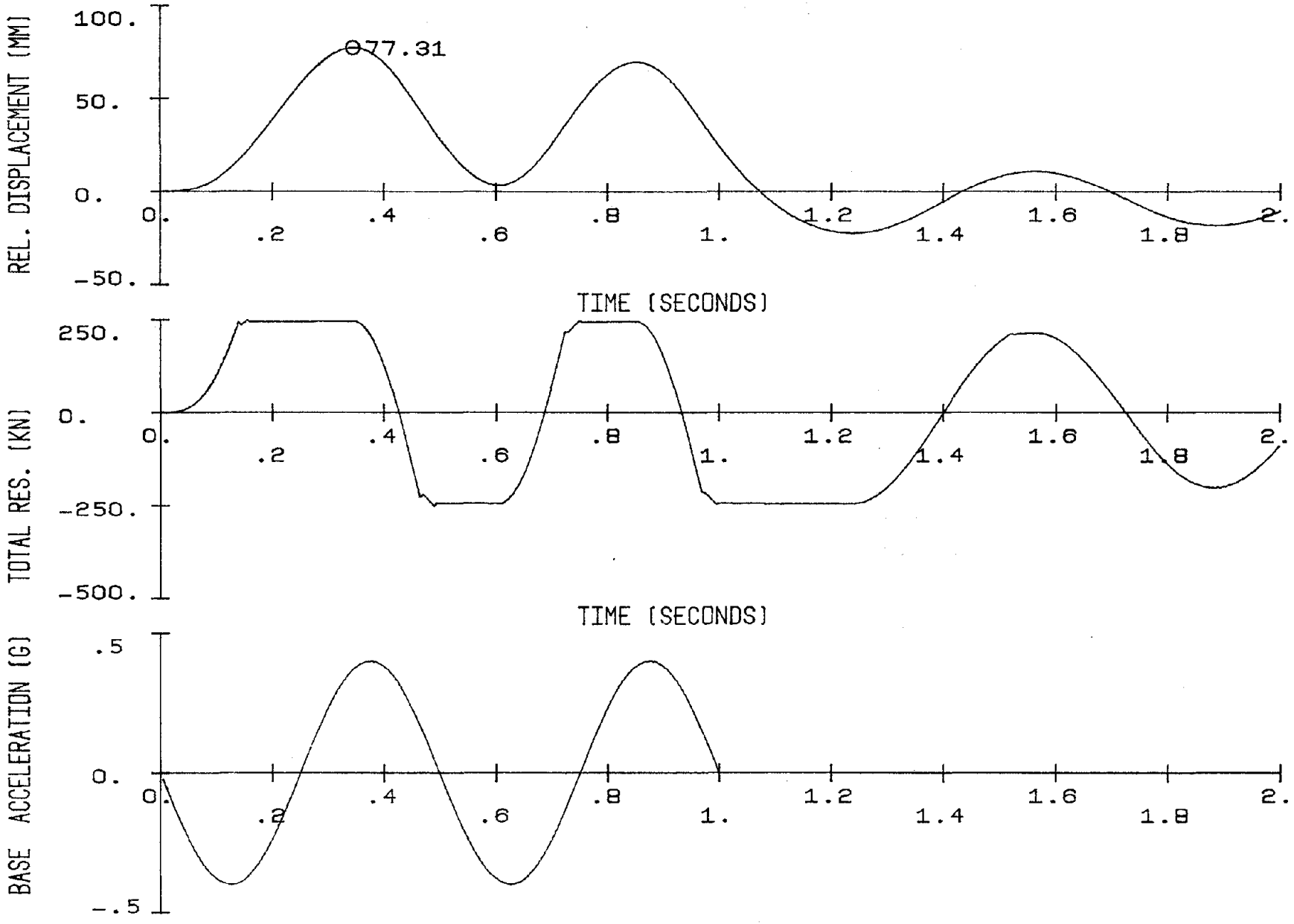

Figure 5.7 Relative Displacement, Total Resistance, and Base Acceleration of the Open Frame

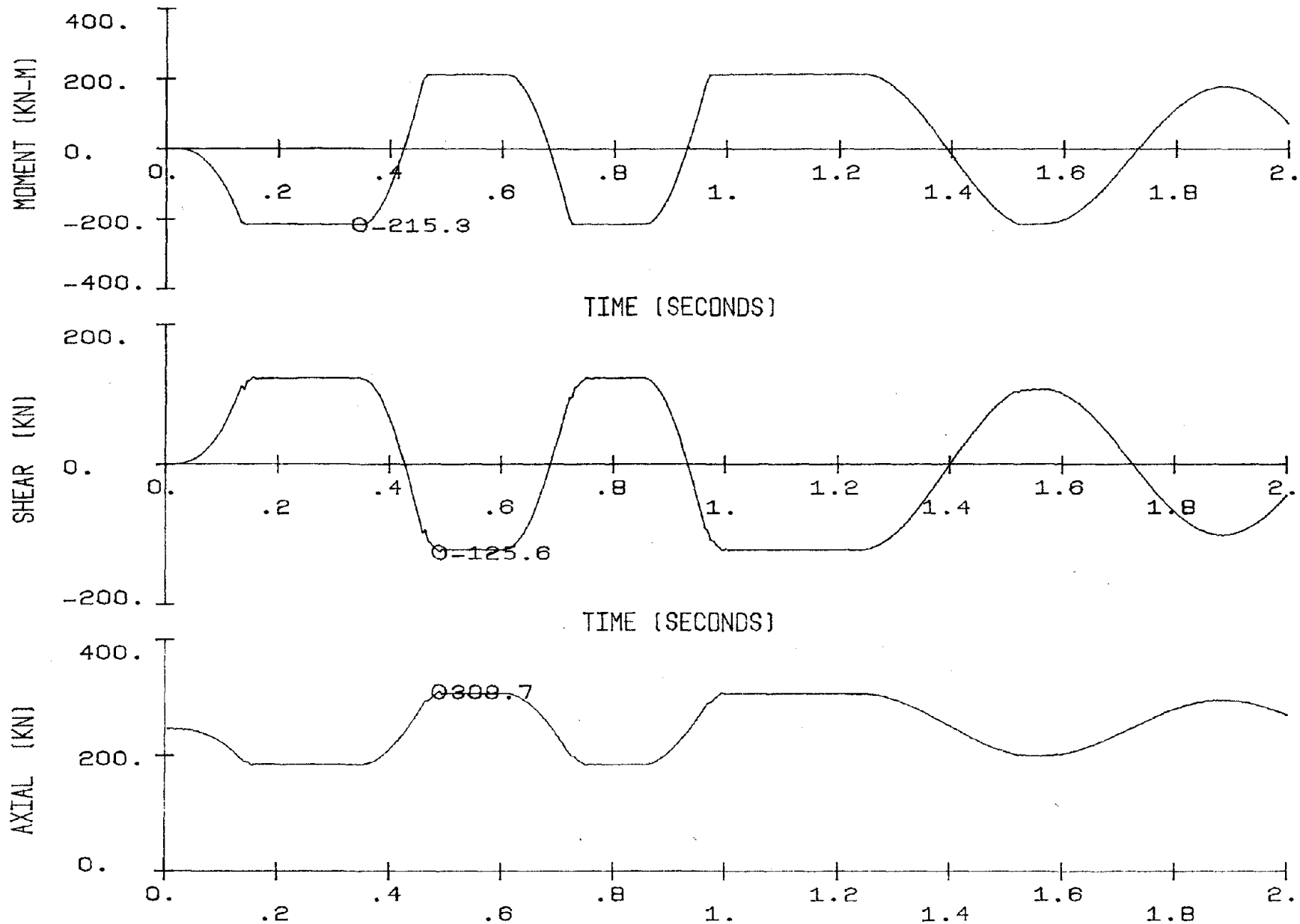

Figure 5.8 Base Moment, Base Shear, and Axial Load for the Left Column of the Open Frame

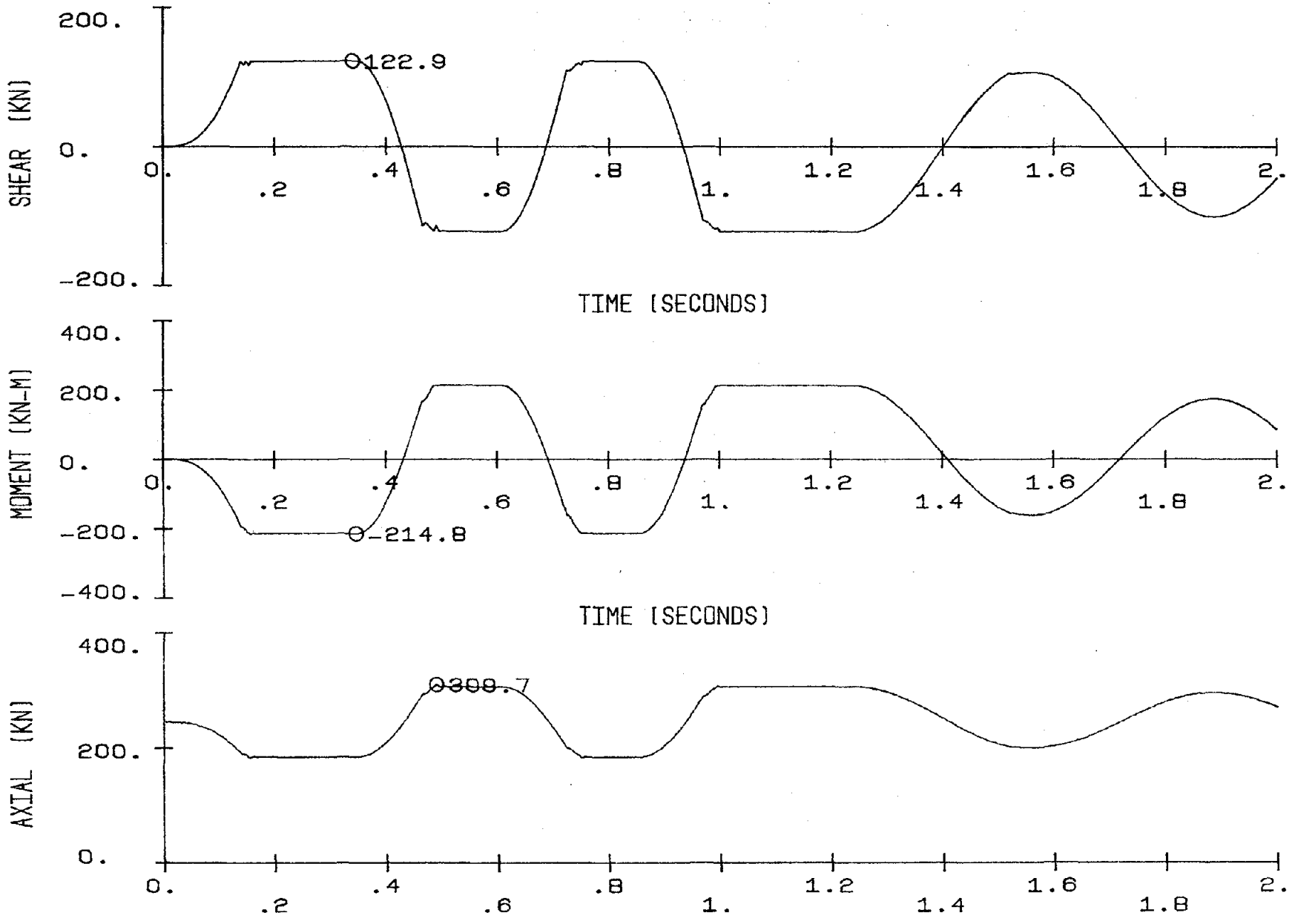

Figure 5.9 Center Shear, Top Moment, and Axial Load for the Left Column of the Open Frame

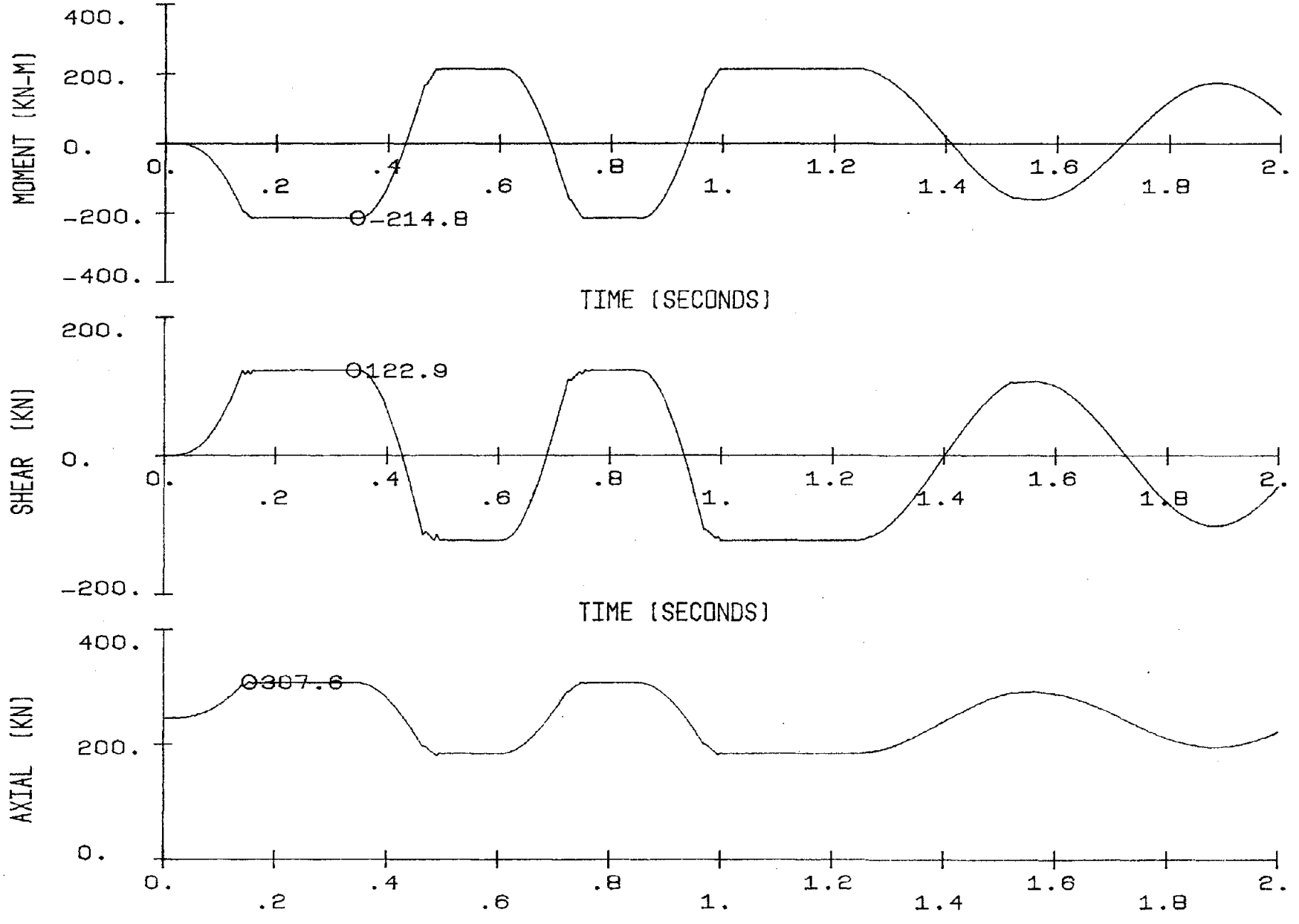

Figure 5.10 Top Moment, Top Shear, and Axial Load for the Right Column of the Open Frame

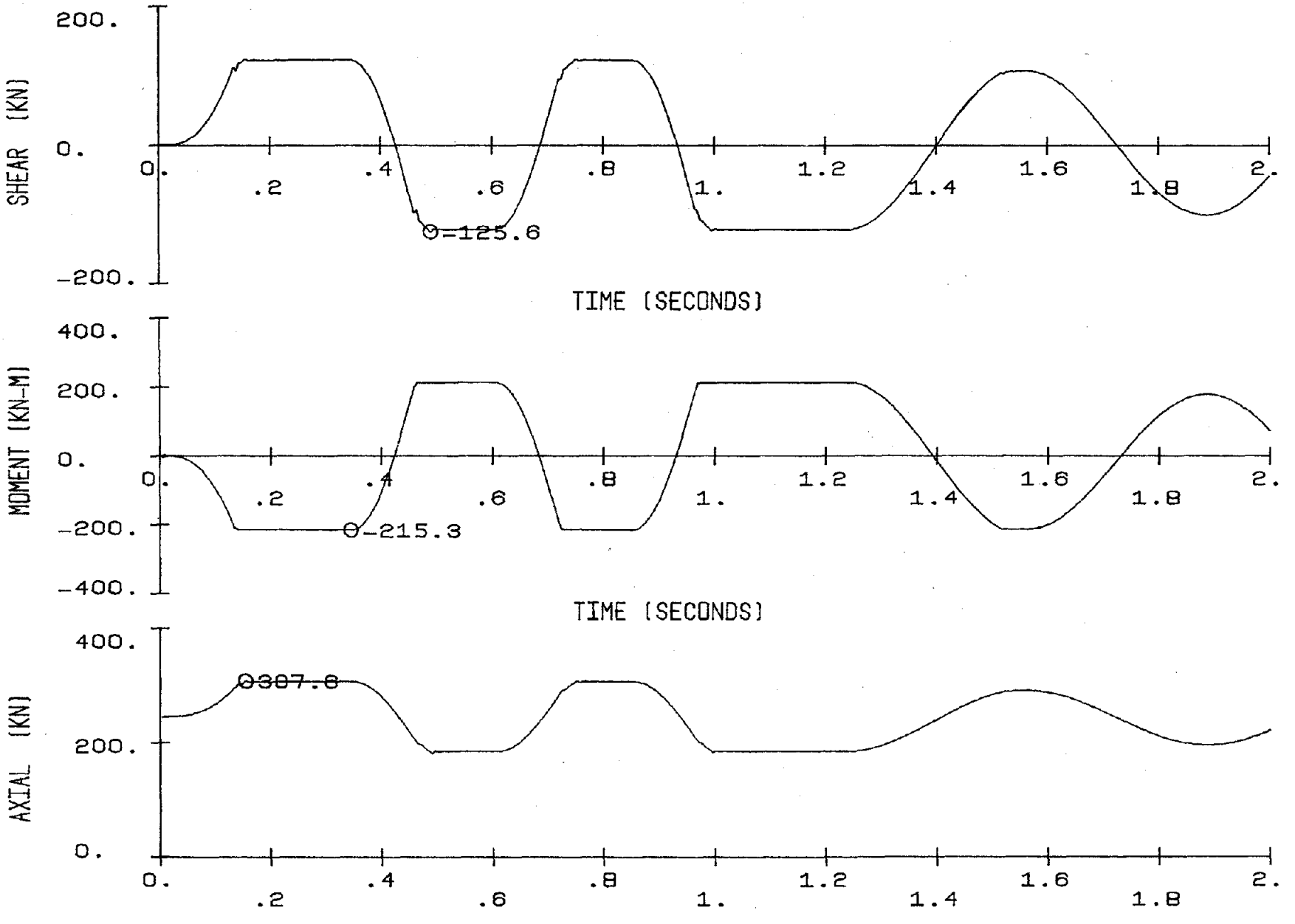

Figure 5.11 Center Shear, Base Moment, and Axial Load for the Right Column of the Open Frame

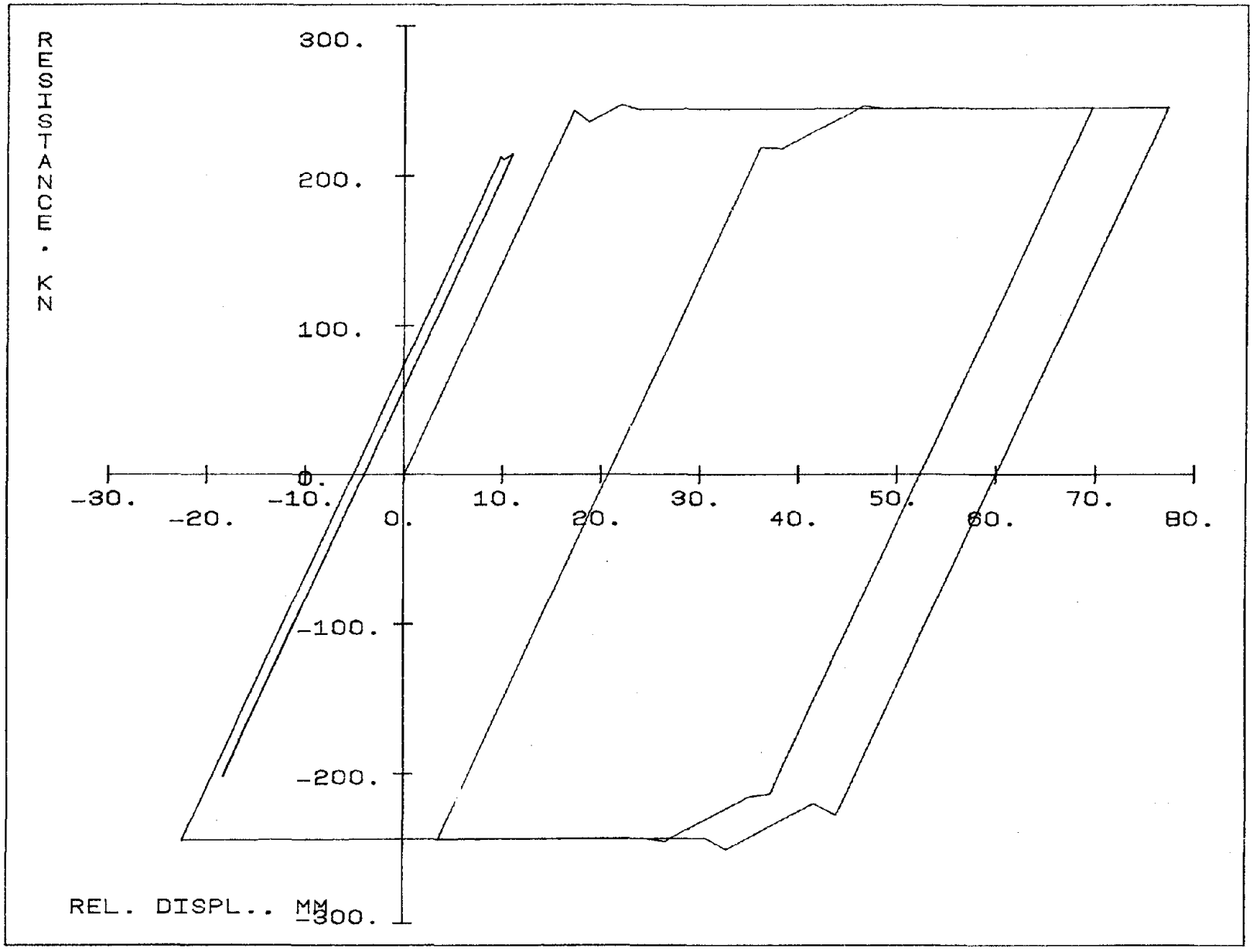

Figure 5.12 Load Displacement Response: Open Frame

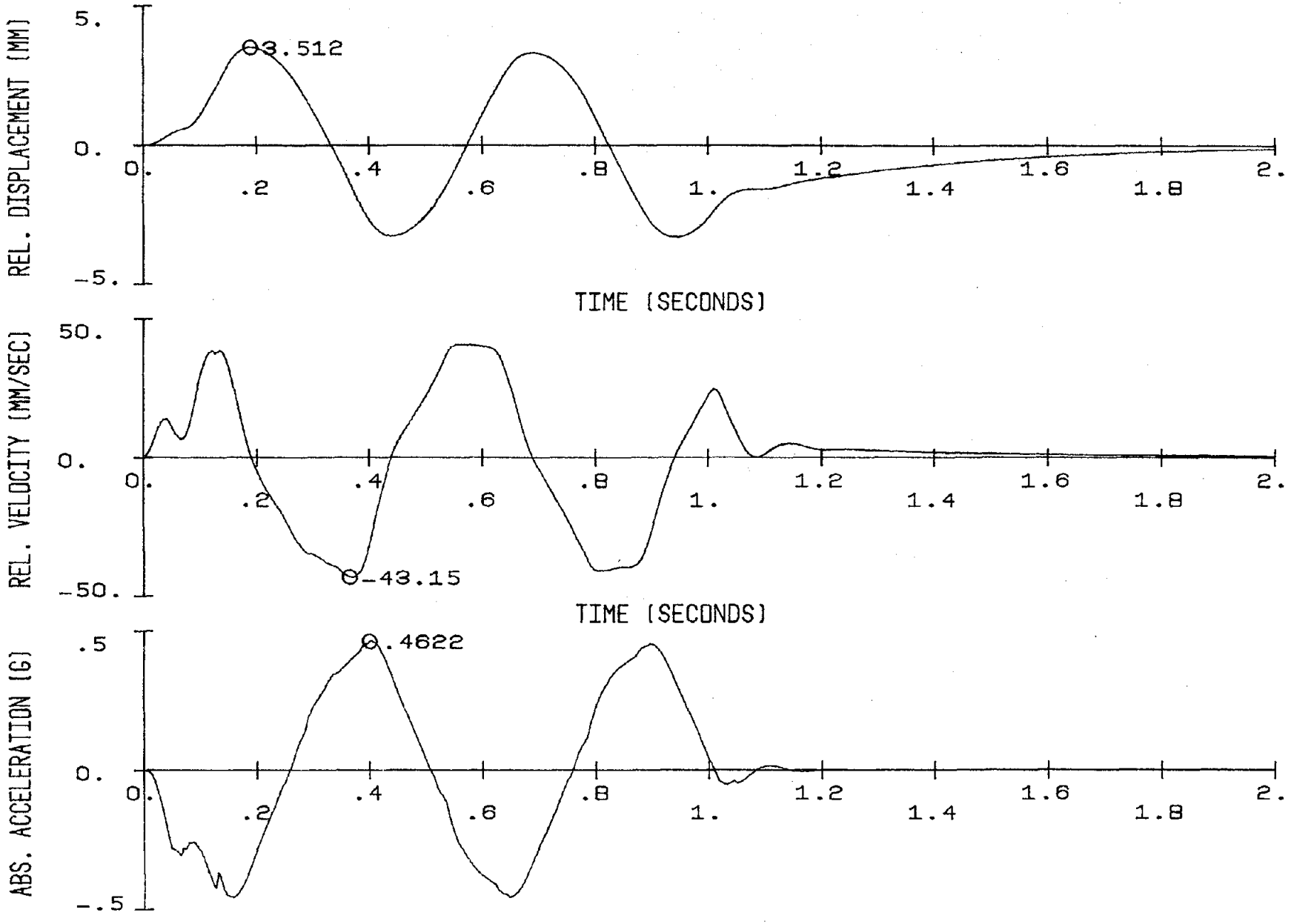

Figure 5.13 Relative Displacement, Velocity, and Absolute Acceleration of the Frame Wall

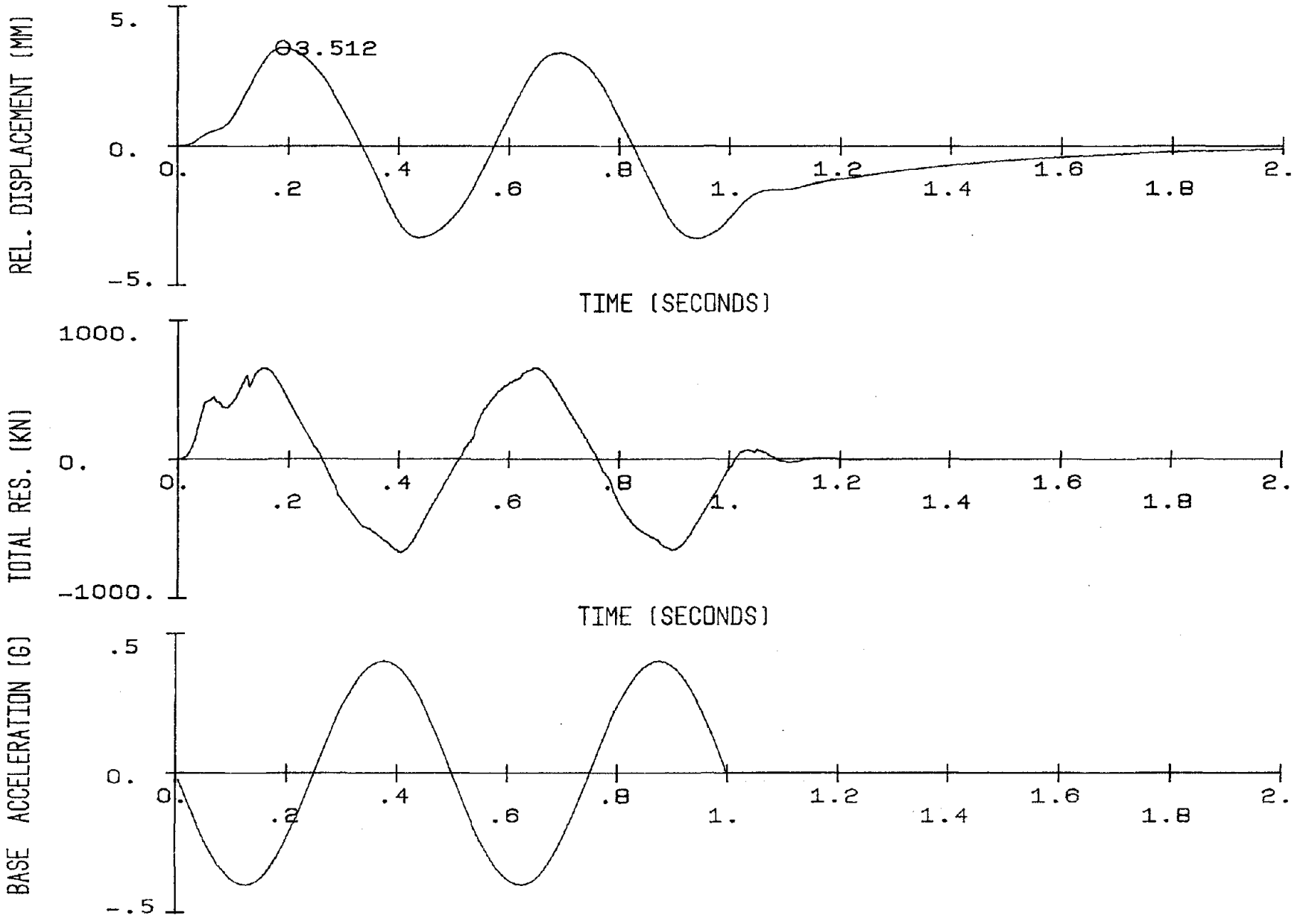

Figure 5.14 Relative Displacement, Total Resistance, and Base Acceleration of the Frame Wall

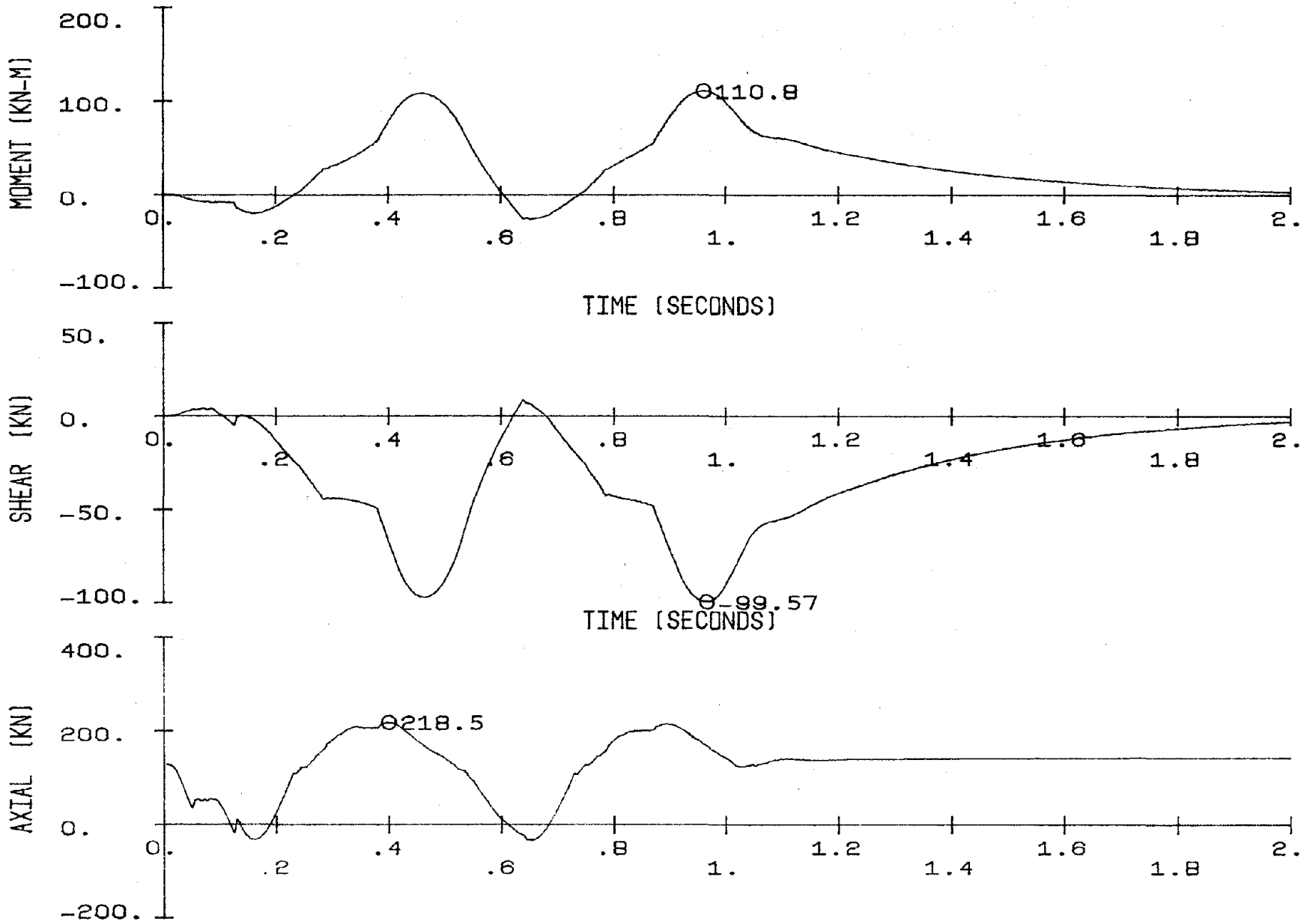

Figure 5.15 Base Moment, Base Shear, and Axial Load for the Left Column of the Frame Wall

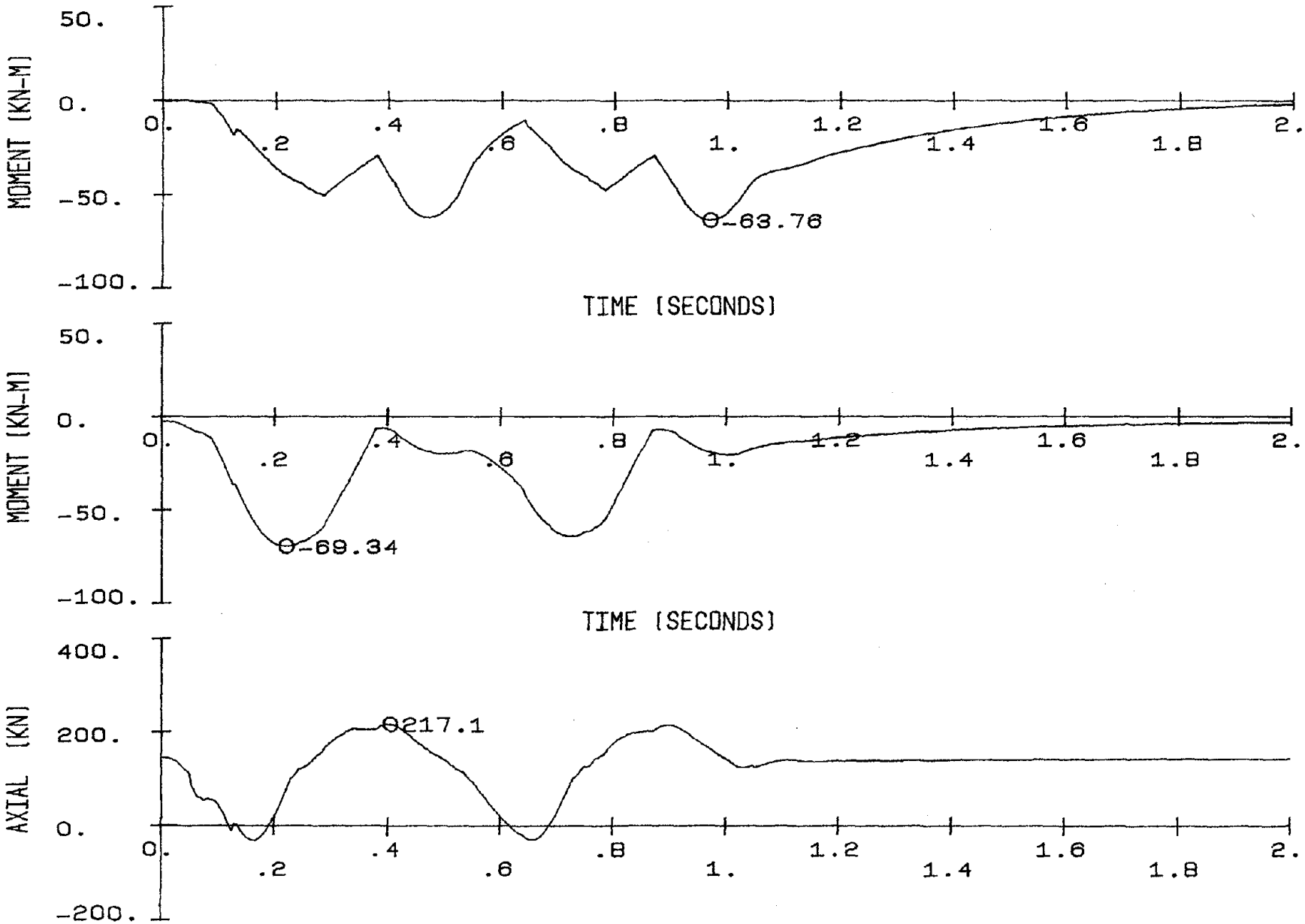

Figure 5.16 Center Moment, Top Moment, and Axial Load for the Left Column of the Frame Wall

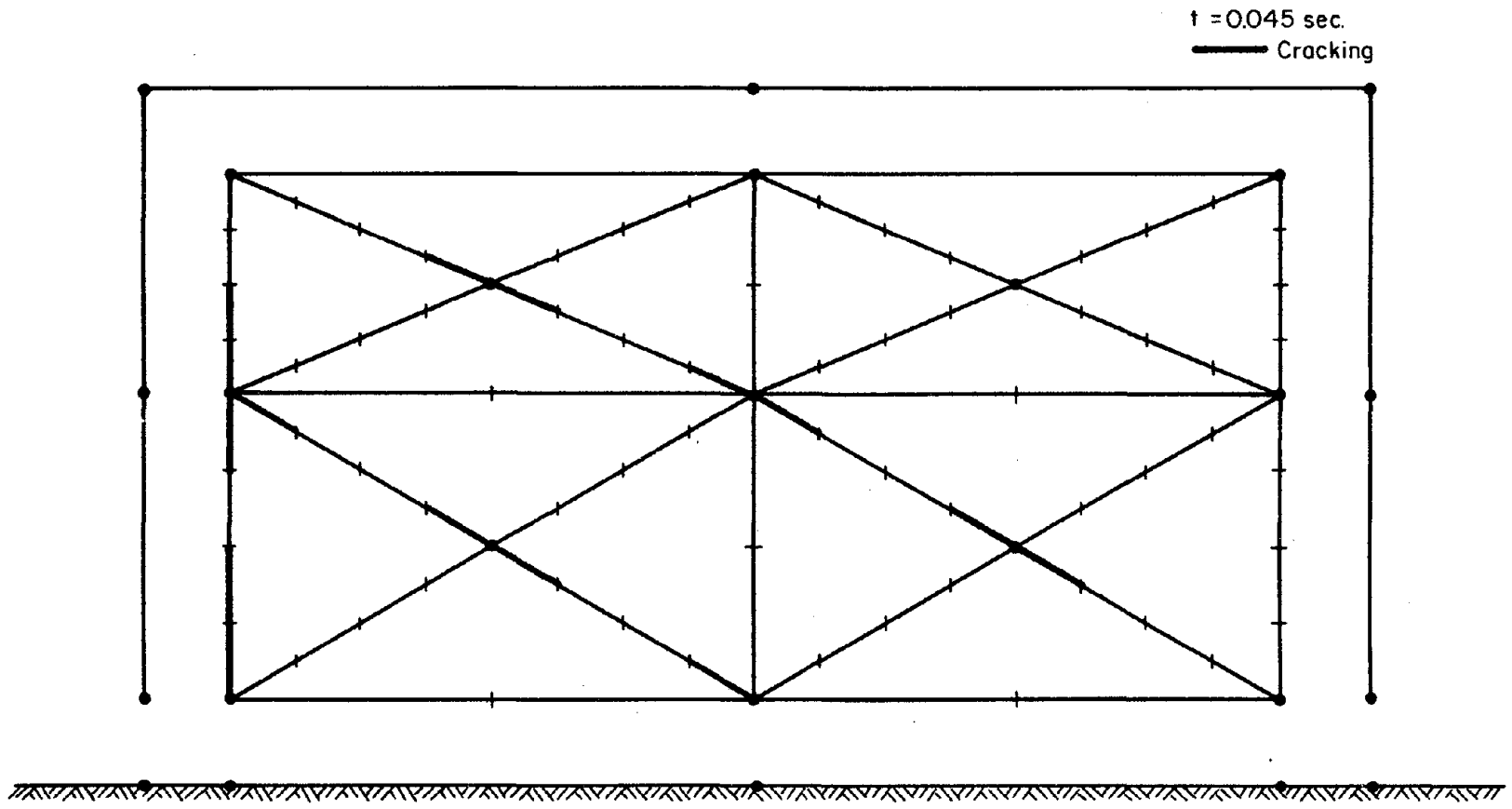

Figure 5.21 Crack Pattern: Frame Wall at t=0.045 sec

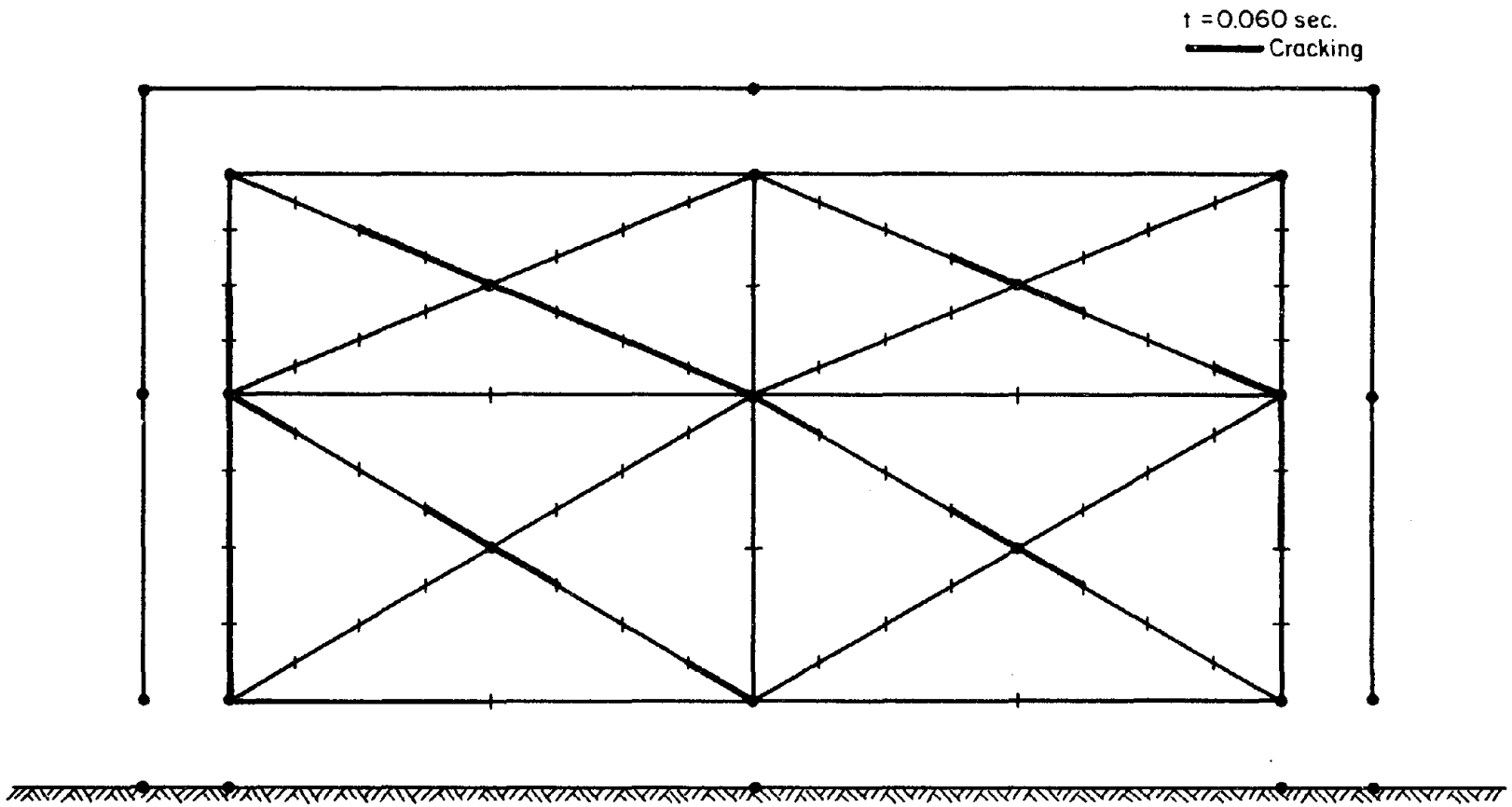

Figure 5.22 Crack Pattern: Frame Wall at t=0.060 sec

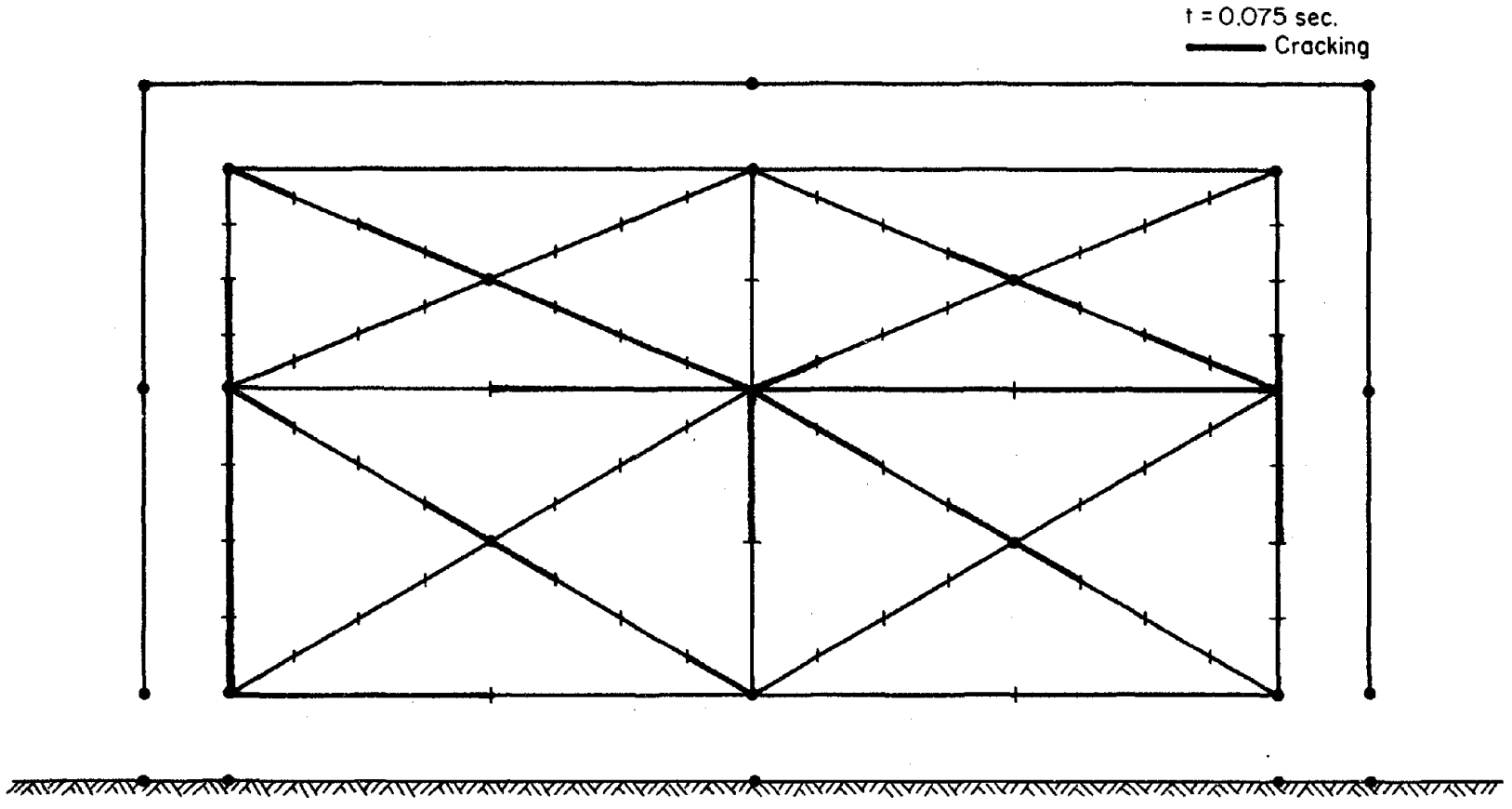

Figure 5.23 Crack Pattern: Frame Wall at t=0.075 sec

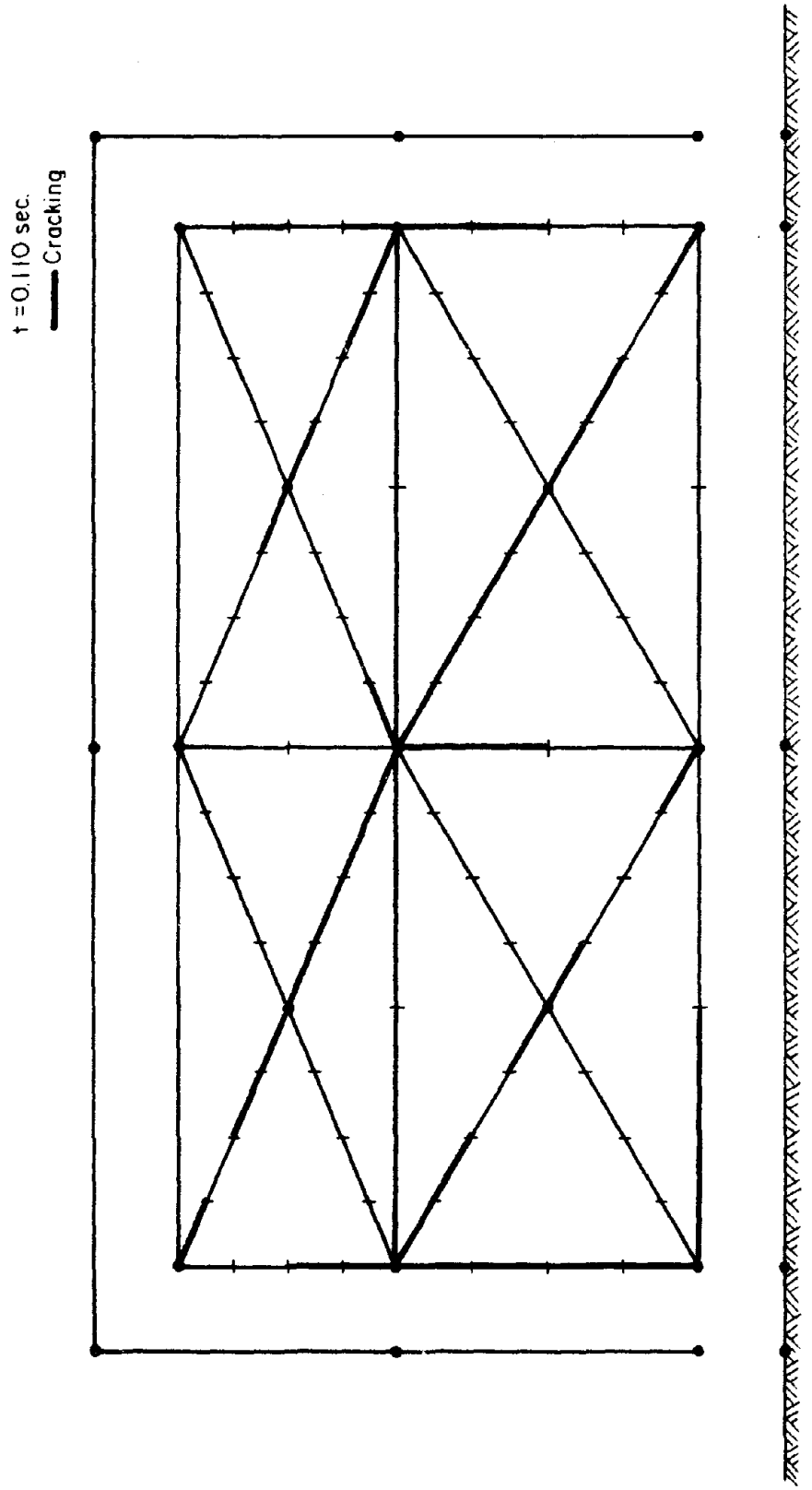

Figure 5.24 Crack Pattern: Frame Wall at t=0.110 sec

1 - t=0.275 sec
2 - t=0.280 sec
3 - t=0.290 sec
4 - t=0.295 sec
5 - t=0.300 sec
6 - t=0.305 sec
7 - t=0.325 sec
8 - t=0.330 sec
9 - t=0.335 sec
10 - t=0.340 sec
11 - t=0.350 sec
12 - t=0.355 sec
13 - t=0.380 sec
14 - t=0.555 sec

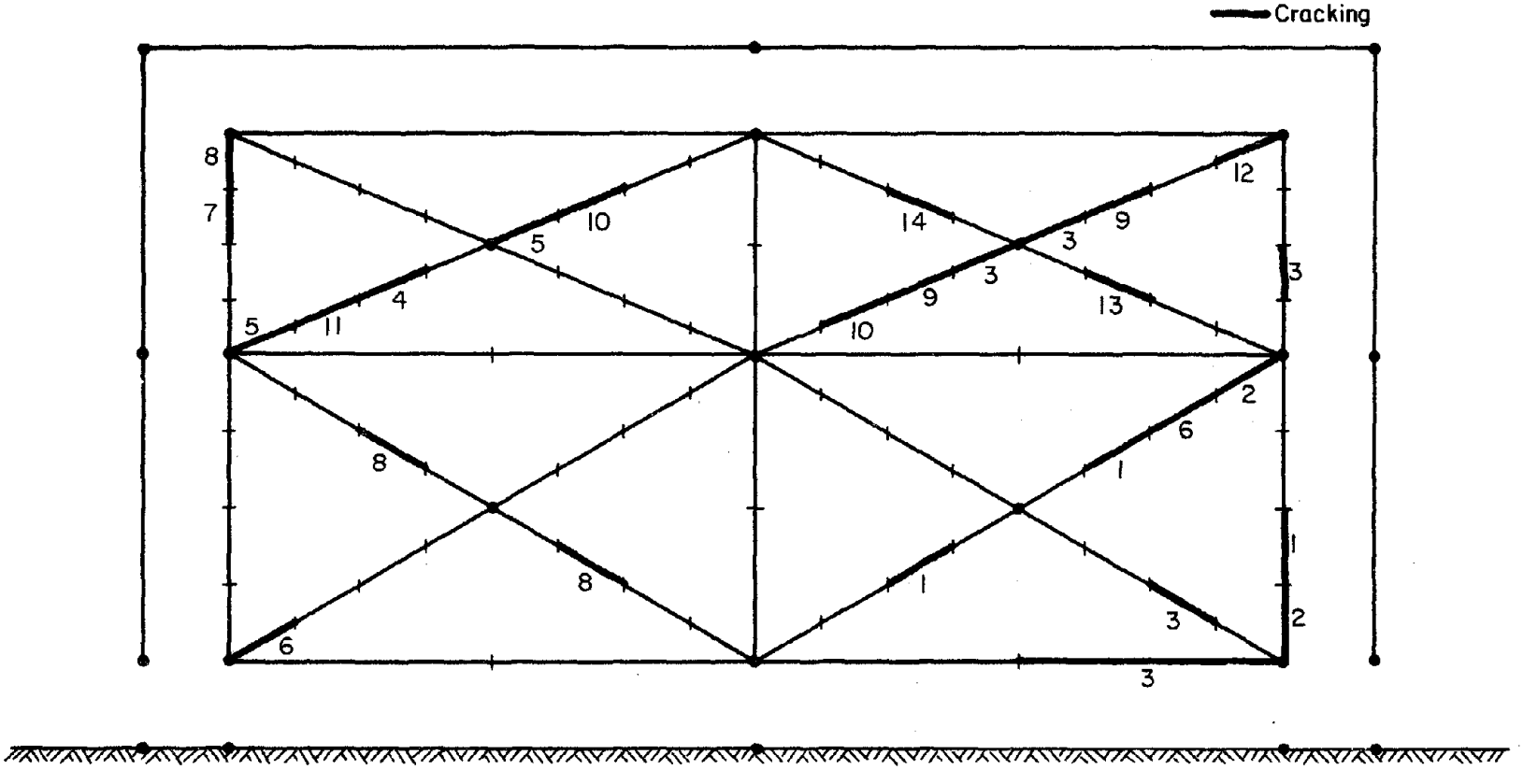

Figure 5.25 Cracking Sequence: Frame Wall from t=0.275 to 0.555 sec

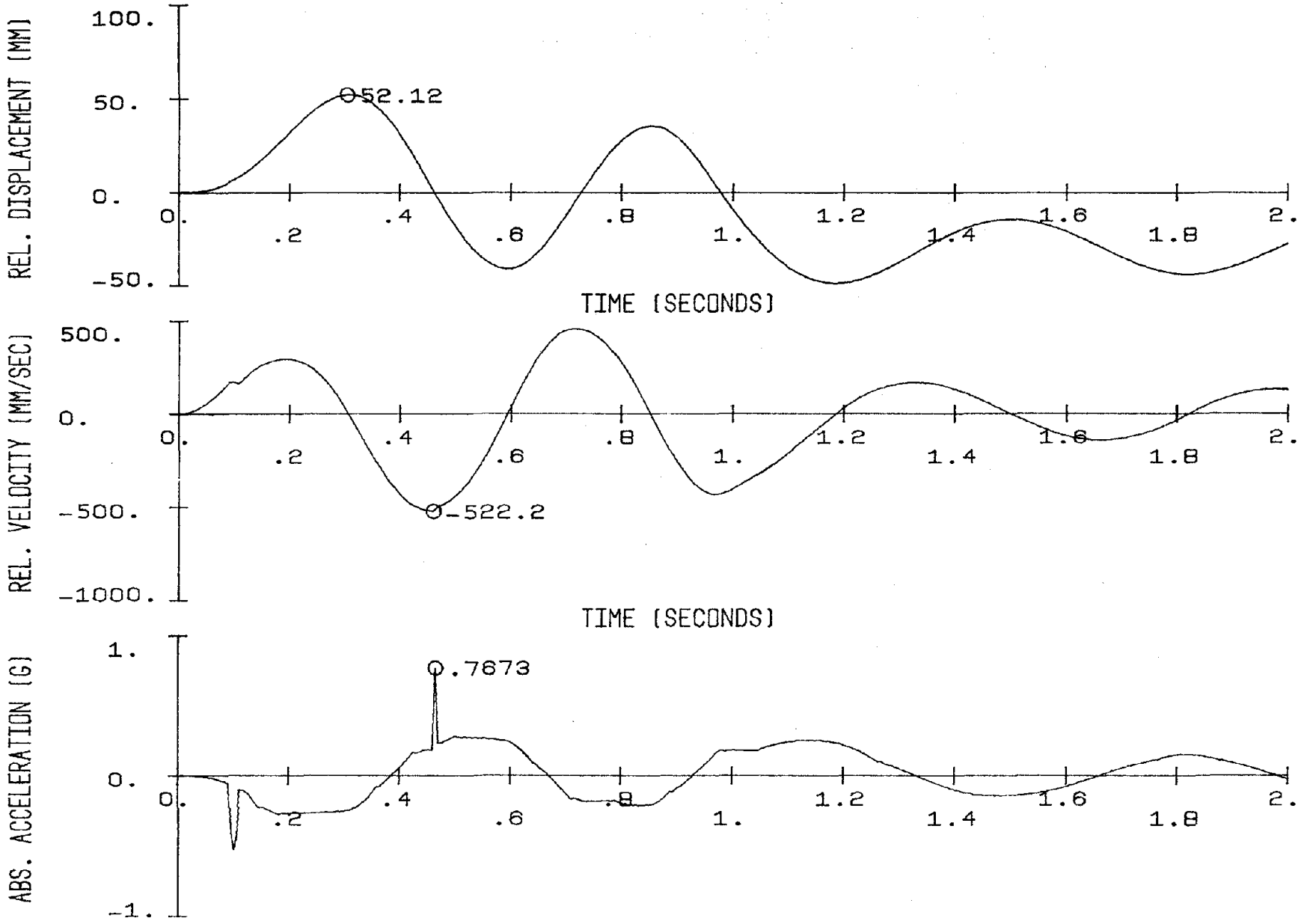

Figure 5.26 Relative Displacement, Velocity, and Absolute Acceleration of the Frame Wall-Gaps(I)

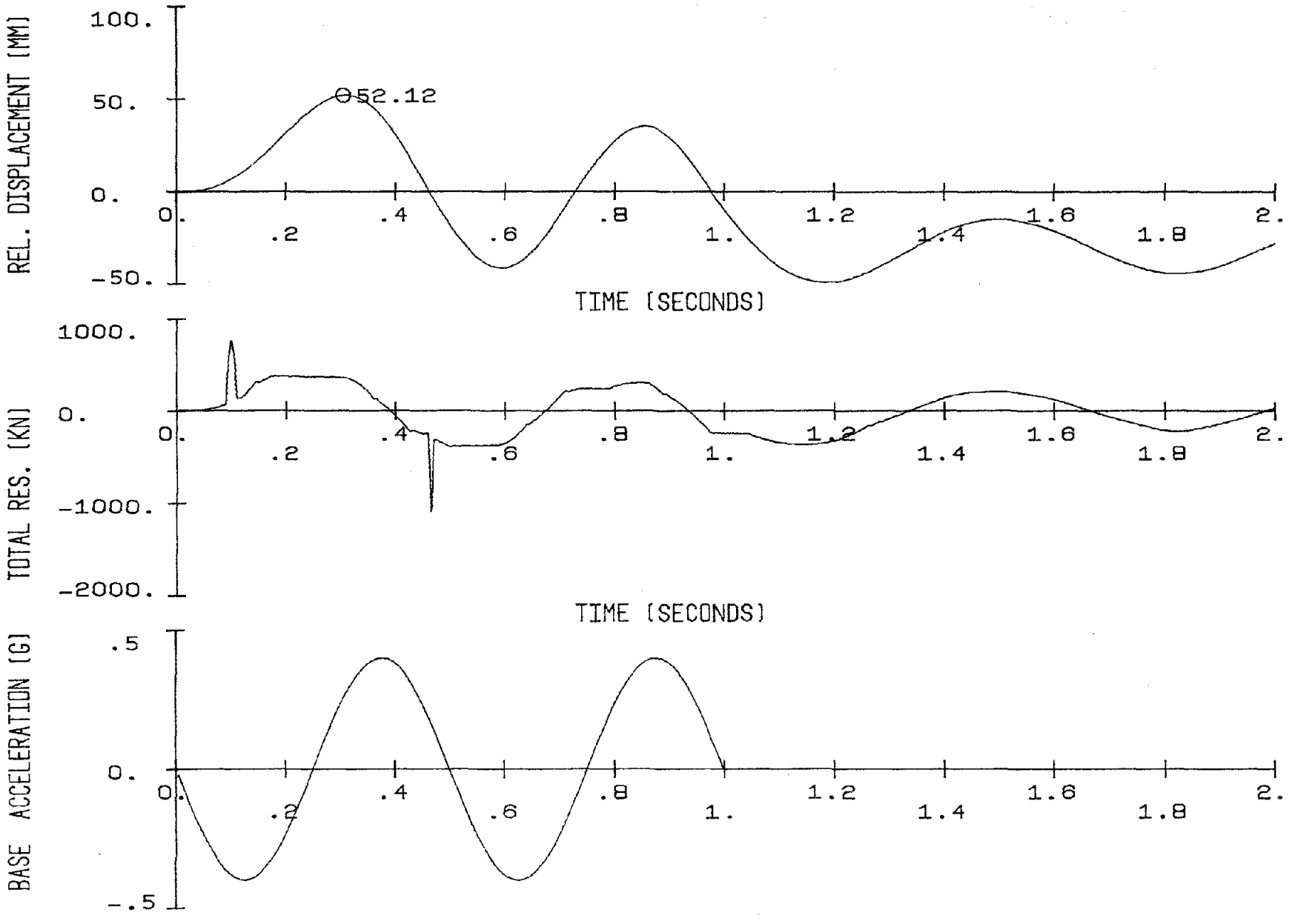

Figure 5.27 Relative Displacement, Total Resistance, and Base Acceleration of the Frame Wall-Gaps(I)

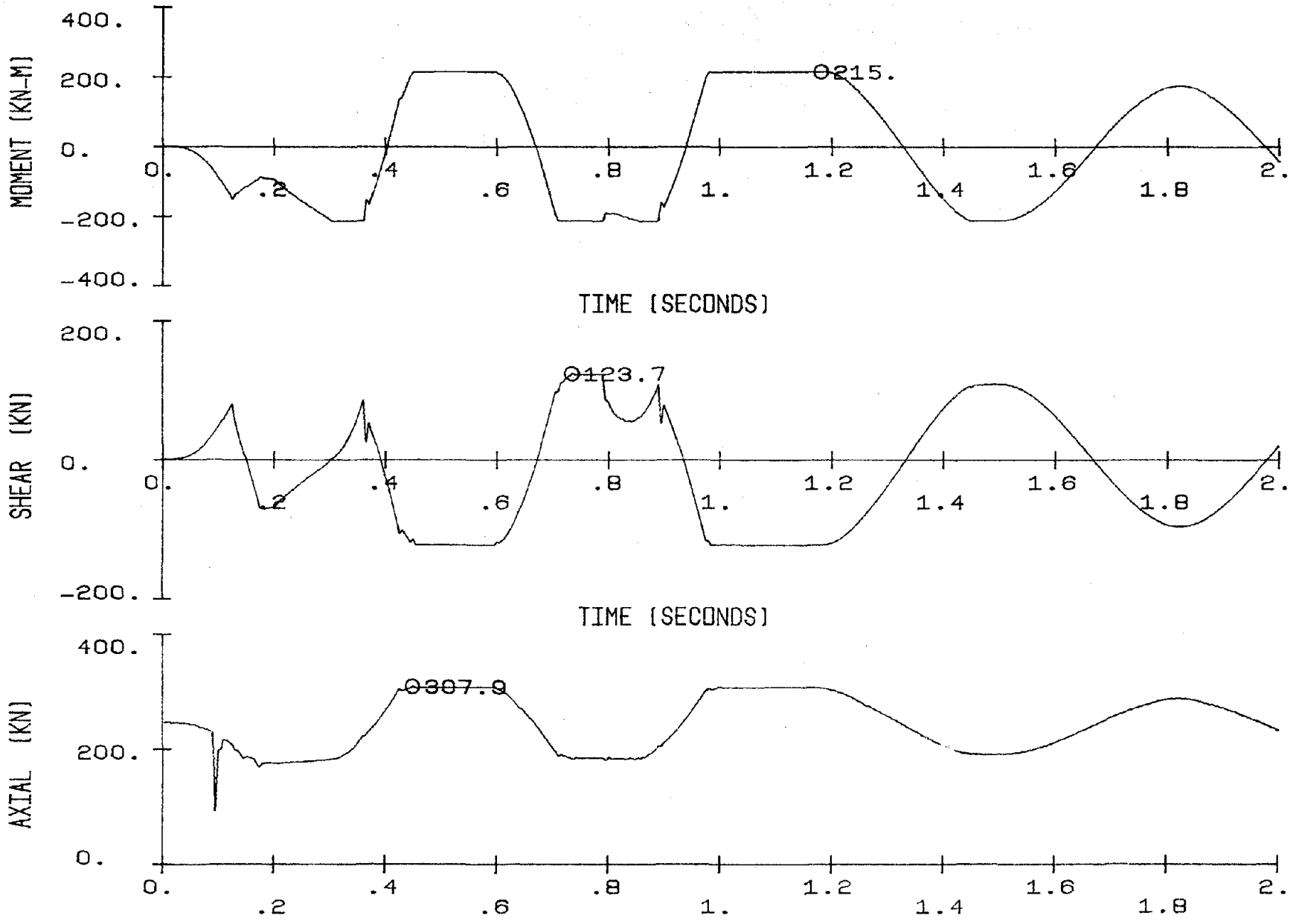

Figure 5.28 Base Moment, Base Shear, and Axial Load for the Left Column of the Frame Wall-Gaps(I)

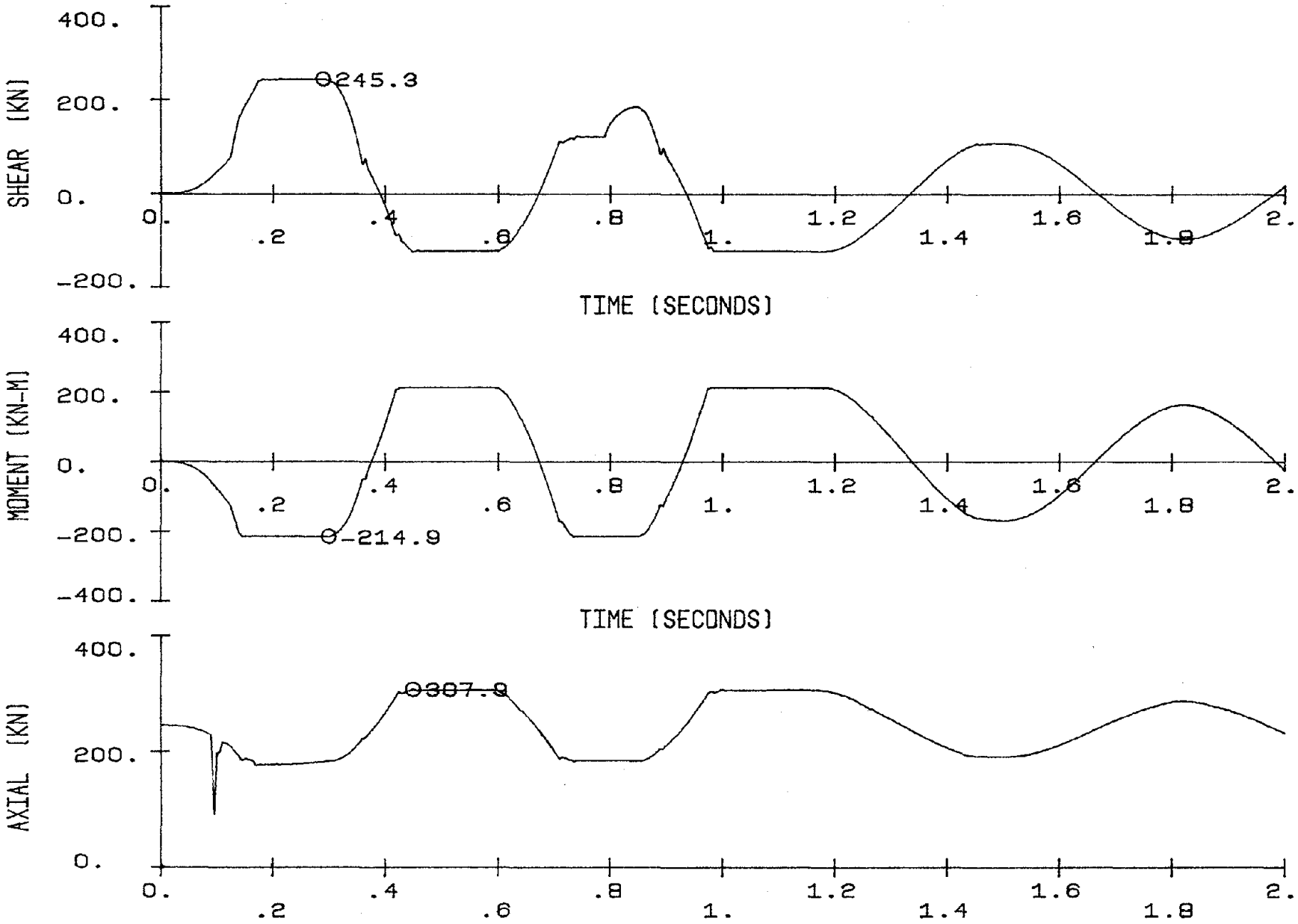

Figure 5.29 Center Shear, Top Moment, and Axial Load for the Left Column of the Frame Wall-Gaps(I)

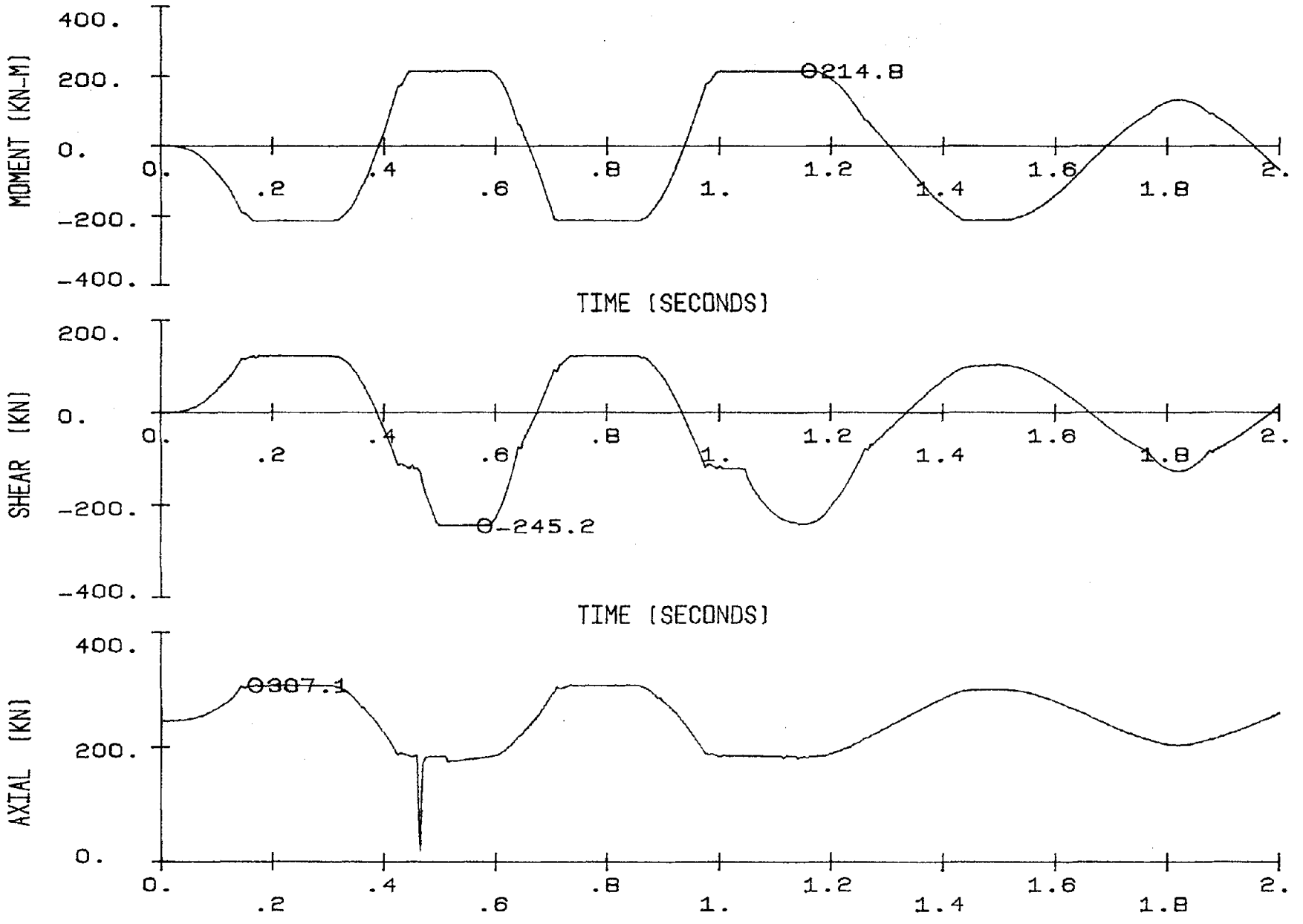

Figure 5.30 Top Moment, Top Shear, and Axial Load for the Right Column of the Frame Wall-Gaps(I)

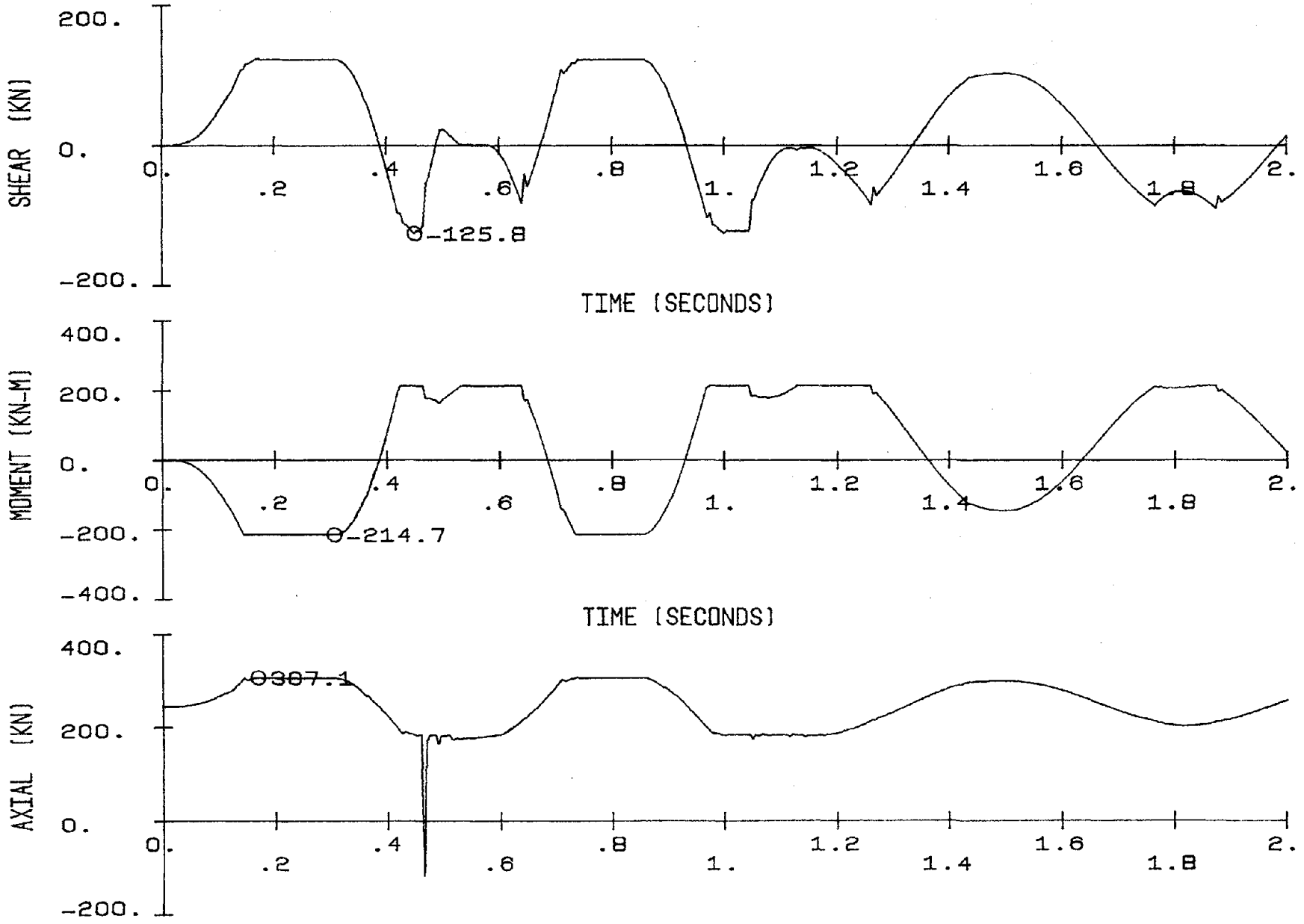

Figure 5.31 Center Shear, Base Moment, and Axial Load for the Right Column of the Frame Wall-Gaps(I)

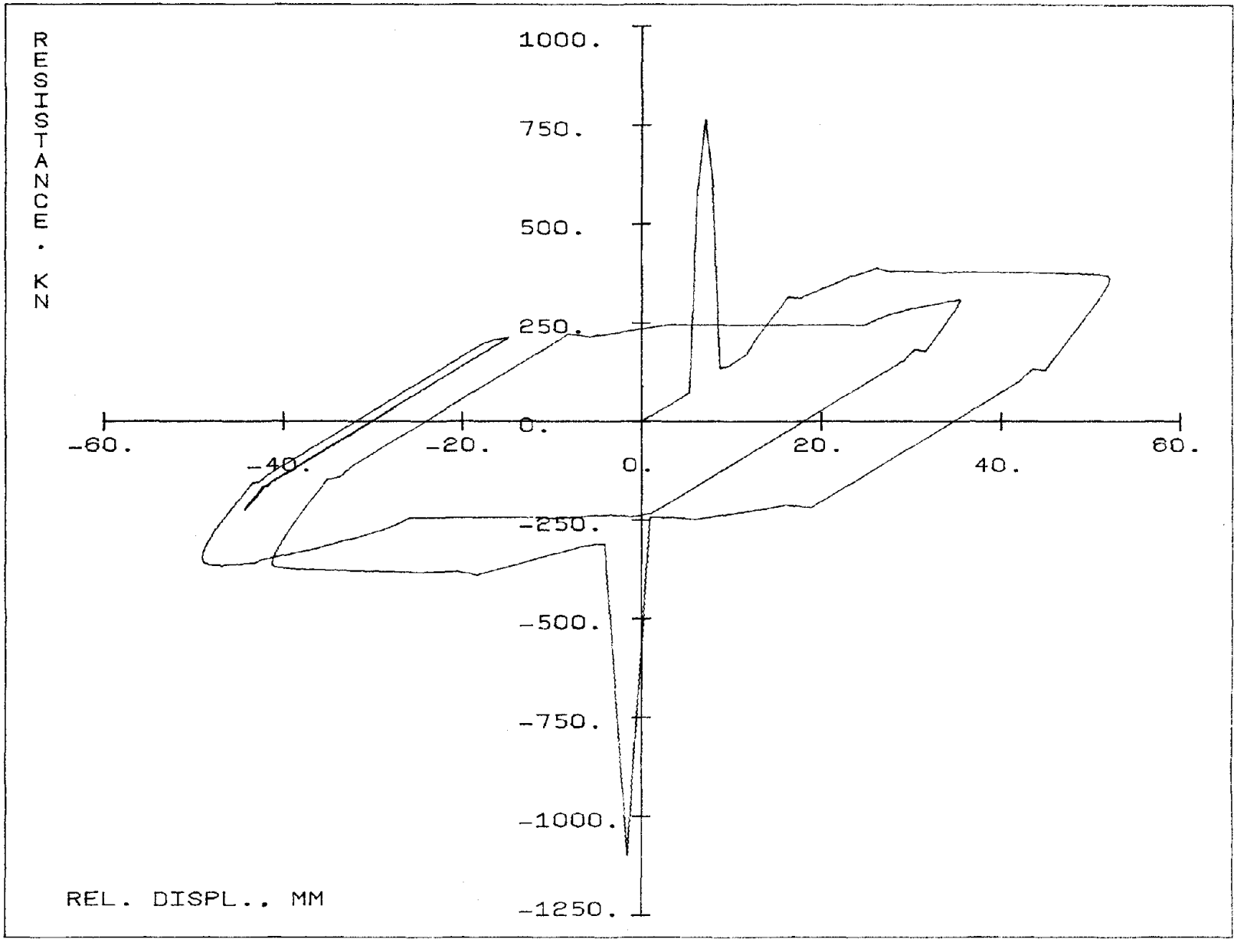

Figure 5.32 Load Displacement Response: Frame Wall-Gaps(I)

1 - t=0.090 sec
2 - t=0.095 sec
3 - t=0.100 sec
4 - t=0.105 sec
5 - t=0.110 sec
6 - t=0.125 sec
7 - t=0.145 sec
8 - t=0.170 sec
9 - t=0.180 sec
10 - t=0.190 sec
11 - t=0.200 sec
12 - t=0.205 sec
13 - t=0.305 sec
14 - t=0.315 sec

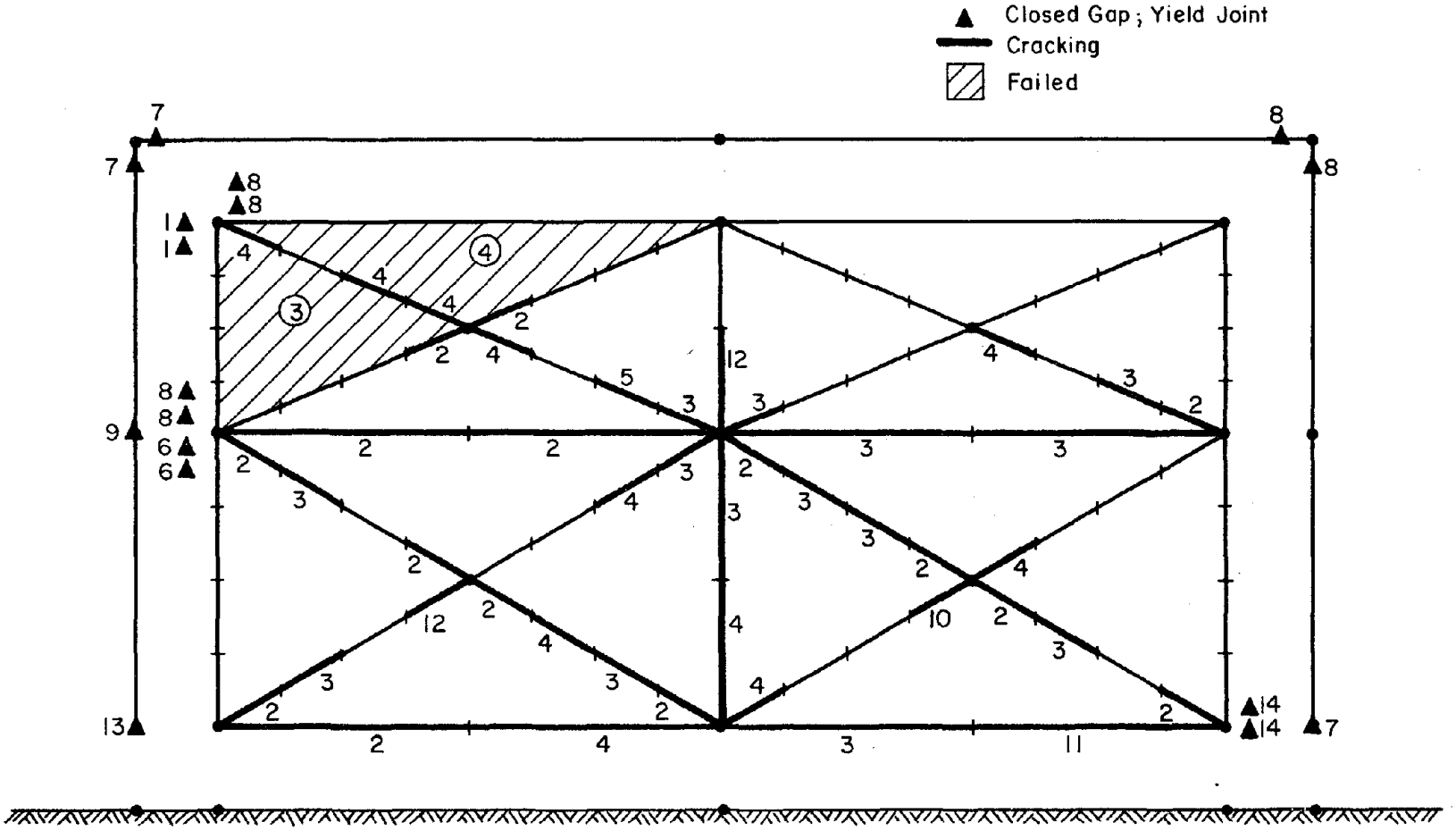

Figure 5.33 Cracking Sequence: Frame Wall-Gaps(I) from t=0.0 to 0.315 sec

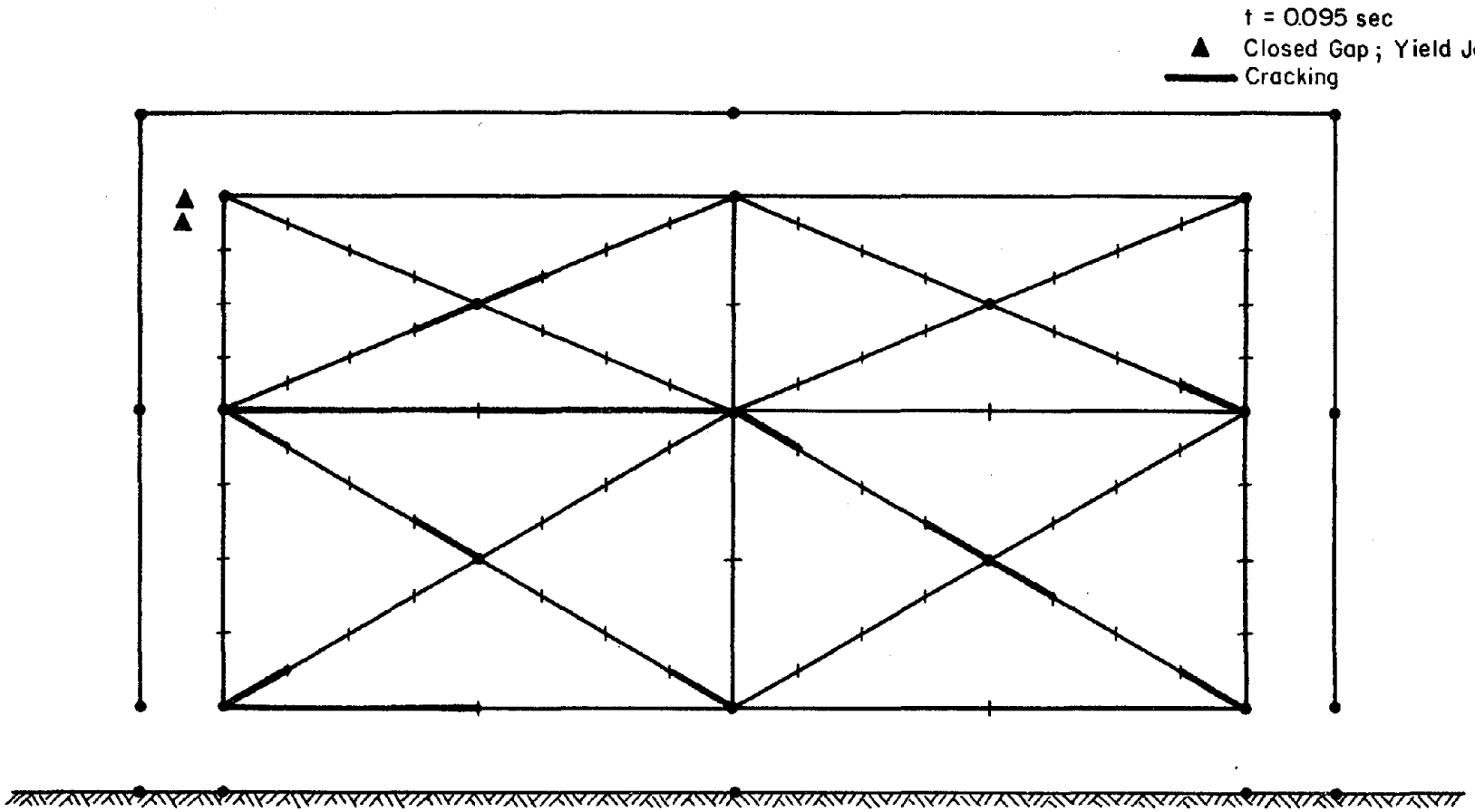

Figure 5.34 Crack Pattern: Frame Wall-Gaps(I) at t=0.095 sec

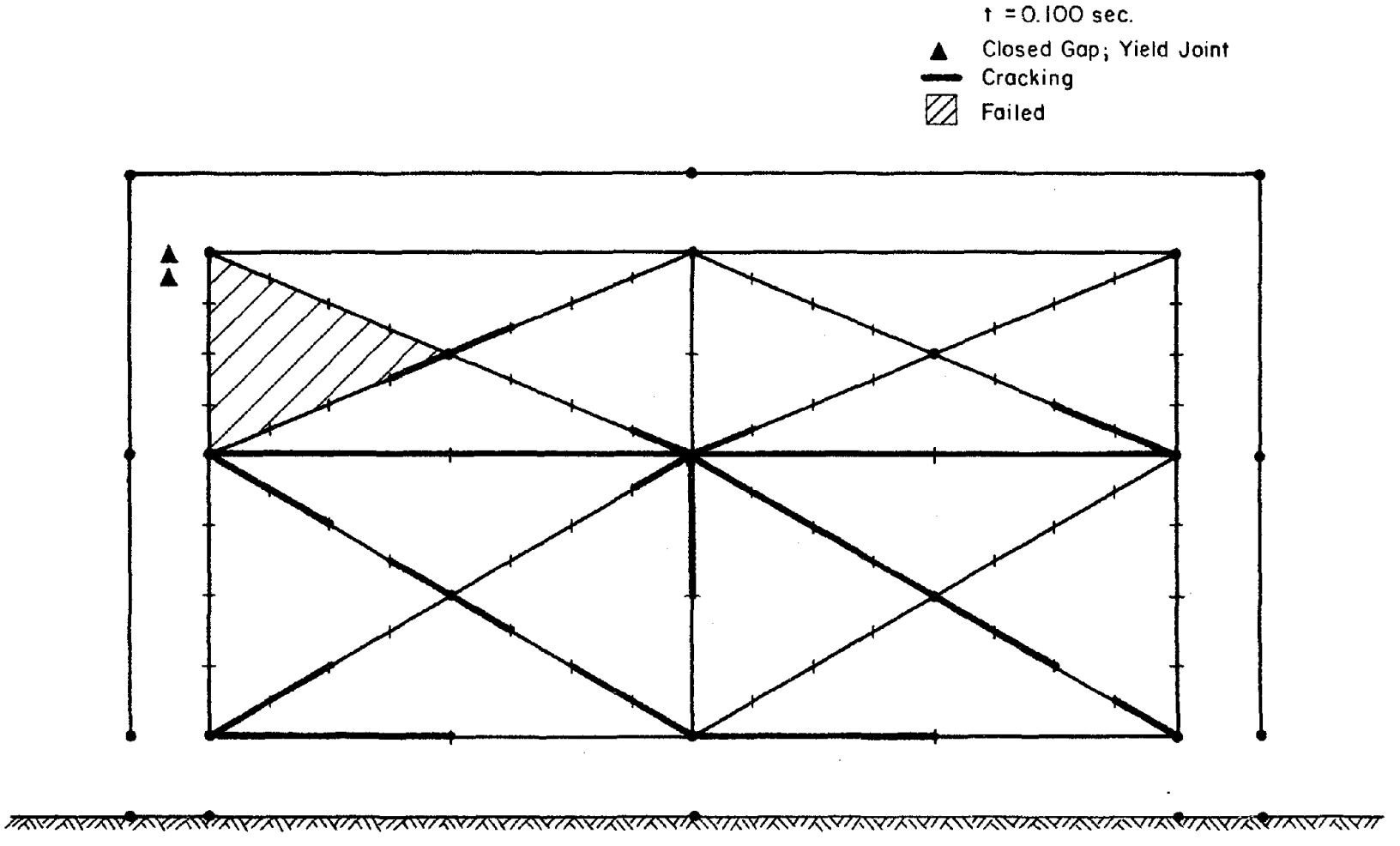

Figure 5.35 Crack Pattern: Frame Wall-Gaps(I) at t=0.100 sec

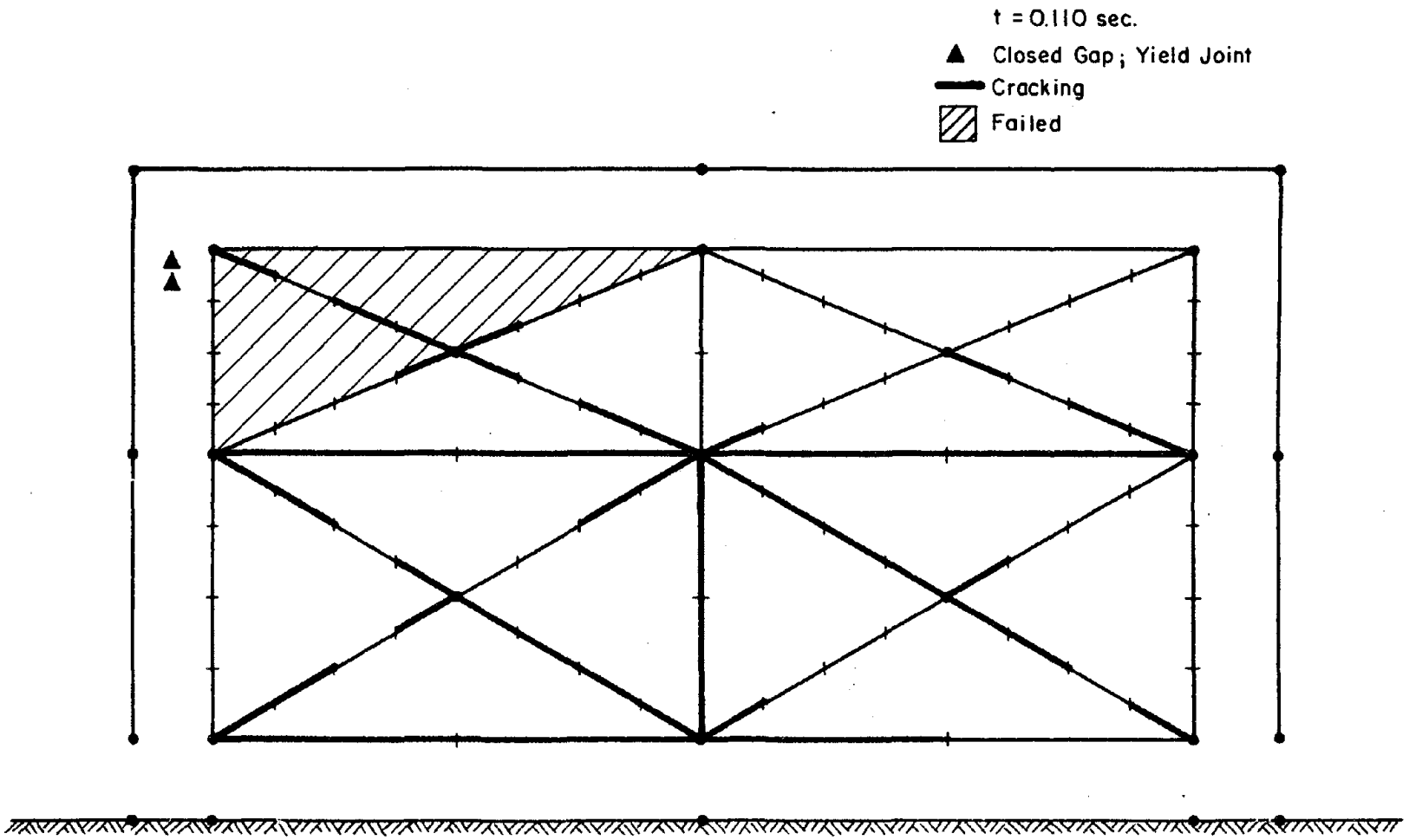

Figure 5.36 Crack Pattern: Frame Wall-Gaps(I) at t=0.110 sec

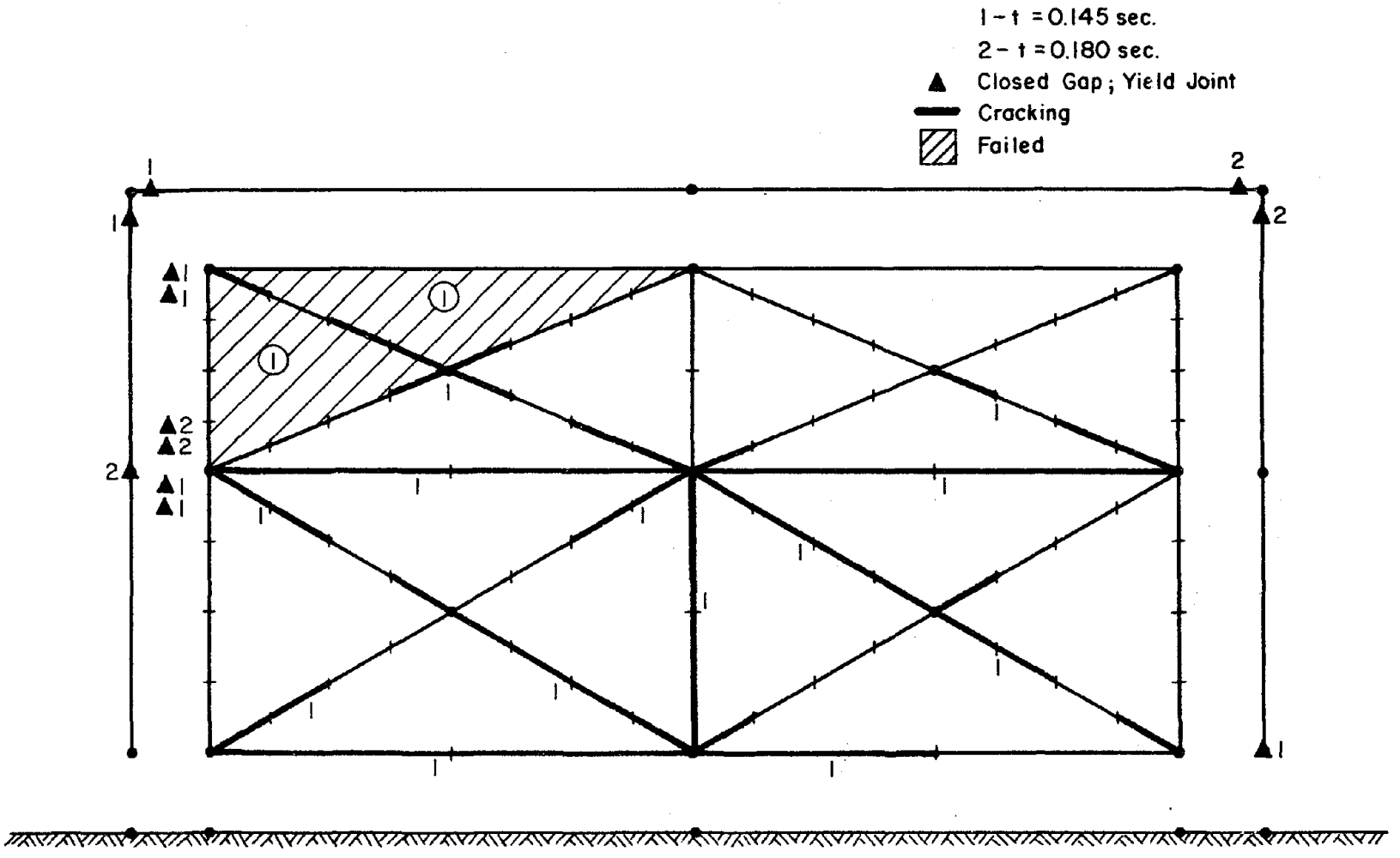

Figure 5.37 Cracking Sequence: Frame Wall-Gaps(I) from t=0.145 to 0.180 sec

1 - t=0.425 sec
2 - t=0.450 sec
3 - t=0.460 sec
4 - t=0.465 sec
5 - t=0.480 sec
6 - t=0.500 sec
7 - t=0.510 sec
8 - t=0.535 sec

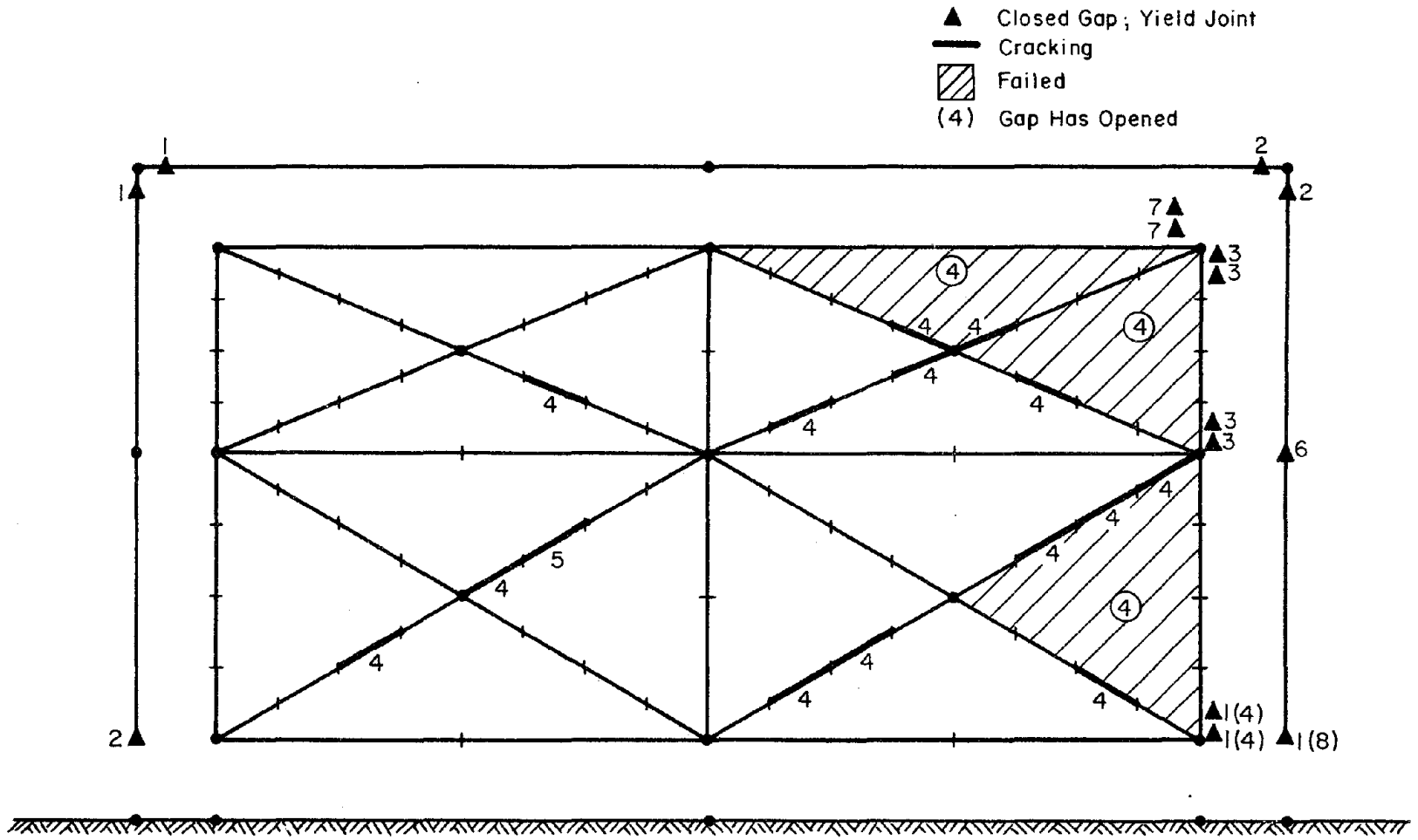

Figure 5.38 Cracking Sequence: Frame Wall-Gaps(I) from t=0.425 to 0.535 sec

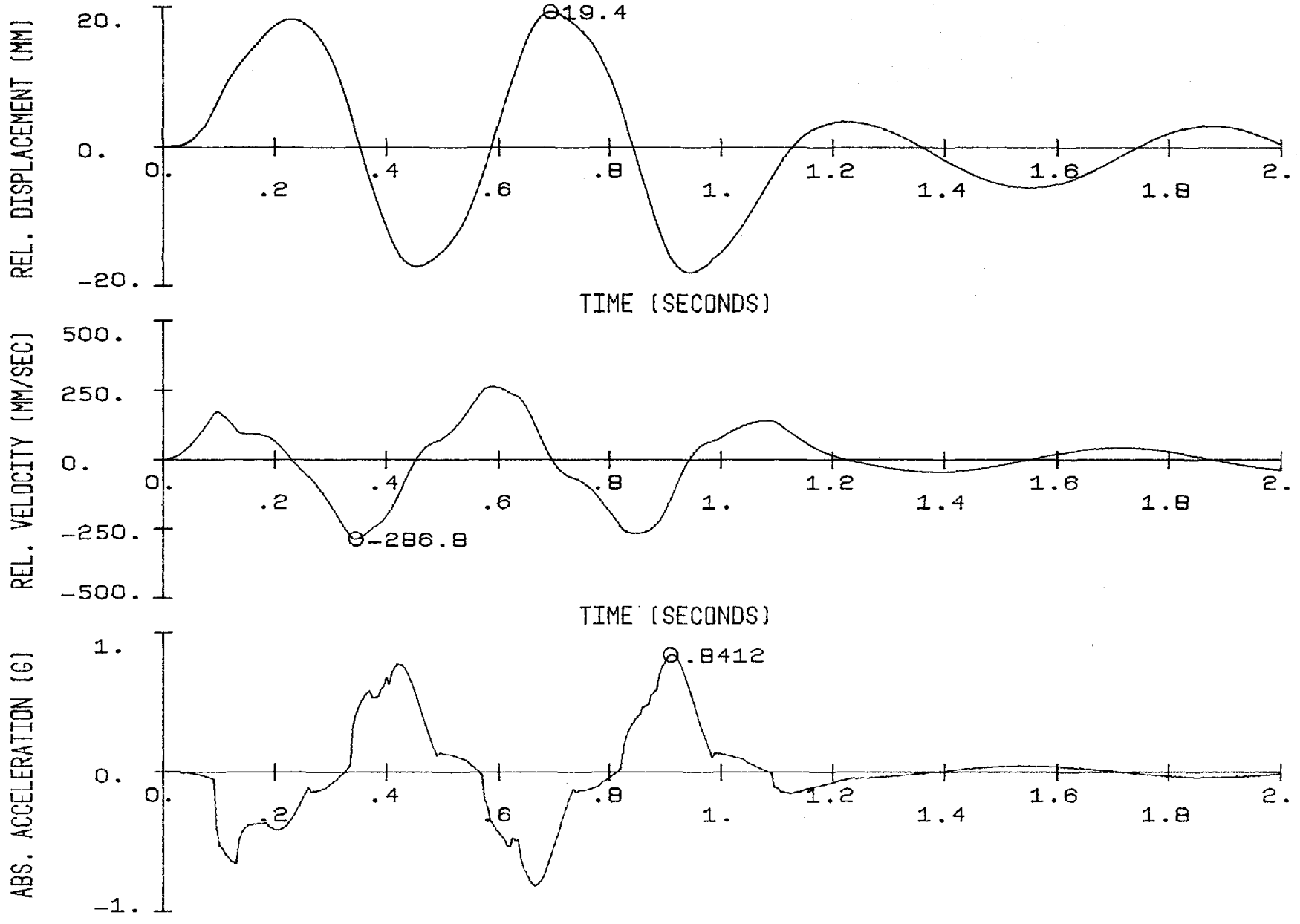

Figure 5.39 Relative Displacement, Velocity, and Absolute Acceleration of the Frame Wall-Gaps(II)

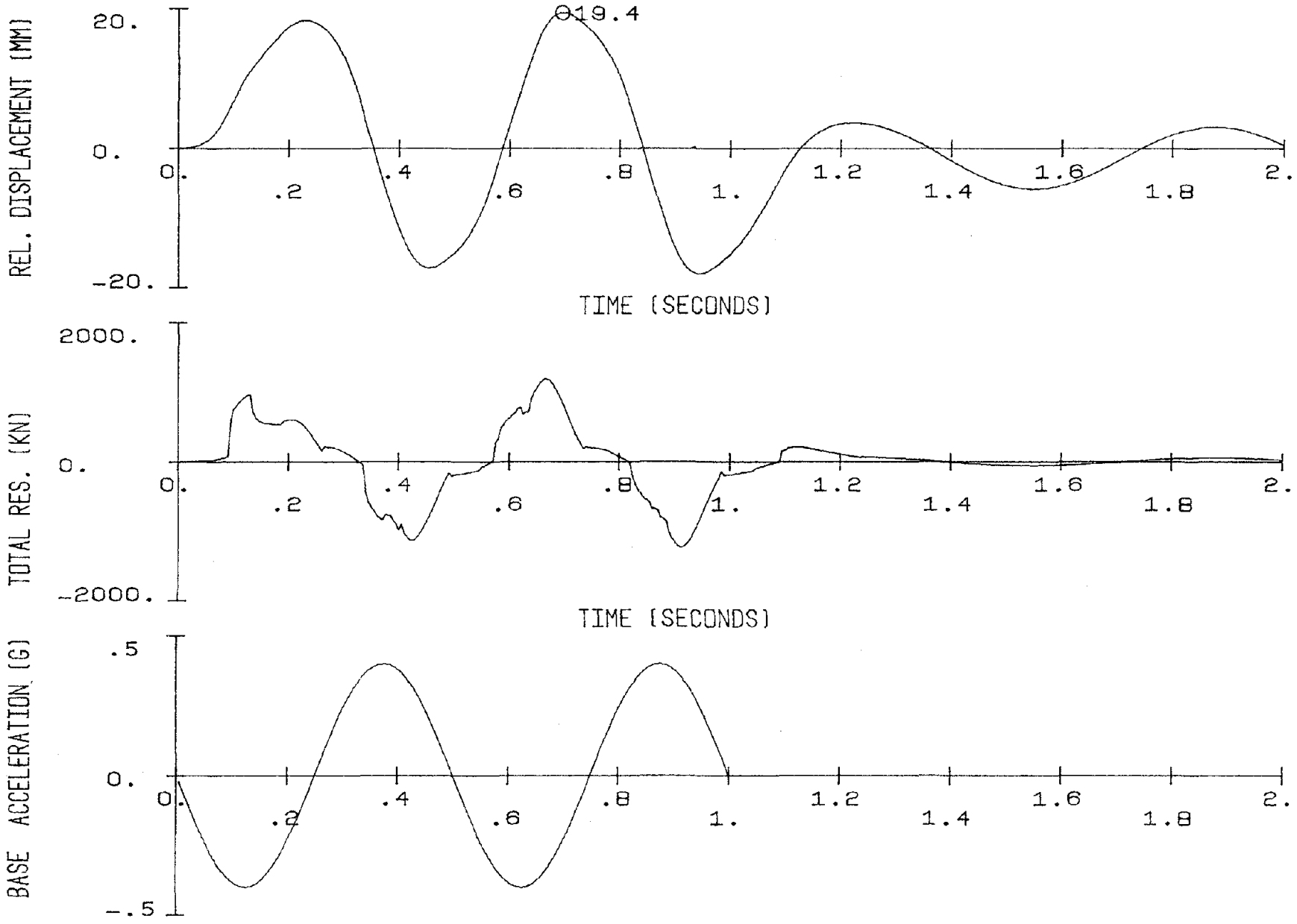

Figure 5.40 Relative Displacement, Total Resistance, and Base Acceleration of the Frame Wall-Gaps(II)

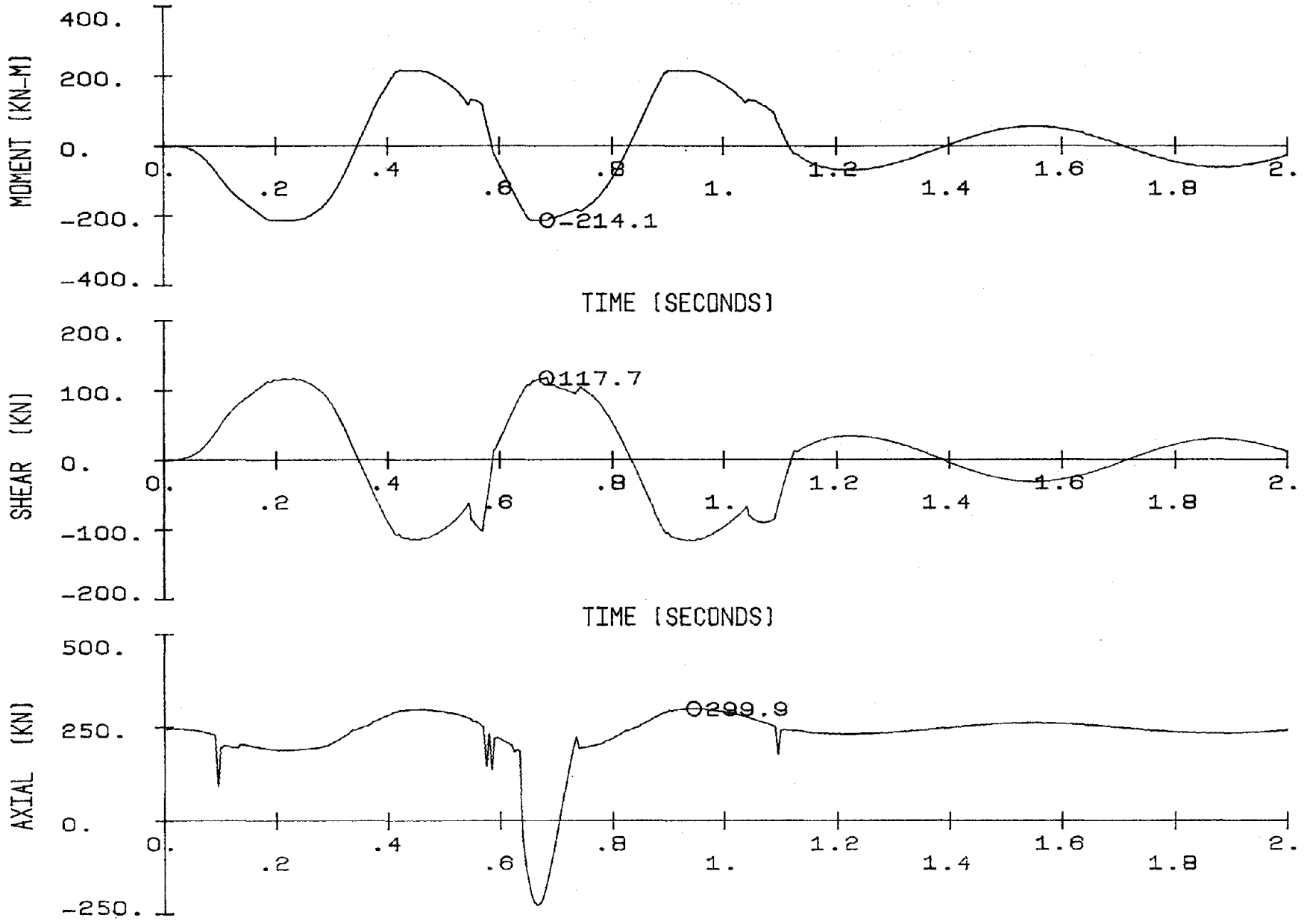

Figure 5.41 Base Moment, Base Shear, and Axial Load for the Left Column of the Frame Wall-Gaps(II)

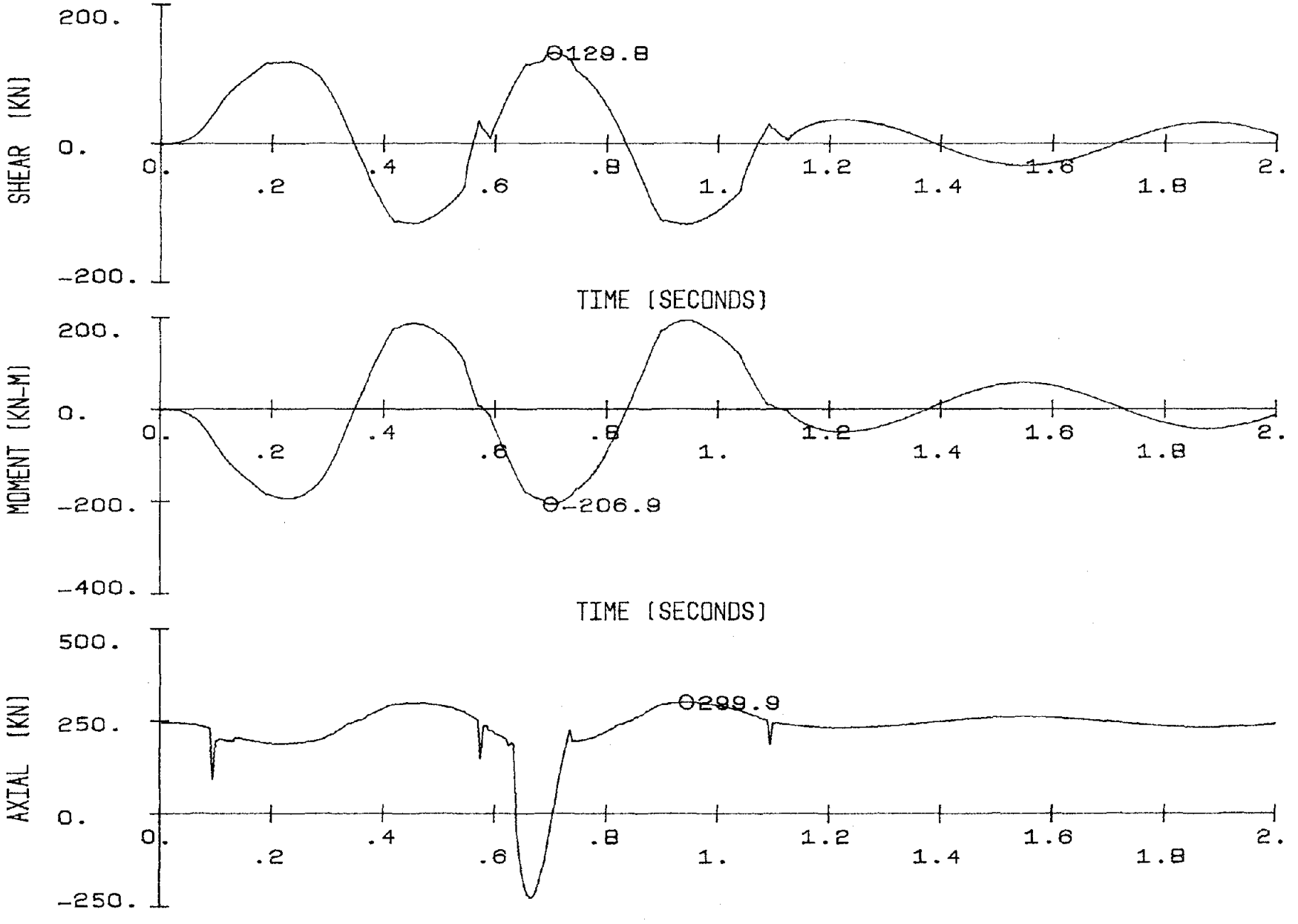

Figure 5.42 Center Shear, Top Moment, and Axial Load for the Left Column of the Frame Wall-Gaps(II)

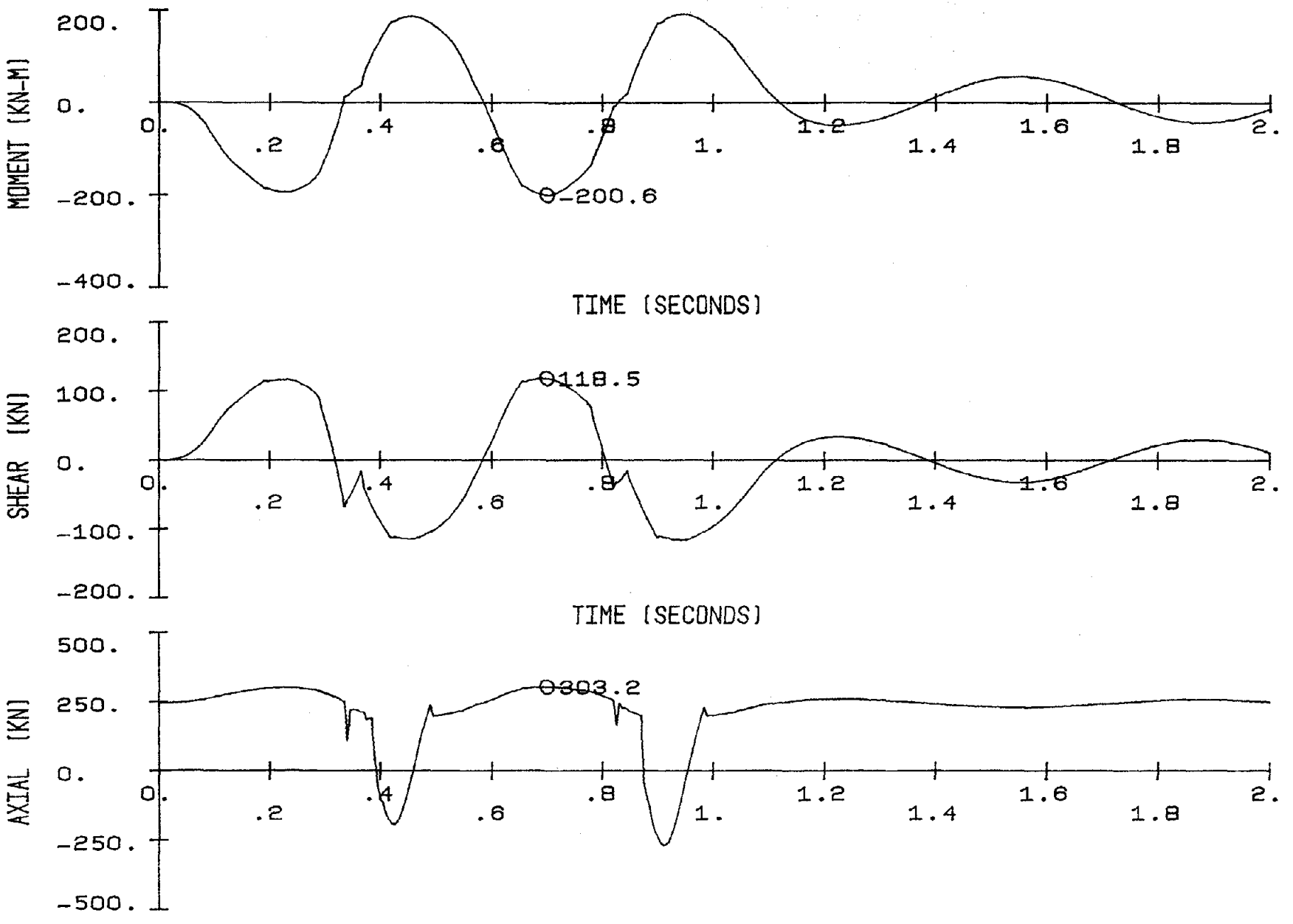

Figure 5.43 Top Moment, Top Shear, and Axial Load for the Right Column of the Frame Wall-Gaps(II)

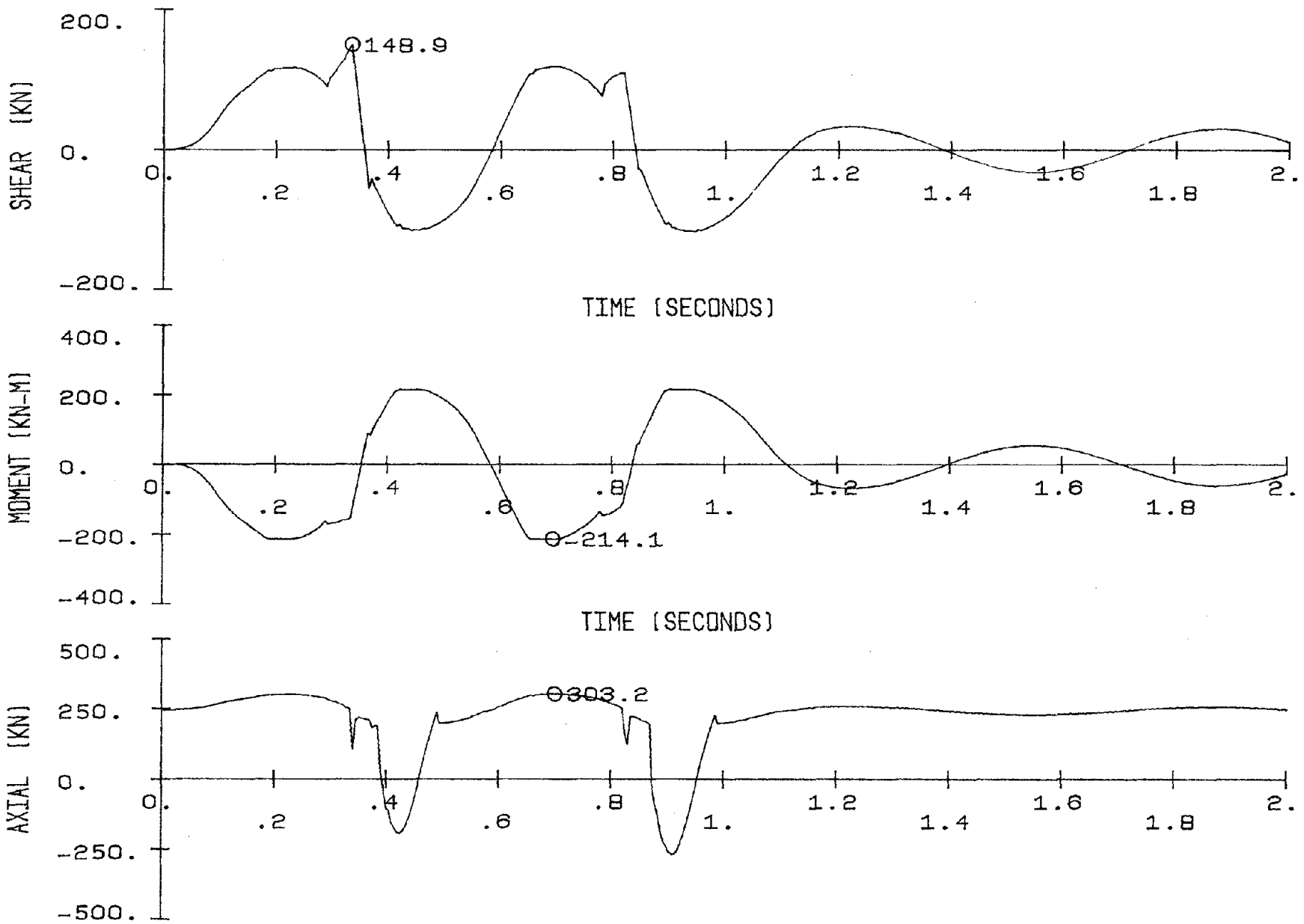

Figure 5.44 Center Shear, Base Moment, and Axial Load for the Right Column of the Frame Wall-Gaps(II)

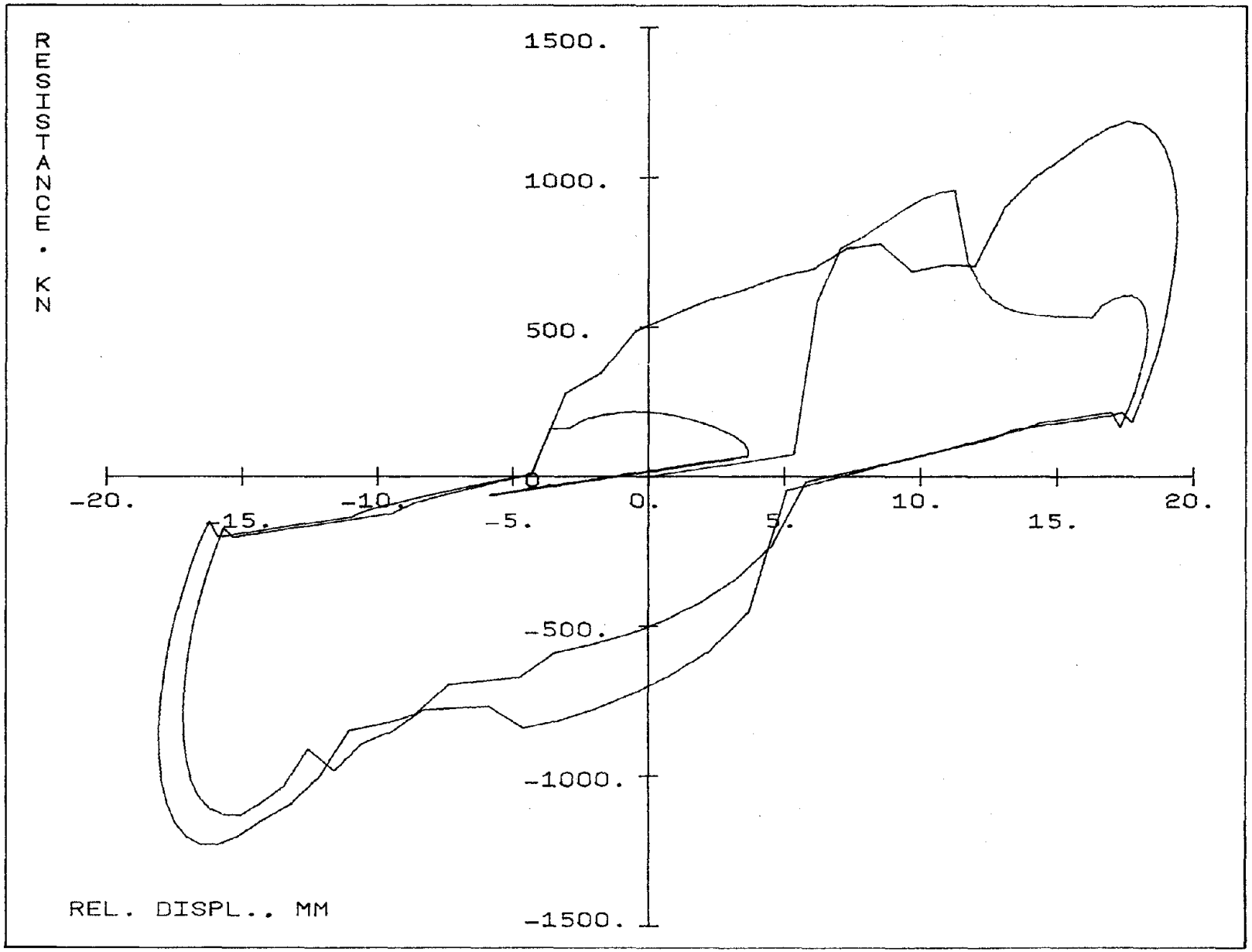

Figure 5.45 Load Displacement Response: Frame Wall-Gaps(II)

1 - t=0.090 sec
2 - t=0.095 sec
3 - t=0.100 sec
4 - t=0.105 sec
5 - t=0.110 sec
6 - t=0.115 sec
7 - t=0.120 sec
8 - t=0.130 sec
9 - t=0.145 sec
10 - t=0.150 sec
11 - t=0.185 sec
12 - t=0.190 sec
13 - t=0.235 sec
14 - t=0.260 sec

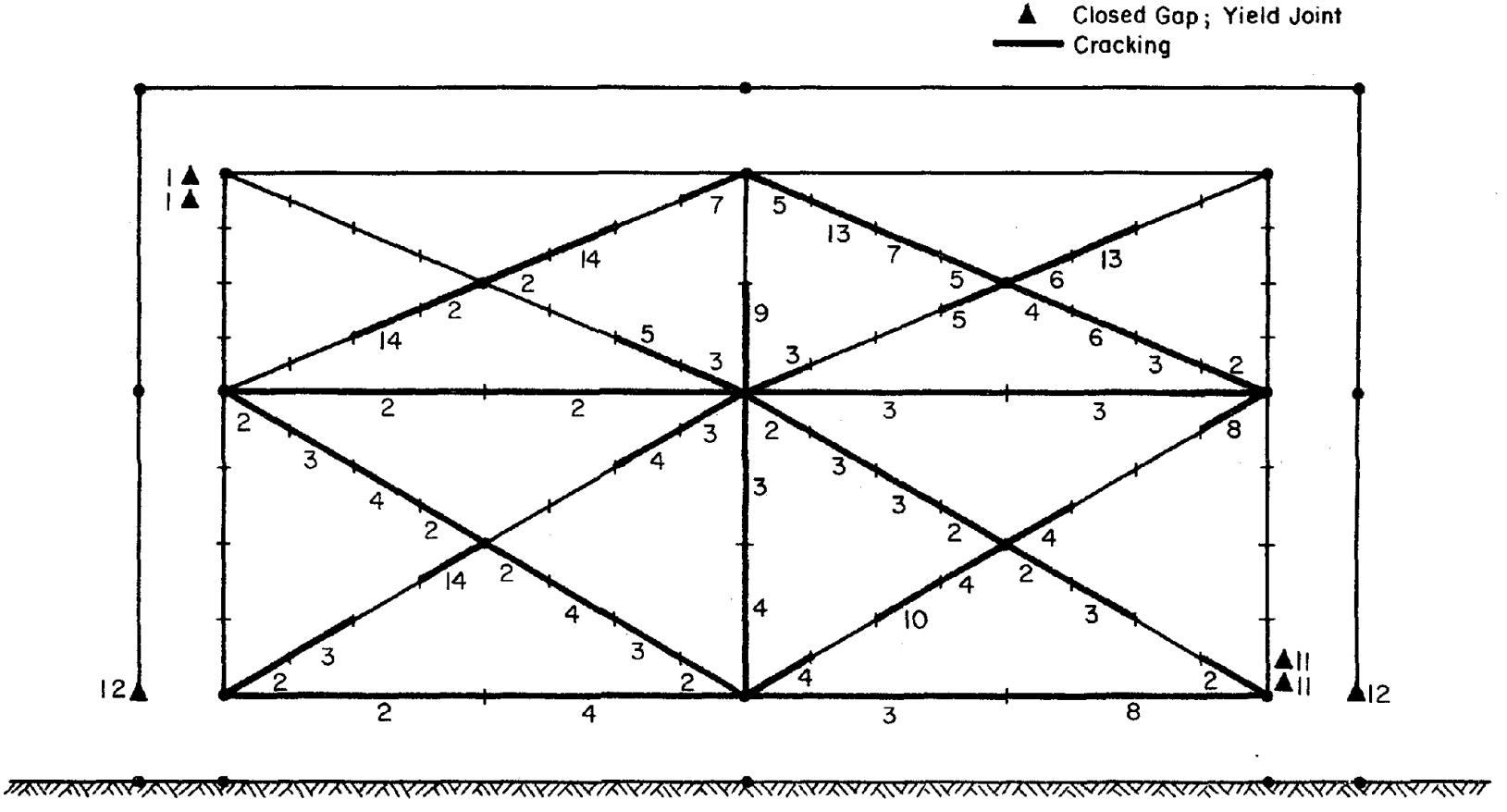

Figure 5.46 Cracking Sequence: Frame Wall-Gaps(II) from t=0.0 to 0.260 sec

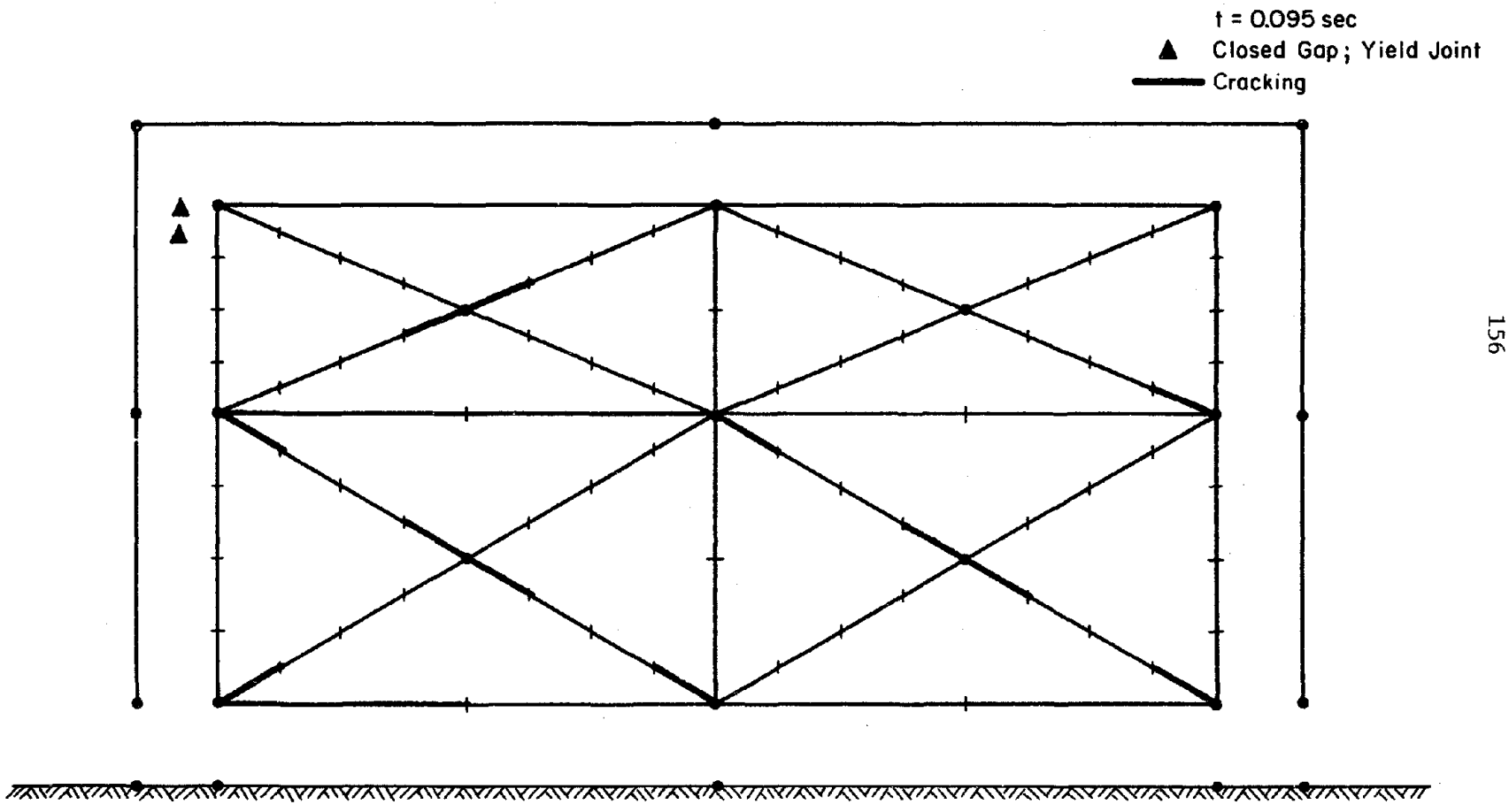

Figure 5.47 Crack Pattern: Frame Wall-Gaps(II) at t=0.095 sec

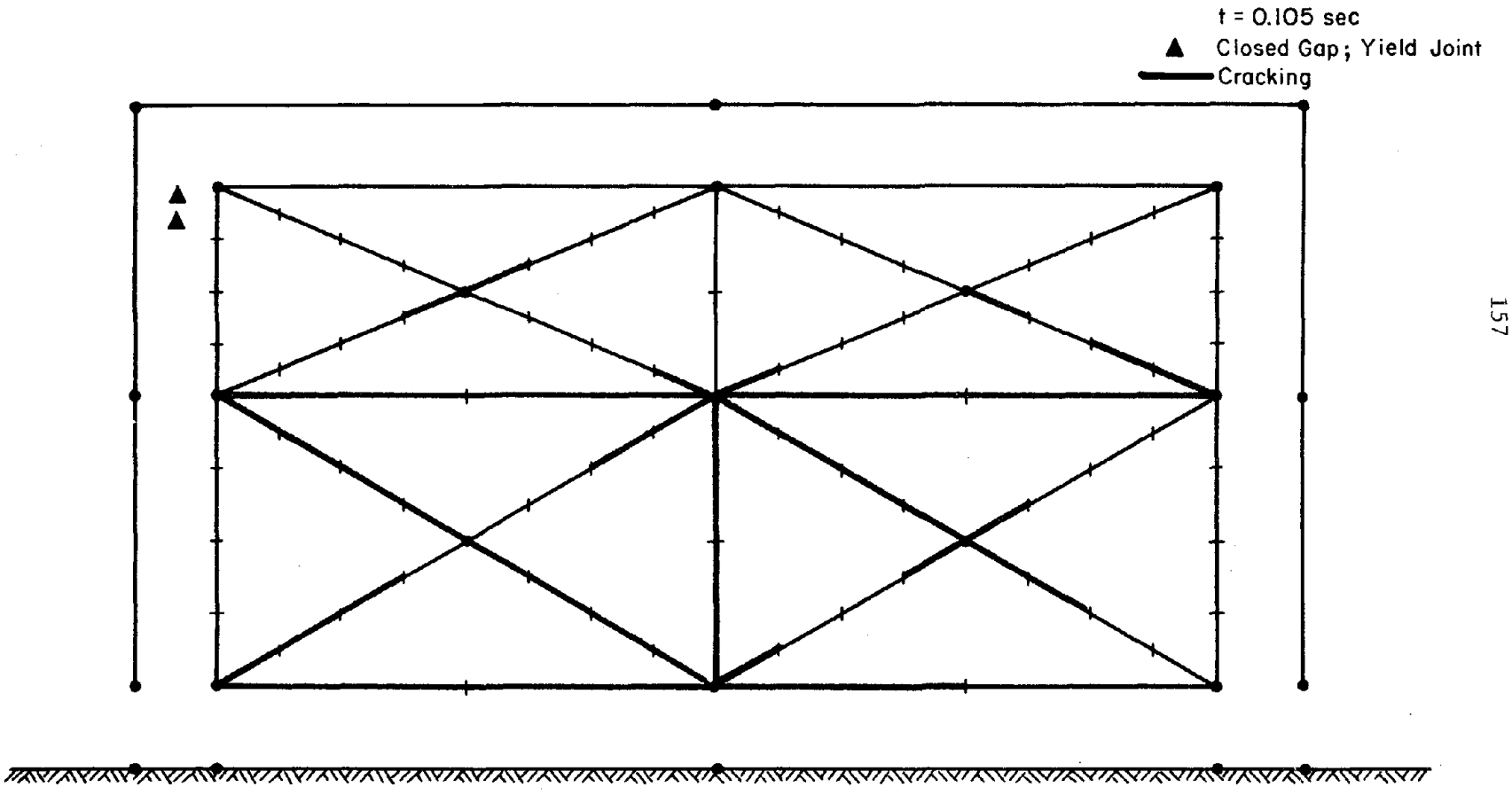

Figure 5.48 Crack Pattern: Frame Wall-Gaps(II) at t=0.105 sec

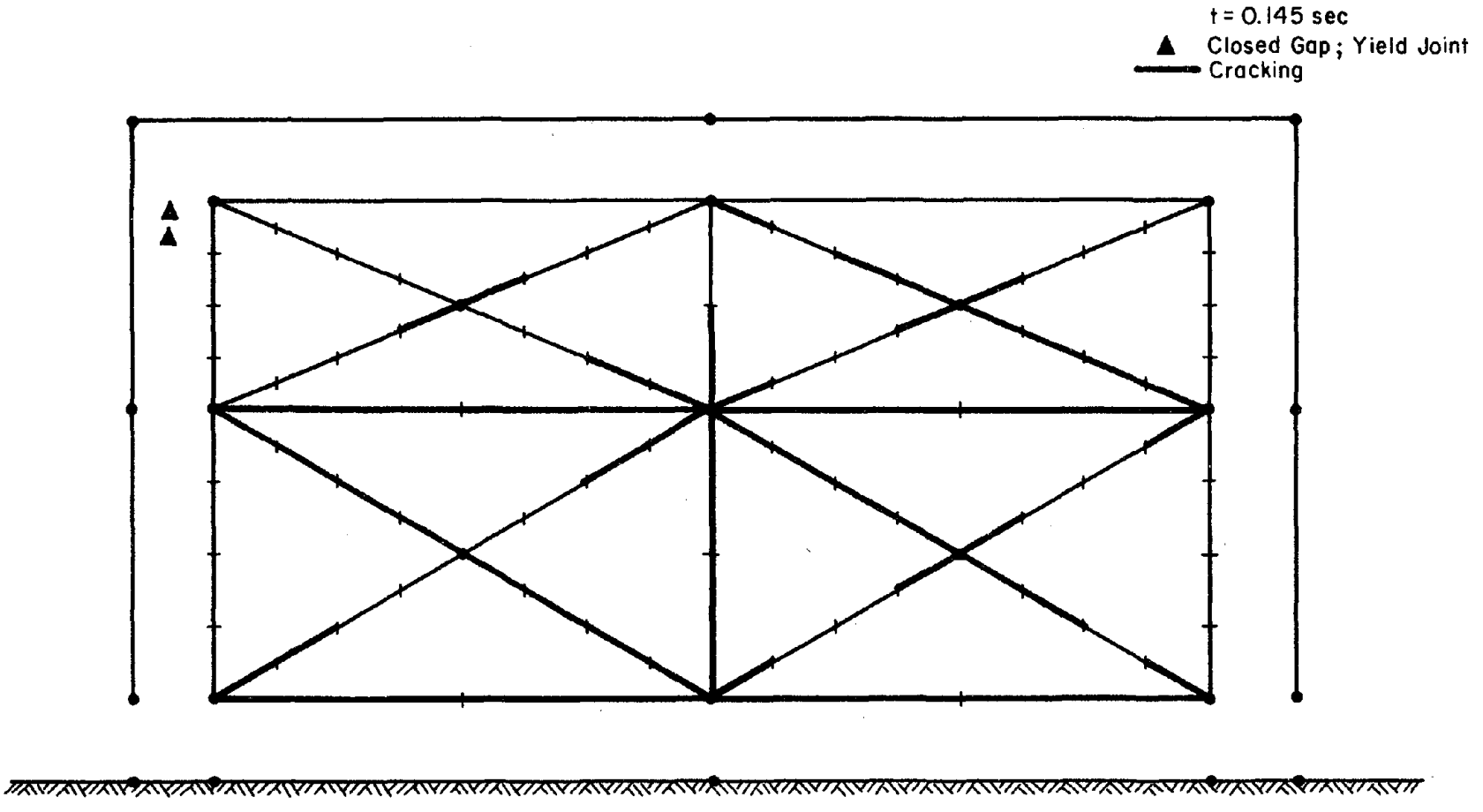

Figure 5.49 Crack Pattern: Frame Wall-Gaps(II) at t=0.145 sec

1 - t=0.290 sec
2 - t=0.310 sec
3 - t=0.315 sec
4 - t=0.320 sec
5 - t=0.330 sec
6 - t=0.335 sec
7 - t=0.340 sec
8 - t=0.345 sec
9 - t=0.350 sec
10 - t=0.355 sec
11 - t=0.360 sec
12 - t=0.365 sec
13 - t=0.370 sec
14 - t=0.380 sec
15 - t=0.390 sec
16 - t=0.405 sec
17 - t=0.455 sec

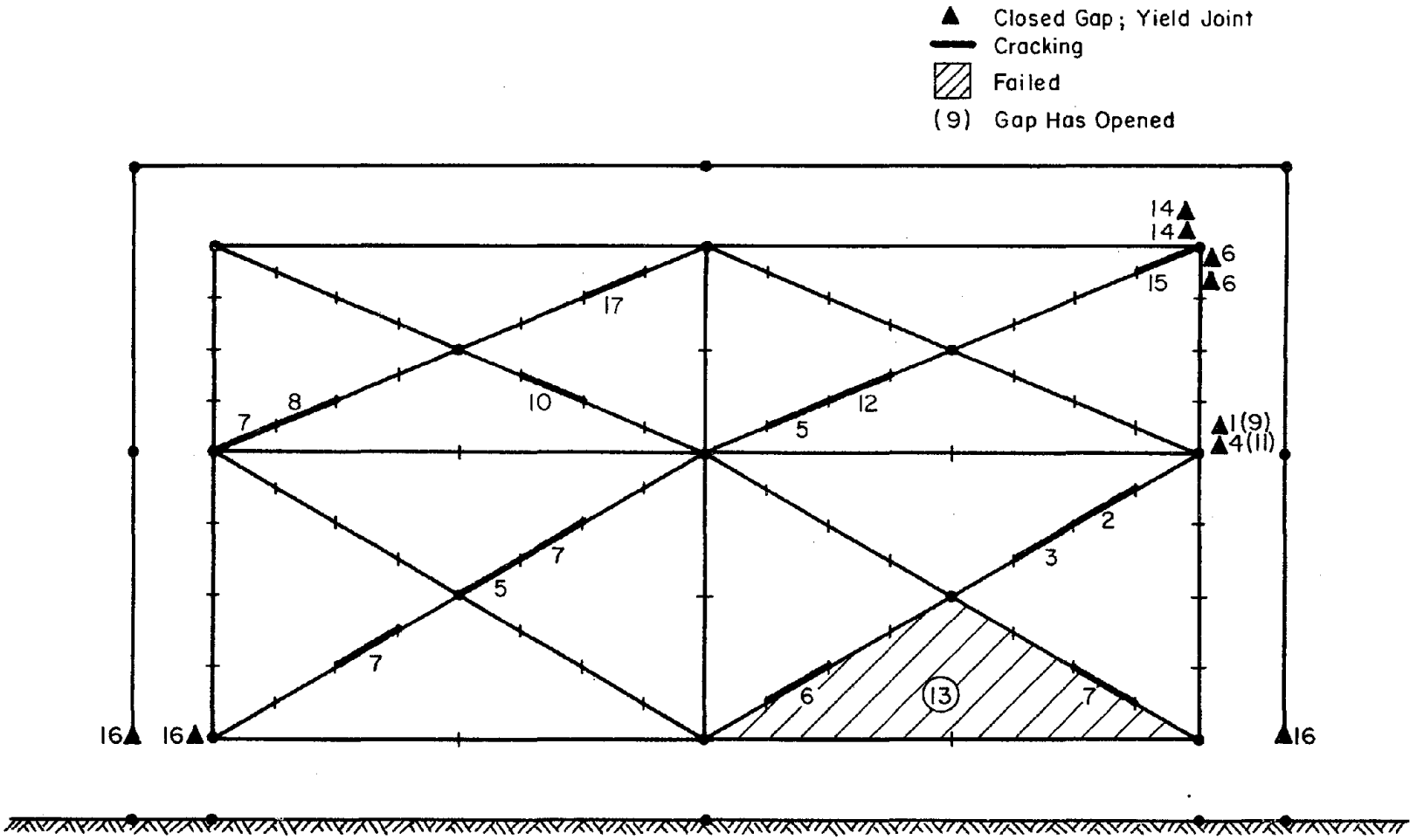

Figure 5.50 Cracking Sequence: Frame Wall-Gaps(II) from t=0.290 to 0.455 sec

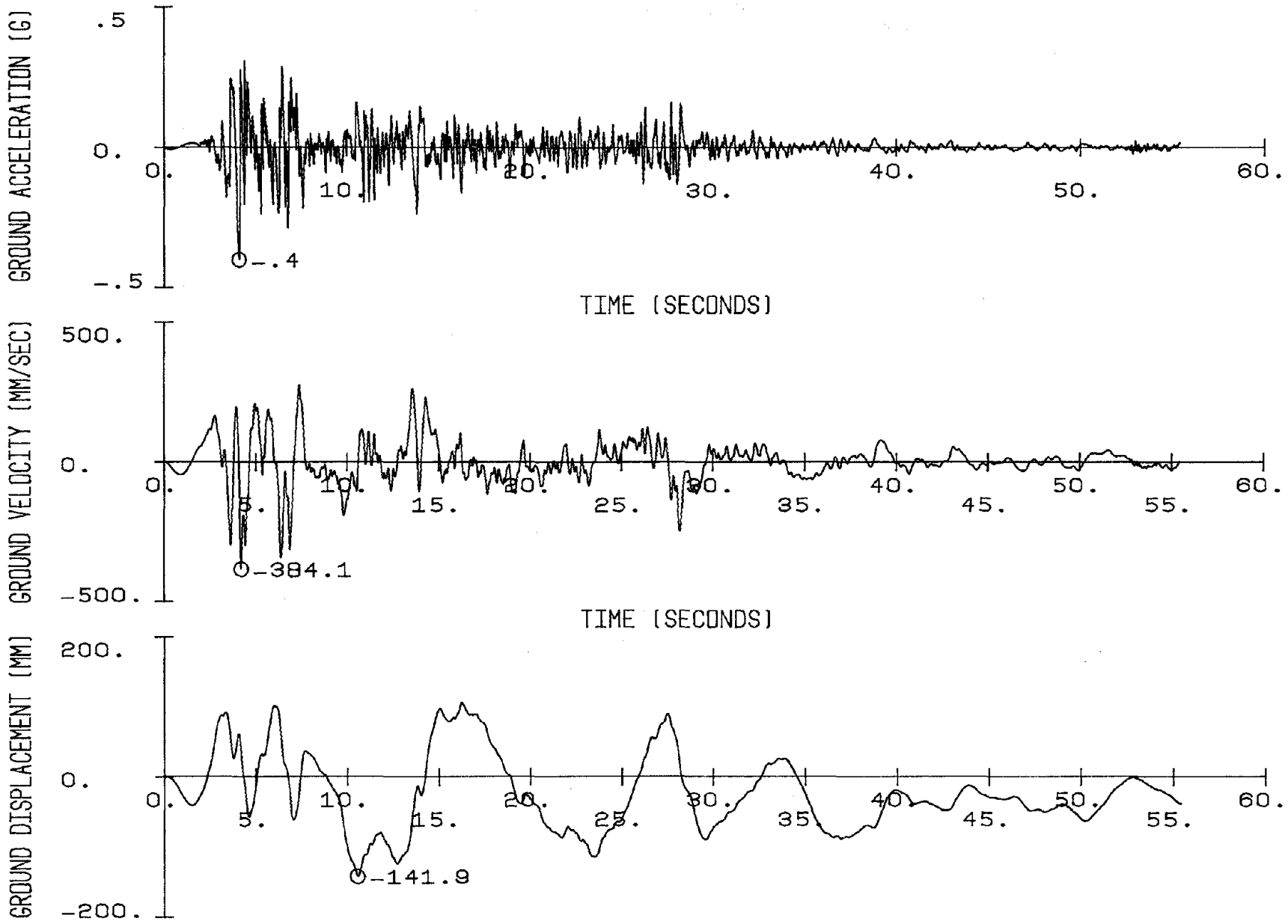

Figure 5.51 Ground Motion for the El Centro Record, May 18, 1940, S00E Component, Scaled to 0.4g

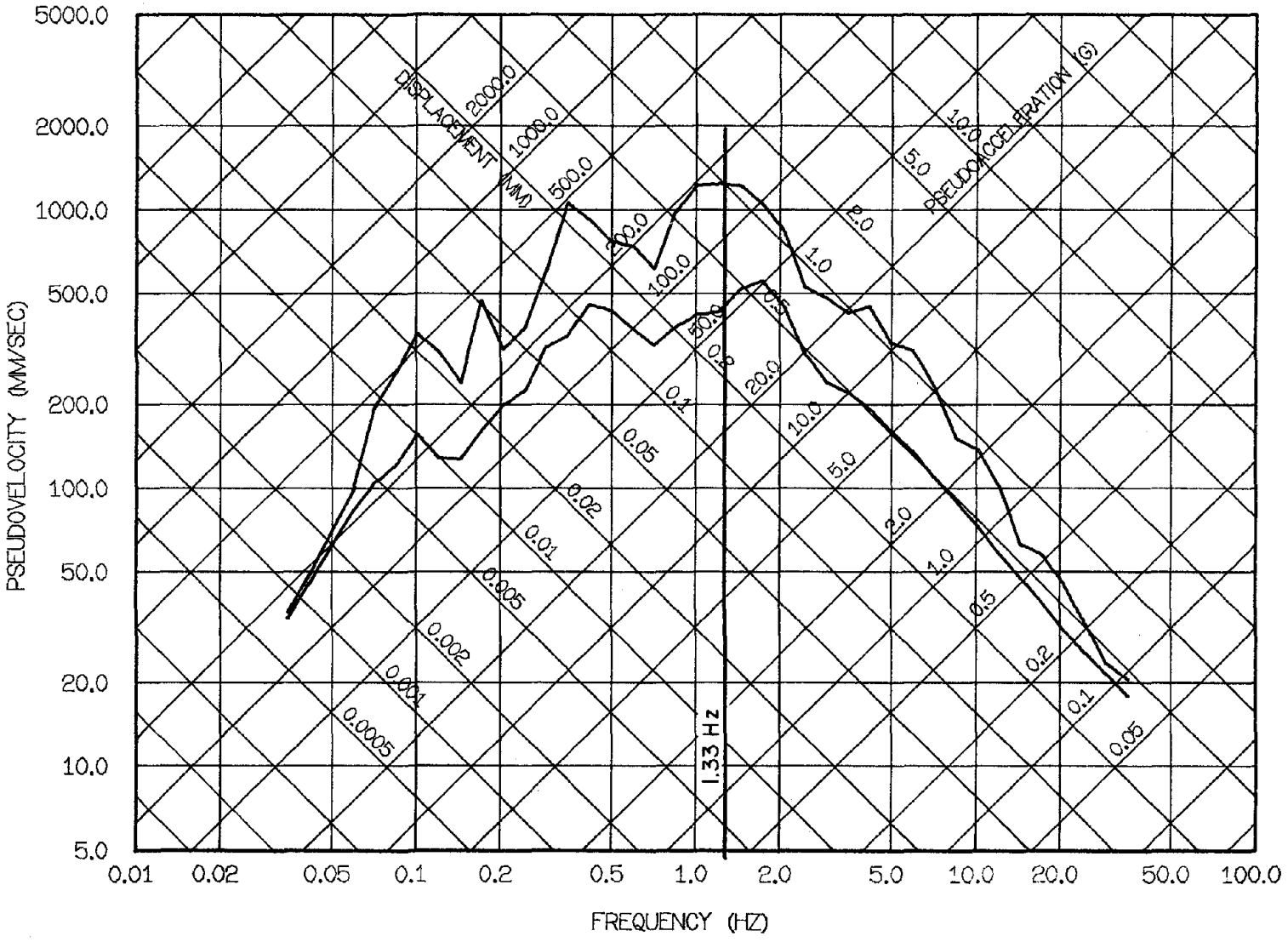

Figure 5.52 Elastic Spectrum at 2% and 20% Damping for the El Centro Record, May 18, 1940, S00E Component, Scaled to 0.4g

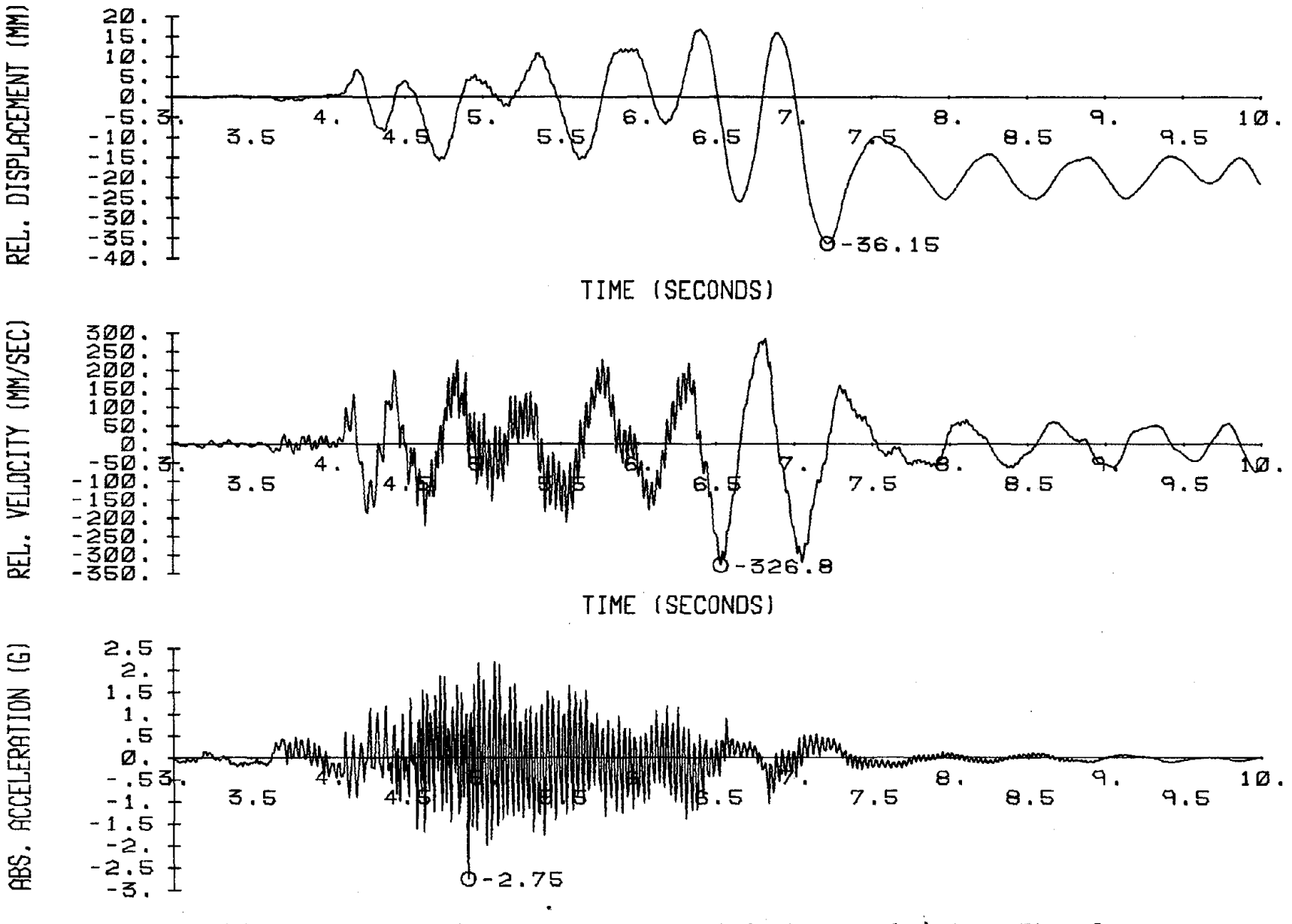

Figure 5.53 Relative Displacement, Velocity, and Absolute Acceleration: First Story

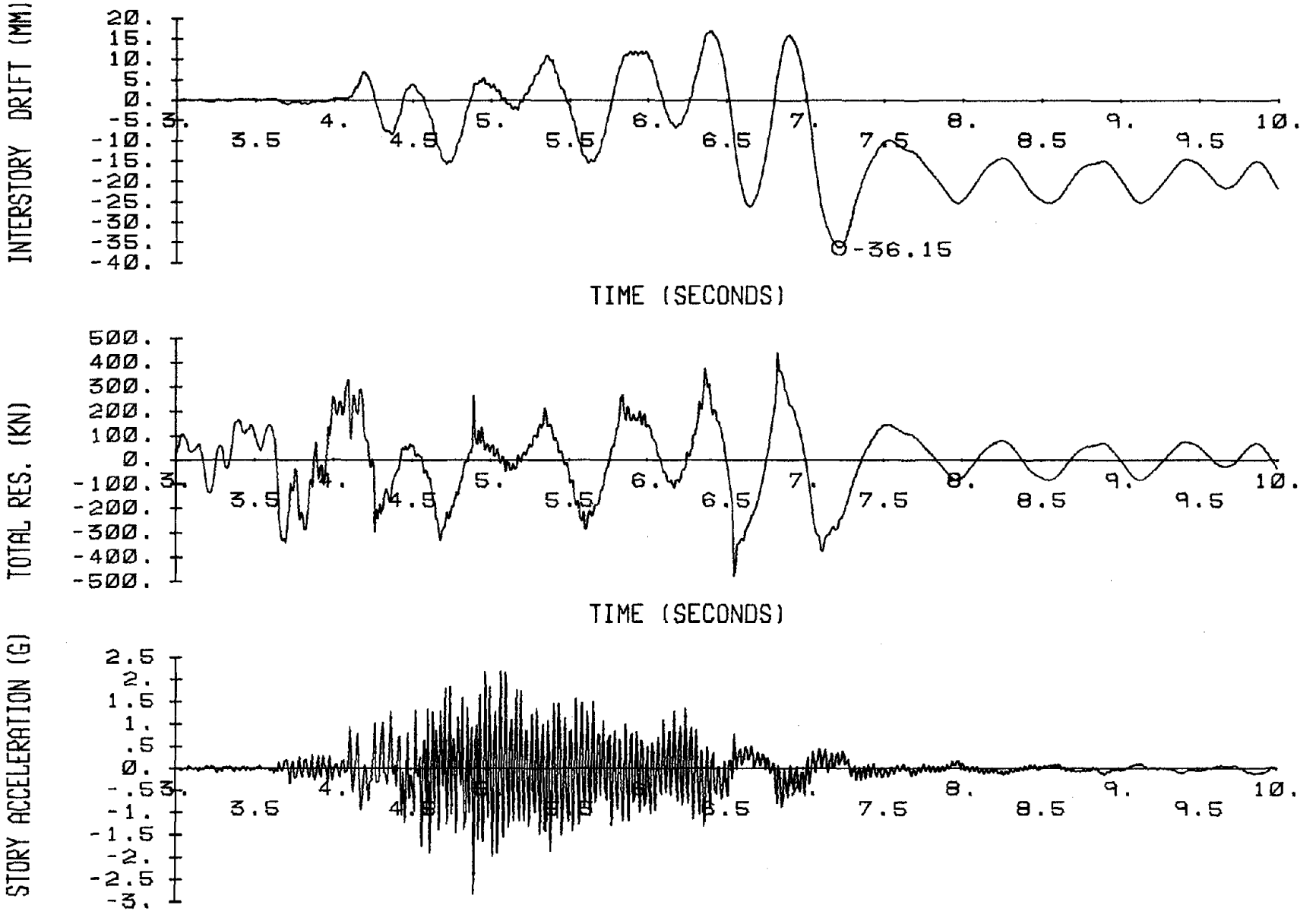

Figure 5.54 Interstory Drift, Total Resistance, and Story Acceleration: First Story

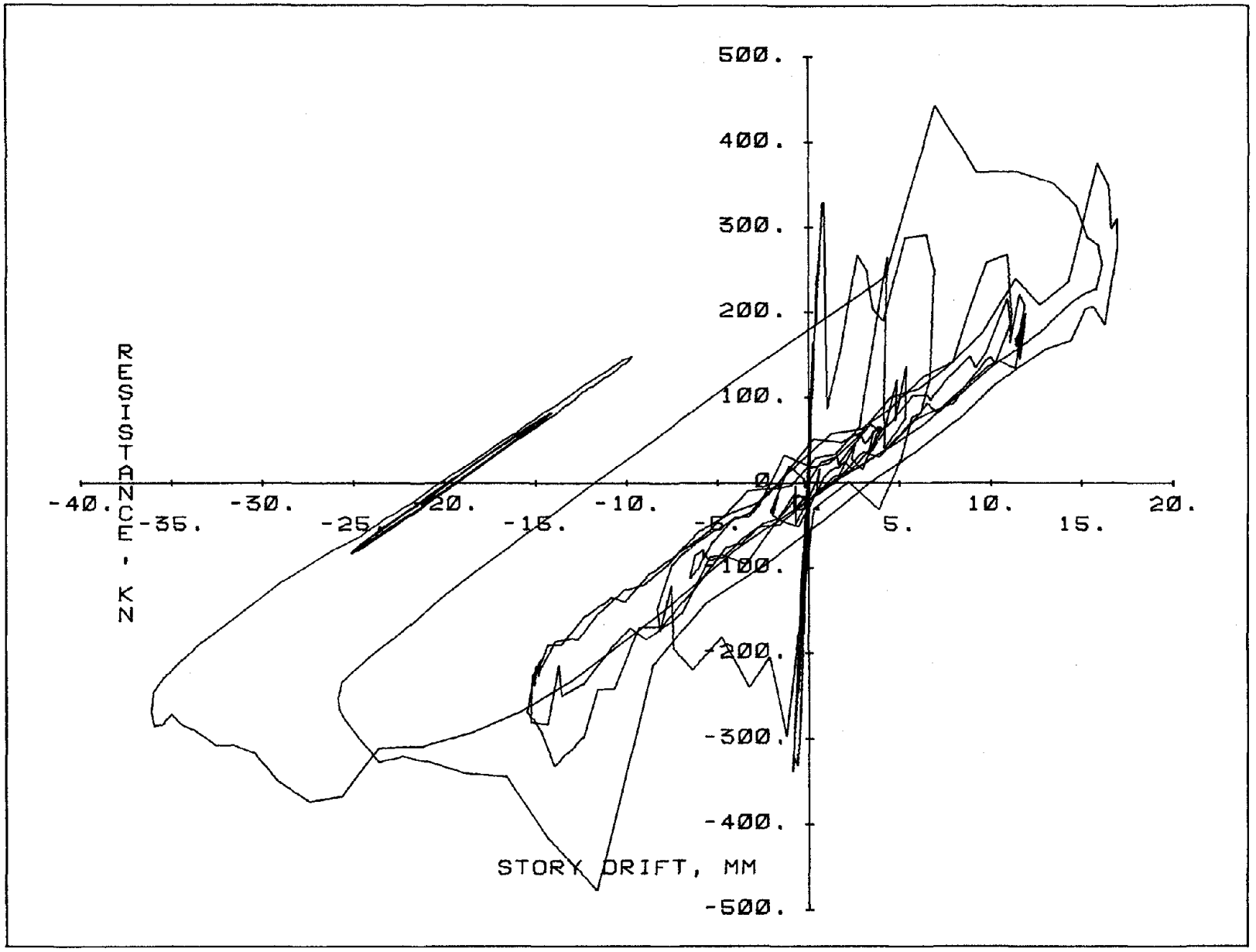

Figure 5.55 Load Displacement Response: First Story

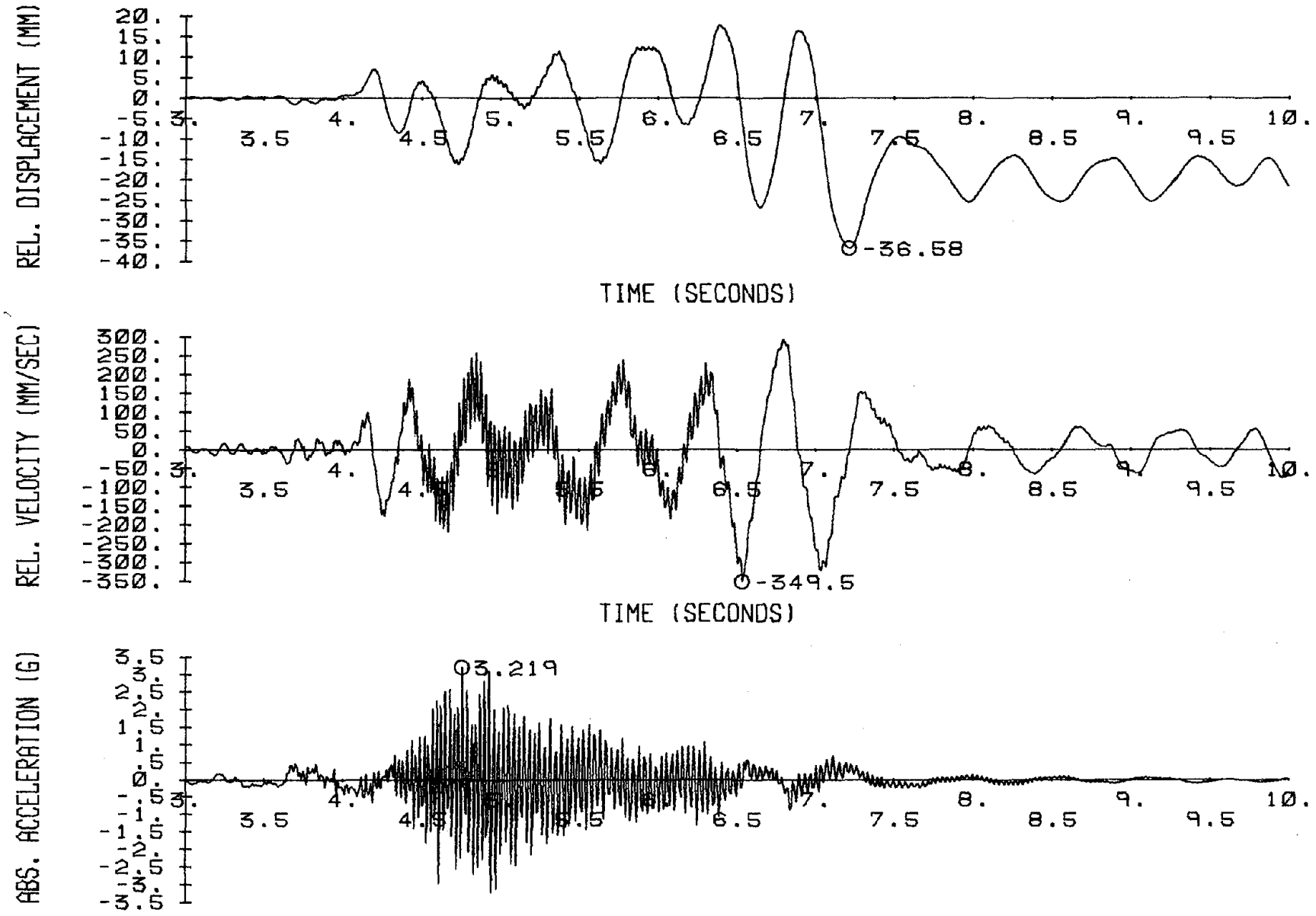

Figure 5.56 Relative Displacement, Velocity, and Absolute Acceleration: Second Story

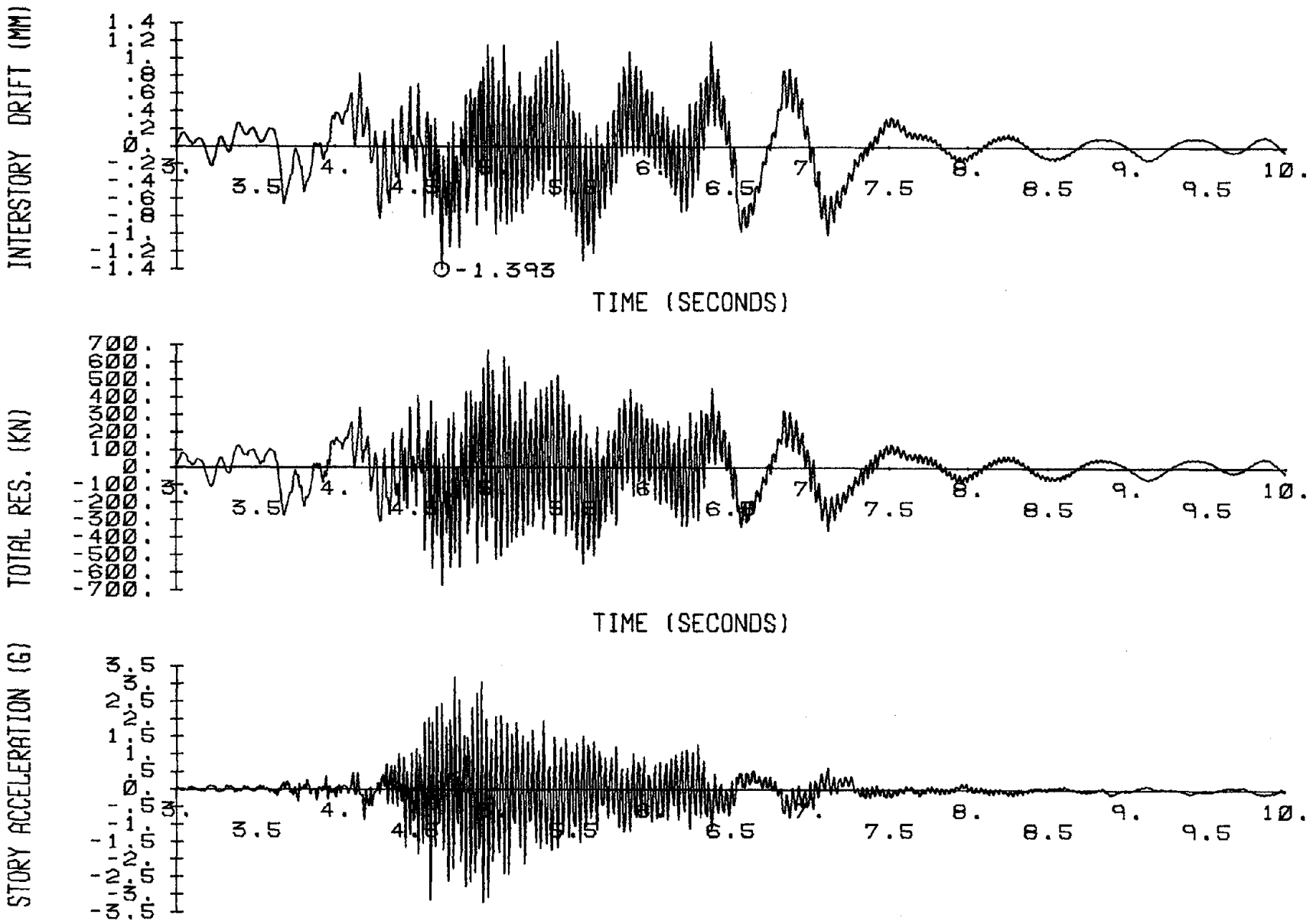

Figure 5.57 Interstory Drift, Total Resistance, and Story Acceleration: Second Story

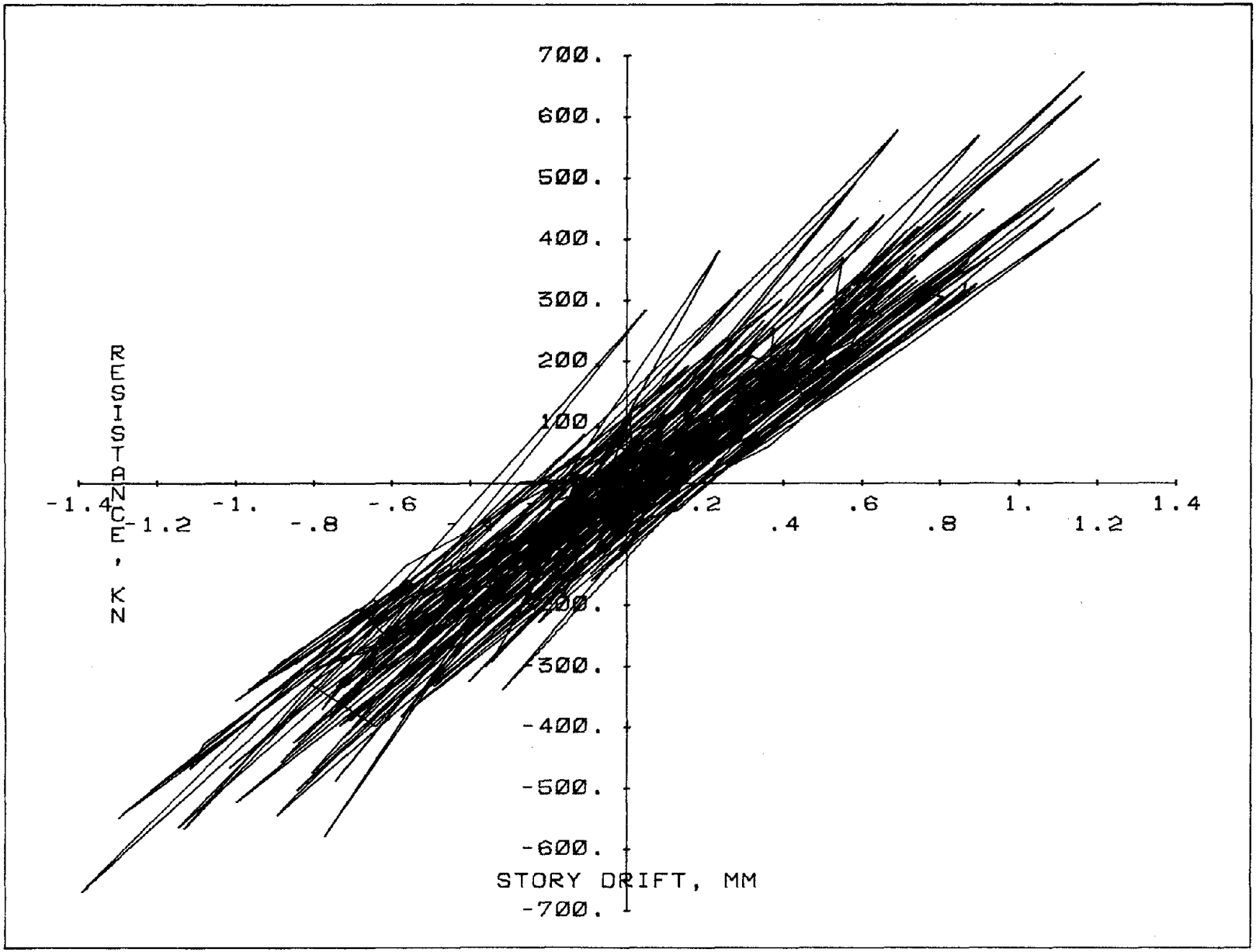

Figure 5.58 Load Displacement Response: Second Story

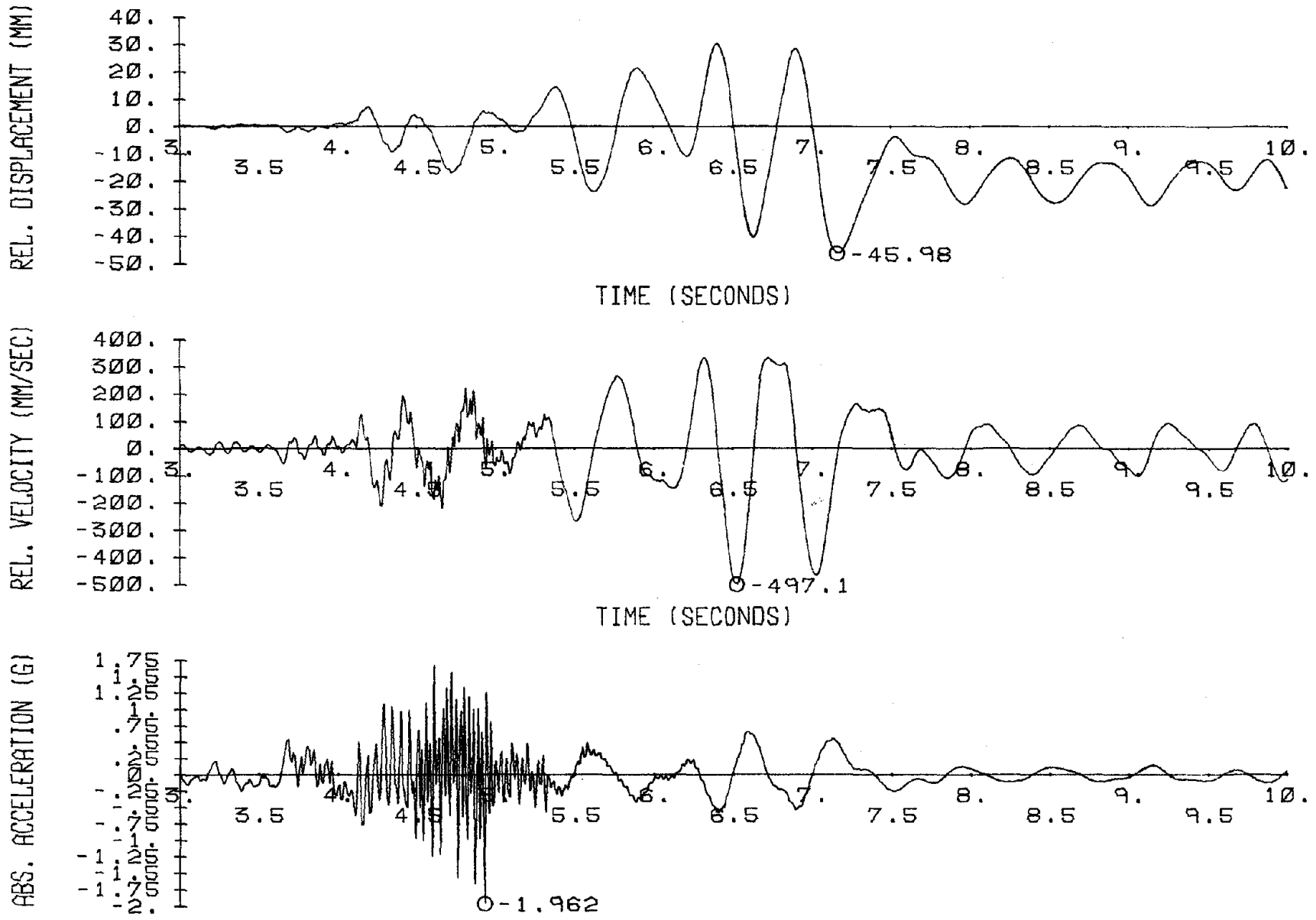

Figure 5.59 Relative Displacement, Velocity, and Absolute Acceleration: Third Story

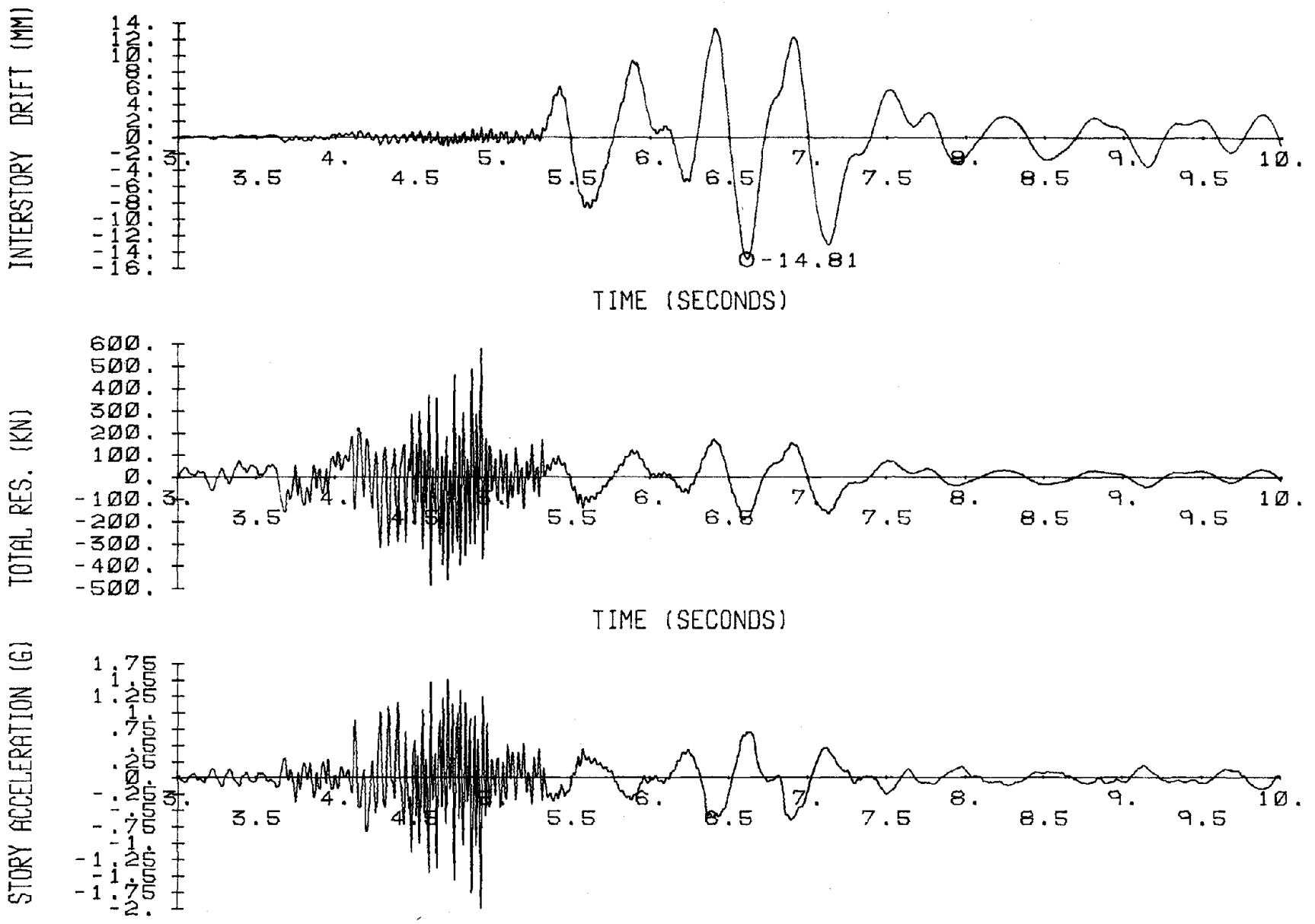

Figure 5.60 Interstory Drift, Total Resistance, and Story Acceleration: Third Story

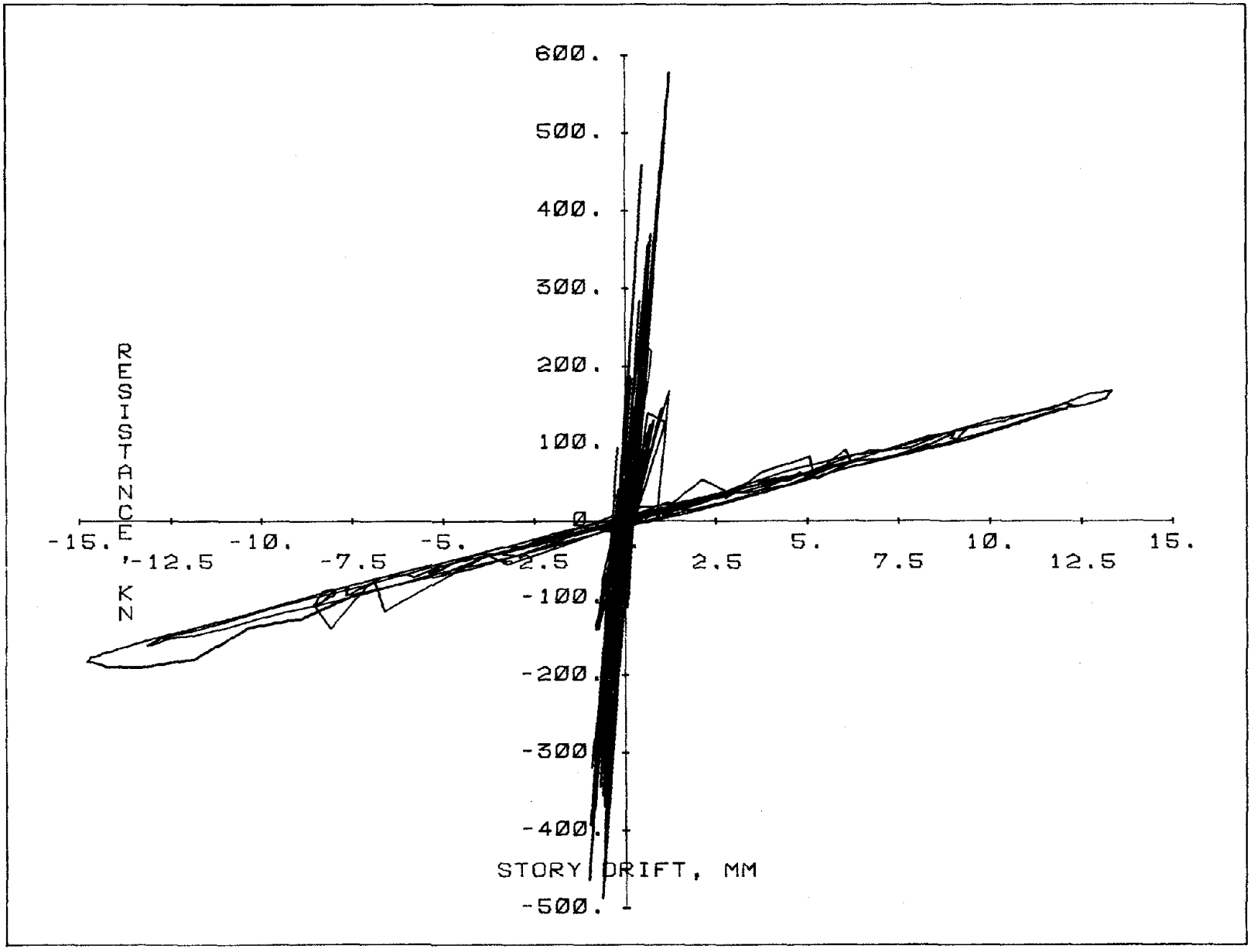

Figure 5.61 Load Displacement Response: Third Story

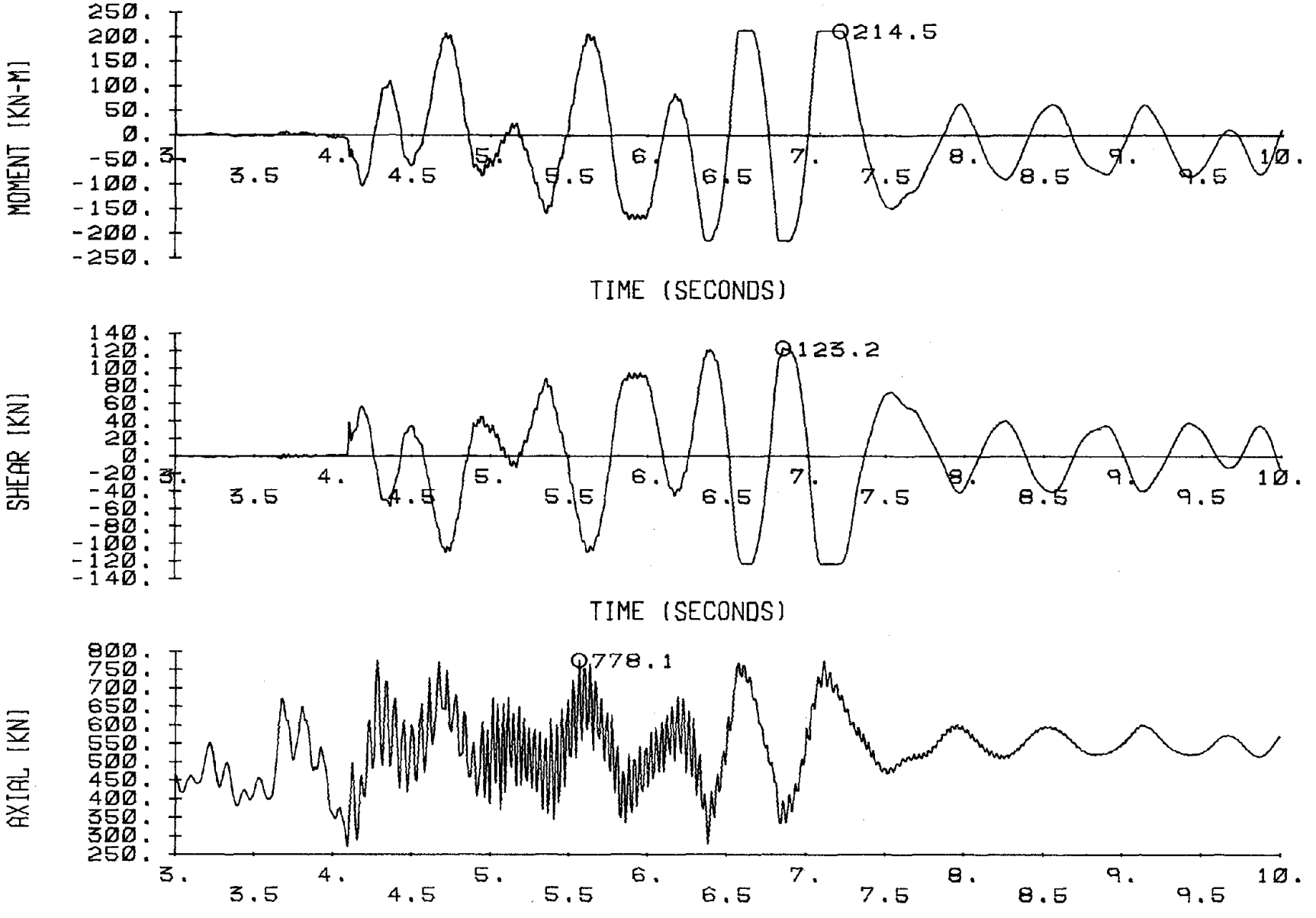

Figure 5.62 Base Moment, Base Shear, and Axial Load for the Left Column: First Story

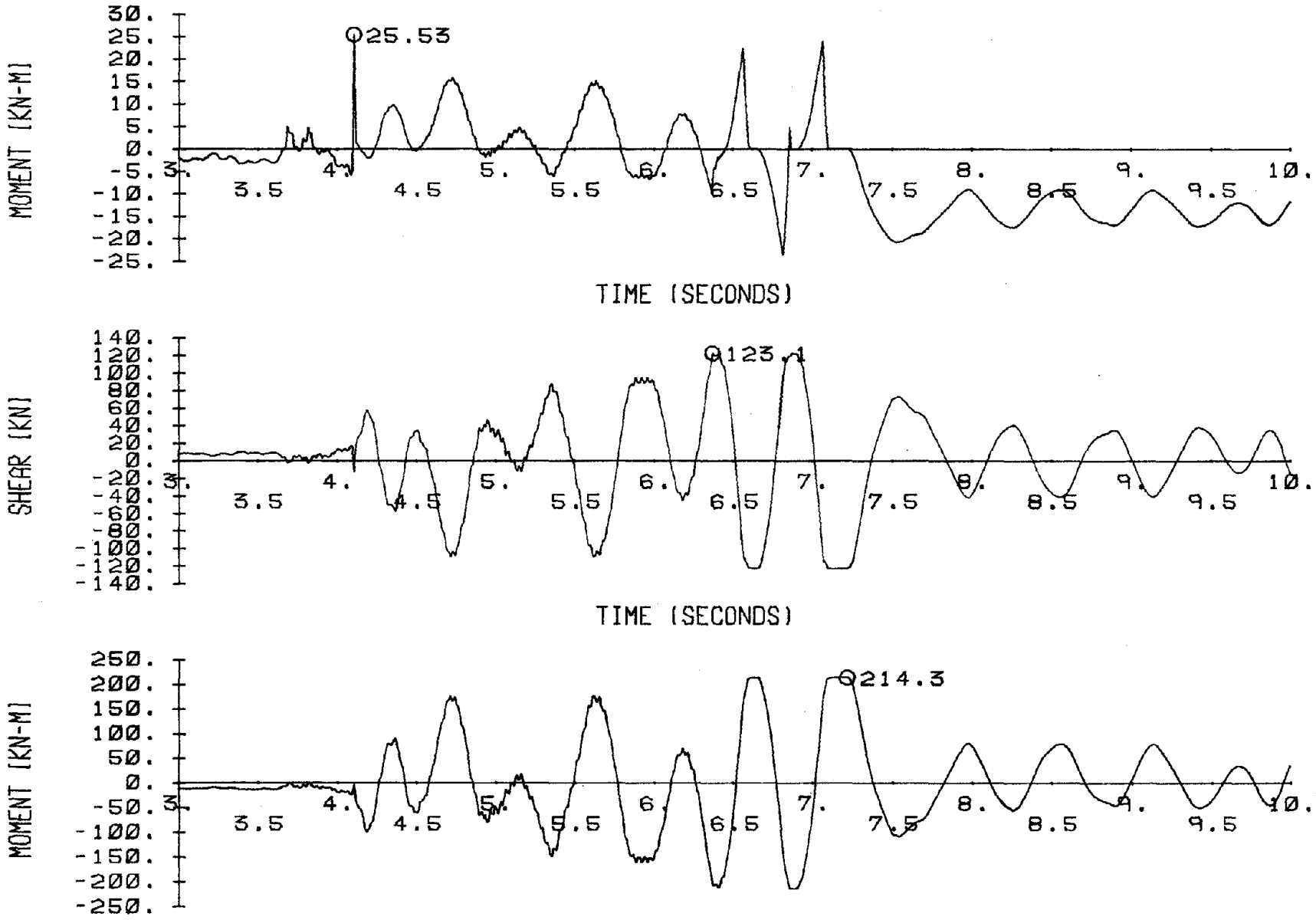

Figure 5.63 Center Moment, Center Shear, and Top Moment for the Left Column: First Story

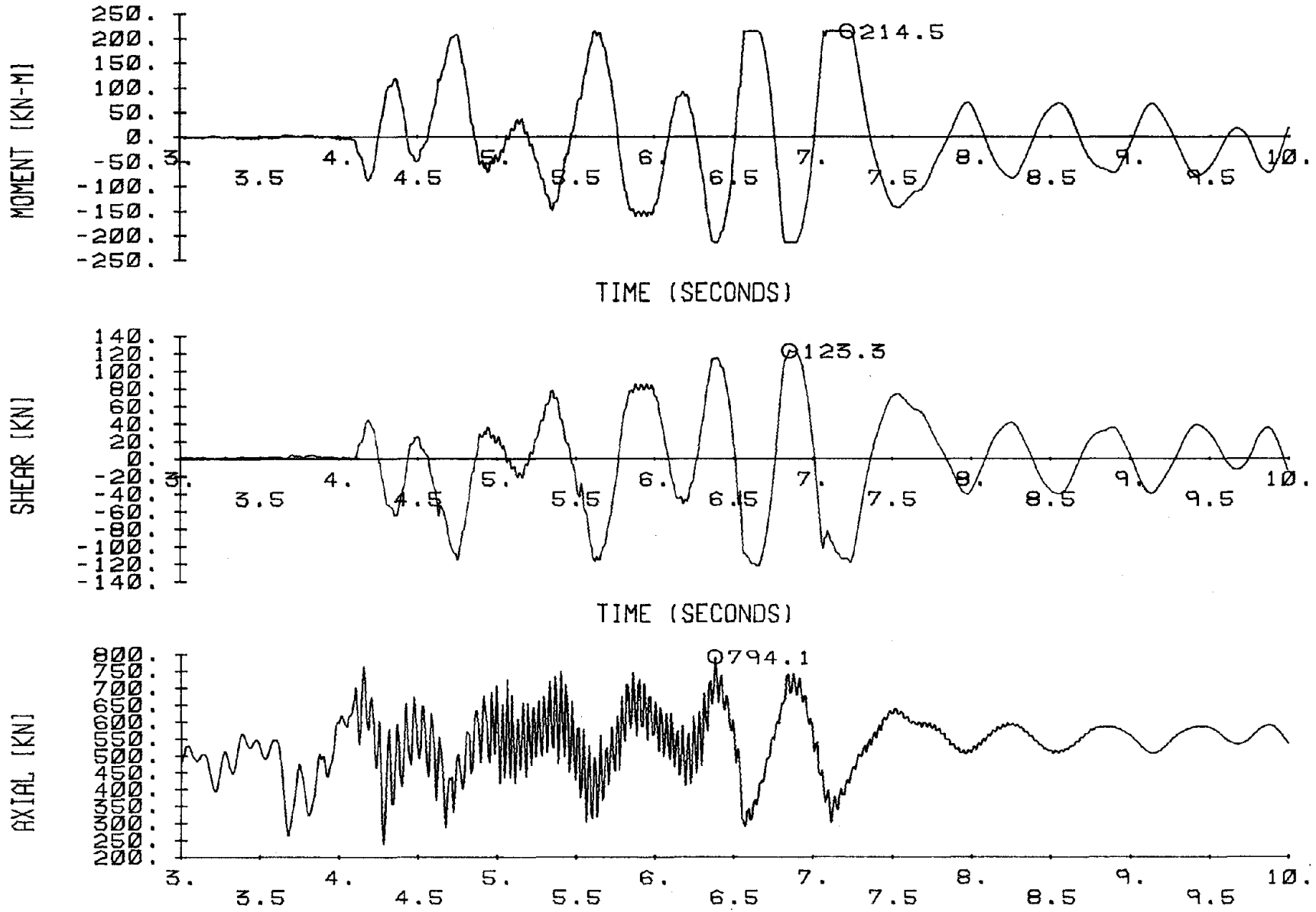

Figure 5.64 Base Moment, Base Shear, and Axial Load for the Right Column: First Story

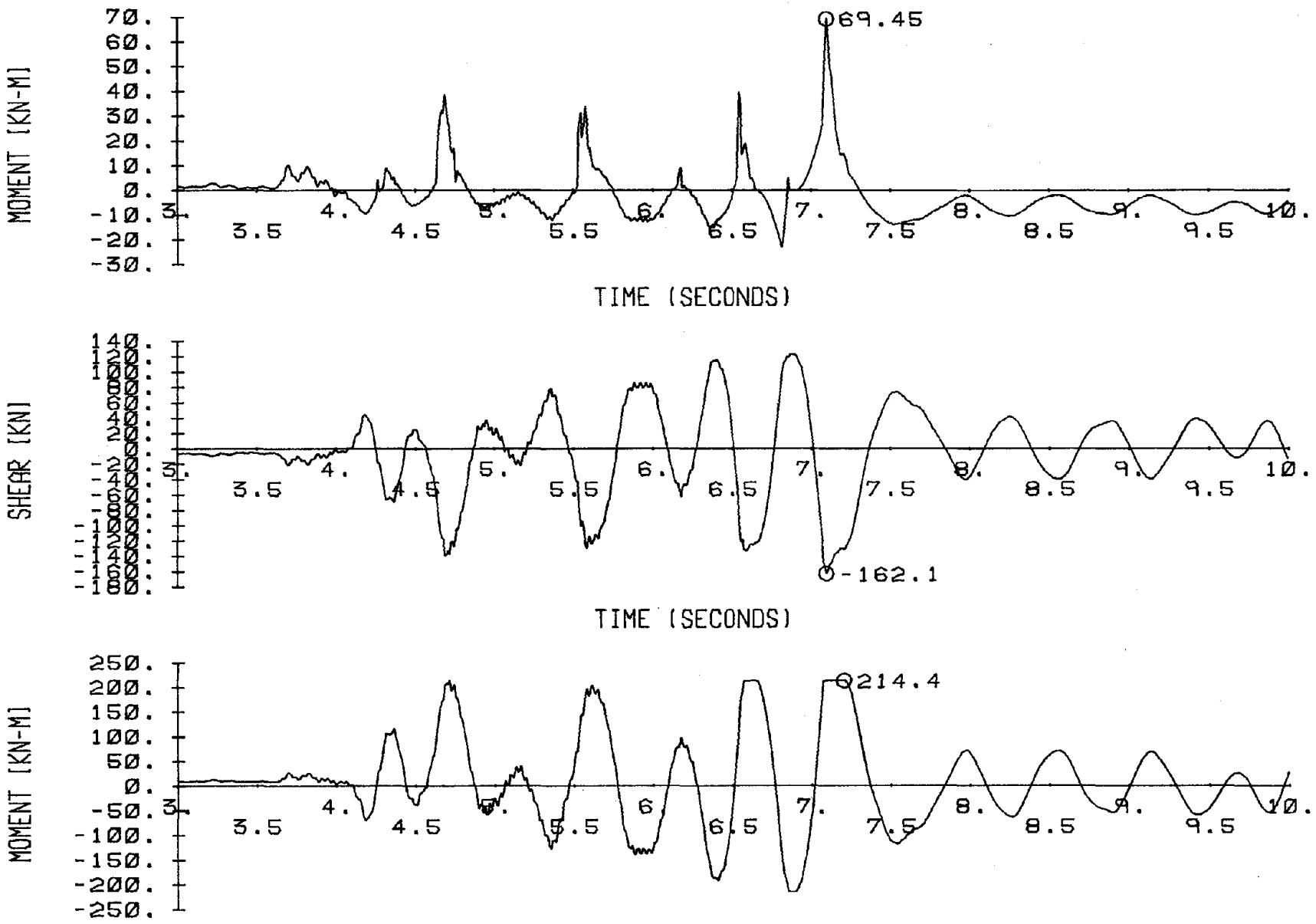

Figure 5.65 Center Moment, Center Shear, and Top Moment for the Right Column: First Story

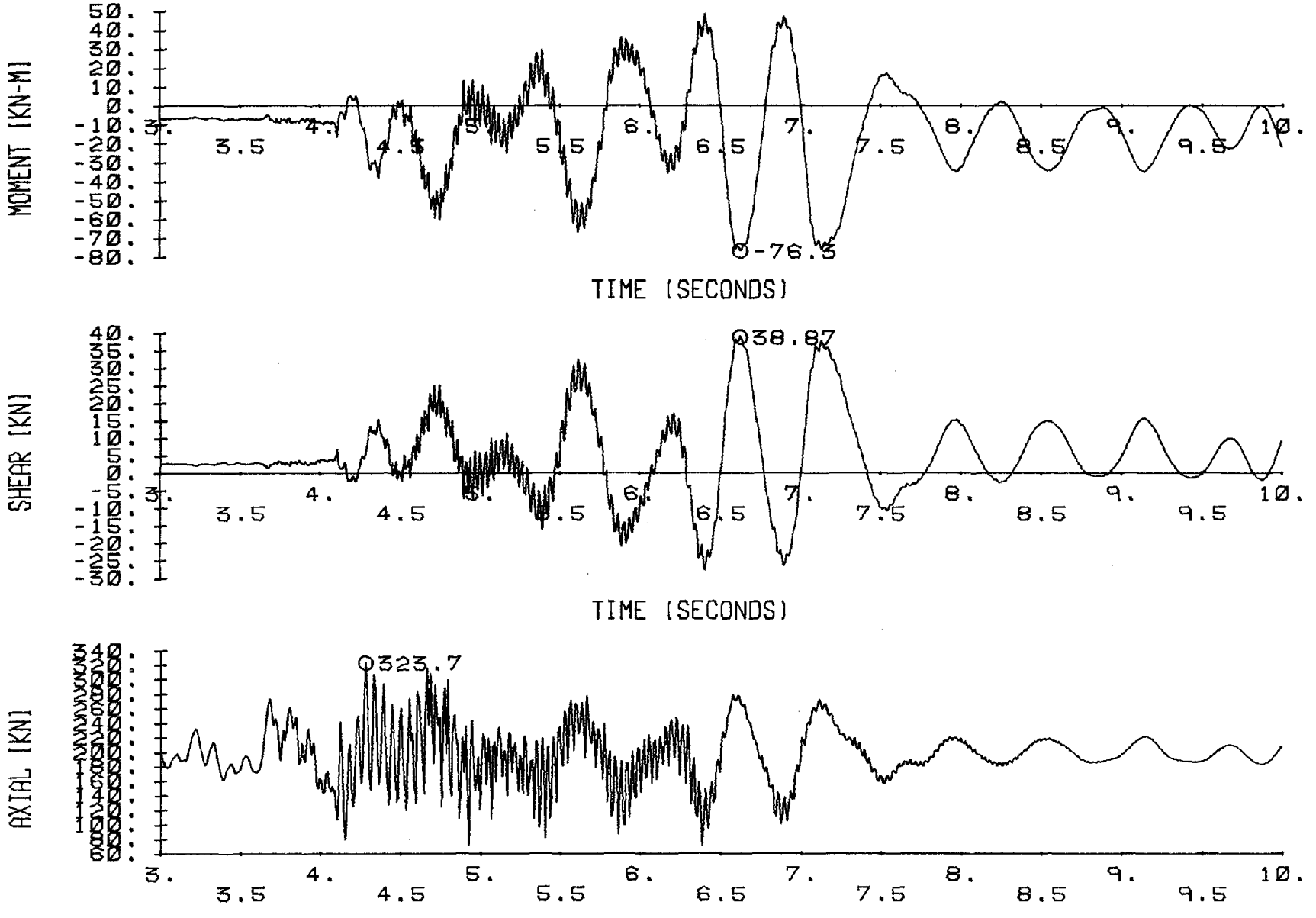

Figure 5.66 Base Moment, Base Shear, and Axial Load for the Left Column: Second Story

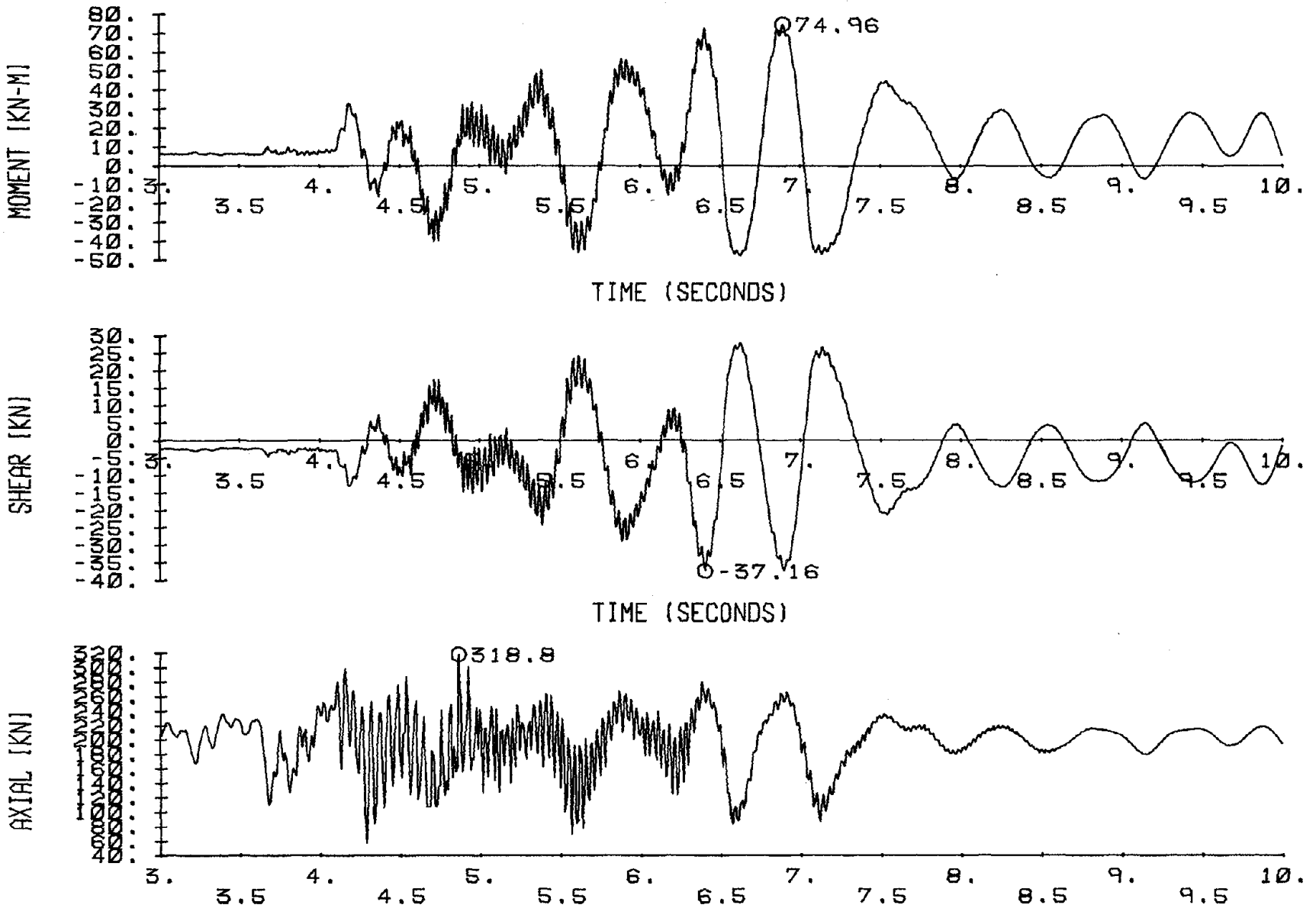

Figure 5.67 Base Moment, Base Shear, and Axial Load for the Right Column: Second Story

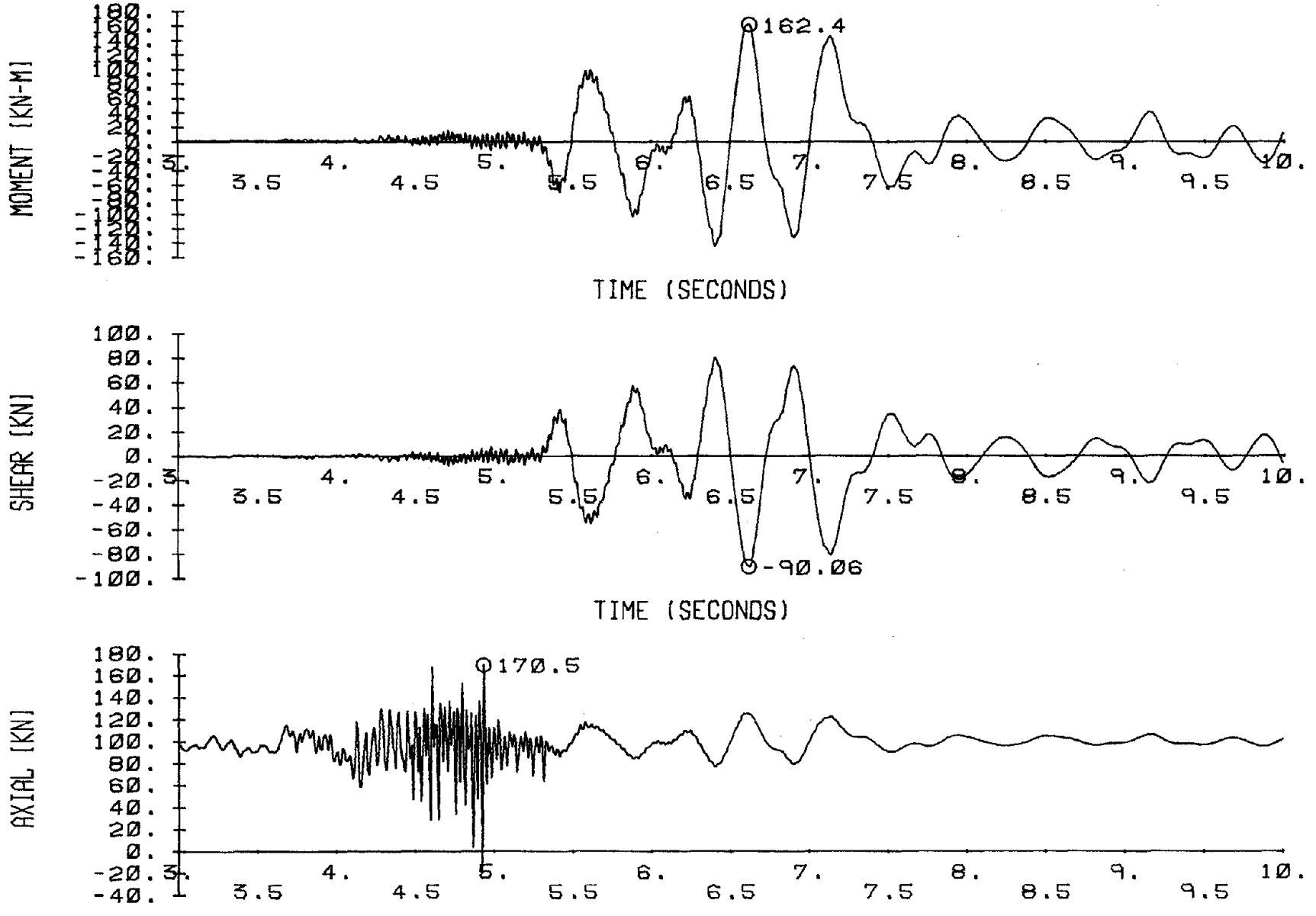

Figure 5.68 Base Moment, Base Shear, and Axial Load for the Left Column: Third Story

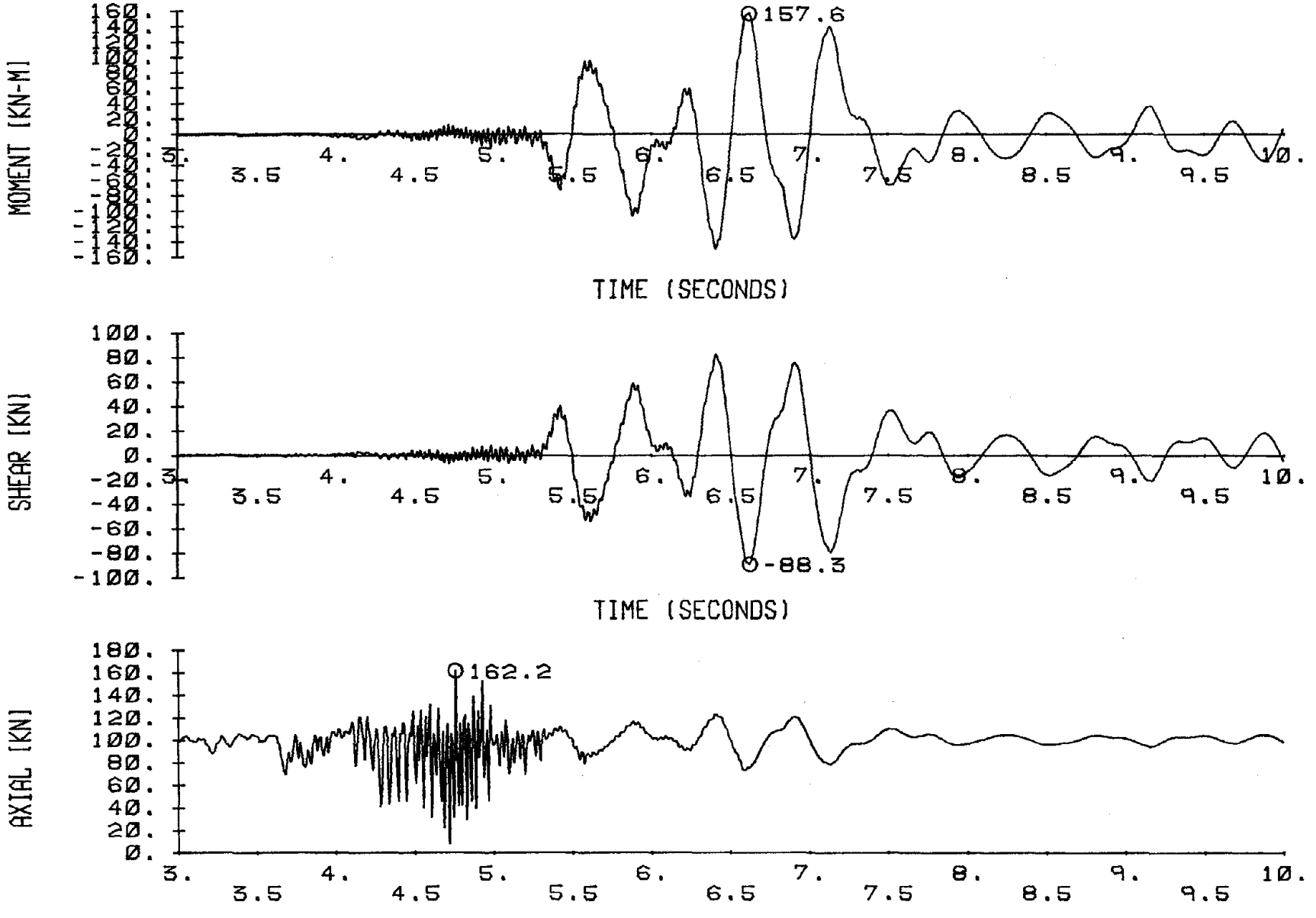

Figure 5.69 Base Moment, Base Shear, and Axial Load for the Right Column: Third Story

APPENDIX A

FAILURE SURFACE FOR MASONRY

A.1 Wall Element Failure Surface

Masonry is a nonhomogeneous, nonisotropic, material; and as stated in Chapter 3 this is difficult to handle analytically. To simplify the problem the assumption was made that masonry could be treated as a homogeneous isotropic material. However, experimental results show that this assumption may not be extended to the failure mechanism for masonry. This implies that the failure surface for masonry is in general not symmetric.

The shape of the failure surface shown in Fig. 3.3 is an assumption based on a linear interpolation between the control points F_1, F_2, F_3, F_4, and F_5. These five control points are in turn a function of the angle that the principal stress makes with the mortar joints. This condition implies that the specific shape of the failure surface shown is not constant and in general depends on the magnitude of the normal and shear stresses applied.

There are two different aspects of the failure surface for masonry which must be coupled to form the failure surface shown in Fig. 3.3. The first is the overall shape of the failure surface for the given angle that the principal stresses make with the mortar joints. The second is the change in the shape of the failure surface due to a change in the angle that the principal

stresses make with mortar joints. These two aspects are in general not independent of each other but an assumption of independence is made to make the problem tractable.

Although there is adequate experimental evidence to support the functional dependence of the control points F_1 through F_4 on the principal stress angle there is little or no direct experimental evidence to support a specific interpolation between these control points except as might be determined in an analogy with plain concrete. Due to the lack of experimental evidence a simple linear interpolation between points F_1 through F_5 is assumed. This is believed to be a conservative assumption.

The control points F_1, F_2, F_3, and F_4 represent a simple uniaxial loading condition. In making these control points a function of the angle that the principal stress makes with the mortar joints a dual purpose is served. First, it allows the failure surface to depend on the principal stress angle without having to undergo a complex analytical or experimental study and second it allows the matching of these conditions to the experimental evidence already available for uniaxial stress tests.

The dependence of the control points F_1 and F_2 on the angle that the principal stress makes with the mortar joints is shown in Fig. 3.4. This figure is based on a test developed by F. B. Johnson and J. N. Thompson to determine the tensile strength of masonry. The test consists of applying a compressive load along

the diameter of a circular masonry disk. This induces a tensile stress in the disk normal to the direction in which the load is applied. Therefore this test provides an indirect measure of the tensile strength of the masonry assemblage. By rotating the disk the angle that the principal stress makes with the mortar joint may be varied. The authors carried out a series of tests and presented their data in a paper at the First International Conference on Masonry Structural Systems in November 1967. Part of this data along with a discussion of the test was later presented in Ref.[41]. Figure 3.4 is an approximation of the experimental results presented in Fig. I-20 of Ref.[41].

The dependence of the control points F_3 and F_4 on the angle that the principal stress makes with the mortar joints is shown in Fig. 3.5. This figure is based on the experimental results presented by Hamid and Drysdale in Ref.[22]. Hamid and Drysdale carried out a series of uniaxial compressive tests where the angle that the mortar joint made with the compressive load was varied. They accomplished this by cutting out from a larger specimen the prism elements to be tested. Figure 3.5 is an approximation of the experimental results presented by the authors in Fig. 4 of Ref.[22].

No experimental evidence is available to define the control point F_5; therefore, the assumption was made to take the largest of the values of either F_3 or F_4. It is believed, based on an analogy with concrete, and possible confining effects, that this is a conservative assumption.

A.2 Joint Element Failure Surface

The joint failure surface presented in Fig. 3.2 is based on the experimental results presented by Benjamin and Williams in Ref.[7]. The authors tested a series of frames with an infilled masonry wall to study their load displacement relation as compared to an open frame.

In their effort to better understand the behavior of the masonry wall they carried out a series of tests on specimens which consisted of two bricks bonded by a mortar joint. These tests consisted in applying normal stresses which were oriented at different angles with respect to the mortar joints. This caused different combinations of shear and normal stress across the mortar joint. These series of tests allowed the authors to determine the mortar joint failure mechanism under combined stresses. Part of the results presented in Ref.[7] were later reprinted in Ref.[41]. Figure 3.2 is an attempt at approximating the experimental results presented in Fig. 6 of Ref.[7].

Figure 3.2 is not confined to failure along the mortar joints as the experiments in Ref.[7] might imply. A series of tests on full masonry panels where the cracking pattern also passed through the bricks showed a similar failure surface as that shown in Fig. 3.2. These results are presented in Refs.[18] and [41].

APPENDIX B

JOINT ELEMENT STIFFNESS MATRIX

The derivation of the stiffness matrix for the joint element is expressed in a straightforward finite element formulation based on Fig. B-1.

Figure B-1 Unidimensional Joint Element

The interpolation functions relating the generalized displacements to the nodal displacements are expressed as follows:

$$\{u\} = [N_1 \;;\; N_2]\,\{u''\} \tag{B-1}$$

where

$\{u\}$ = generalized displacements

$N_1 = N_2$ = [1 - X/t], [X/t]; interpolation functions

t = joint thickness

$\{u''\}$ = nodal displacements

Based on these functions the strains are given as follows

$$\{e_x \;;\; e_{xy}\} = \begin{bmatrix} \frac{\partial}{\partial x} & 0 \\ 0 & \frac{\partial}{\partial x} \end{bmatrix} \{u\} \tag{B-2}$$

where

$\{e_x; e_{xy}\}$ = normal and shear strain

$\{u\}$ = generalized displacements

Subtitution of Eq. B-1 into B-2 gives

$$\{e_x \quad ; \quad e_{xy}\} = \begin{bmatrix} \frac{\partial N_1}{\partial x} & 0 \\ 0 & \frac{\partial N_2}{\partial x} \end{bmatrix} \{u''\} \qquad \text{(B-3)}$$

Using Eq. B-3 and a stress strain relationship for uniaxial compression and pure shear one arrives at the following equation using the principle of virtual work

$$\{p\} = \frac{A}{t} \begin{bmatrix} K_1 & 0 \\ 0 & K_2 \end{bmatrix} \{u''\} \qquad \text{(B-4)}$$

where

$\{p\}$ = nodal loads on the joint

A = area of the joint

t = thickness of the joint

K_1 = a 2x2 stiffness matrix whose elements are the elastic modulus

K_2 = a 2x2 stiffness matrix whose elements are the shear modulus

The relationship needed to substitute in the equations formulated in Chapter 4 are of the incremental type. Equation B-4 can be made incremental by simply allowing the nodal loads and displacements to represent incremental quantities rather than the total loads and displacements as derived. The changes in the incremental stiffness which introduce the nonlinearities are provided by the changes in the stress strain relationship of the material. Before failure of the joint occurs, the relationship between stress and strain is assumed linear. This provides both an internal resistance as well as an incremental stiffness. After failure the incremental stiffness as well as the internal resistance depend on the state of stress. If the normal stress is tension, the incremental stiffness as well as the internal resistance will be zero. If the normal stress is compression then an incremental stiffness will exist as in the elastic case before failure. However, the internal resistance will only be provided by the normal stress present in the joint.

LIST OF REFERENCES

1. Anaguostopaulos S.A., Haviland R., Biggs J., "Use of Inelastic Spectra in Aseismic Design", Journal of the Structural Division, ASCE, vol. 104, ST1, January 1978.

2. Anderson J.C., Gupta R.P., "Earthquake Resistance Design of Unbraced Frames", Journal of the Structural Division, ASCE, vol. 94, ST1, January 1968.

3. Arnold P., Adams D., Le-Wu Lu, "Strength and Behavior of an Inelastic Hybrid Frame", Journal of the Structural Division, ASCE, vol. 94, ST1, January 1968.

4. Axley J.W., Bertero V.V., "Infilled Panels: Their Influence on the Siesmic Response of Buildings", Earthquake Engineering Research Center, University of California, Berkeley, EERC 79-28, September 1979.

5. Baura H.K., Mallick S., "Behavior of One-Story Reinforced Concrete Frame Infilled with Brickwork Under Lateral Loads", Sixth World Conference on Earthquake Engineering, New Delhi, India, 1977, vol. II.

6. Bazan E., Rosenblueth E., "Seismic Response of One-Story X-Braced Frames", Journal of the Structural Division, ASCE, vol. 100, ST2, February 1974.

7. Benjamin J.R., Williams H.A., "The Behavior of One-Story Brick Shear Walls", Journal of the Structural Division, ASCE, vol. 84, ST4, July 1958.

8. Benjamin J.R., Williams H.A., "The Behavior of One-Story Reinforced Concrete Shear Walls", Journal of the Structural

Division, ASCE, vol. 83, ST3, May 1957.

9. Benjamin J.R., Williams H.A., "The Behavior of One-Story Reinforced Concrete Shear Walls Containing Openings", Journal of the American Concrete Institute, vol. 30, No. 5, November 1958.

10. Clough R.W., Benuska K.L., "Nonlinear Earthquake Behavior of Tall Buildings", Journal of the Engineering Mechanics Division, ASCE, vol. 93, No. EM3, June 1967.

11. Clough R.W., Benuska K.L., Wilson E.L., "Inelastic Earthquake Response of Tall Buildings", Third World Conference on Earthquake Engineering, New Zealand, vol. II, 1965.

12. Clough R.W., Penzien J., "Dynamics of Structures", McGraw Hill Book Company, 1975.

13. Clough R.W., Tang D., "Seismic Response of a Steel Building", Proceedings of the U.S. National Conference on Earthquake Engineering, Ann Arbor, Michigan, June 1975.

14. Dawson R.V., Ward M.A., "Dynamic Response of Framed Structures with Infilled Walls", Proceedings of the Fifth World Conference on Earthquake Engineering, Rome, 1973.

15. Derecho A.T., Ghosh S.K., Iqbal M., Freskaskis G., Fintel M., "Structural Walls in Earthquake Resistant Buildings: Parametric Study", Research and Development Construction Technology Laboratories, Portland Cement Association, March 1978.

16. Esteva L., "Behavior Under Alternating Loads of Masonry Diaphragms Framed by Reinforced Concrete Members",

International Symposium on the Effects of Repeated Loading on Materials and Structures, Rilem-Instituto de Ingenieria, Vol 5, Mexico, September 1966.

17. Fedorkiw J.P., Sozen M.A., "A Lump Parameter Model to Simulate the Response of Reinforced Concrete Frames with Masonry Filler Walls", Civil Engineering Studies, Structural Research Series, No. 338, Urbana, Illinois.
18. Fiorato A.E., Sozen M.A., Gamble W.L., "An Investigation of Reinforced Concrete Frames with Masonry Filler Walls", Civil Egineering Studies, Structural Research Series, No. 370, Urbana, Illinois, November 1970.
19. Franklin H.A., "Non-Linear Analysis of Reinforced Concrete Frame and Panels", Structures and Materials Research, Department of Civil Engineering, University of California, Berkeley, March 1970, SESM 70-5.
20. Giberson M.F., "Two Nonlinear Beams with the Definitions of Ductility", Journal of the Structural Division, ASCE, vol. 96, ST2, February 1969.
21. Hanson R.H., "Characteristics of Steel Members and Connections", Proceedings of the U.S. National Conference on Earthquake Engineering, Ann Arbor, Michigan, pp. 225-267, June 1975.
22. Hamid A.A., Drysdale R.G., "Concrete Masonry Under Combined Shear and Compression Along Mortar Joints", Journal of the American Concrete Institute, proc., vol. 77, September-October 1980.

23. Hegemier G.A., Krishnamoorthy G., Isenberg J., Ewing R.D., "Earthquake Response and Damage Prediction of Reinforced Concrete Masonry Multi-story Buildings Part I: Program Definition", Sixth World Conference on Earthquake Engineering, New Delhi, India, vol. II, 1977.

24. Hegemier G.A., Krishnamoorthy G., Isenberg J., Ewing R.D., "Earthquake Response and Damage Prediction of Reinforced Concrete Masonry Multi-story Buildings Part II: Selected results", Sixth World Conference on Earthquake Engineering, New Delhi, India, vol. II, 1977.

25. Holmes M., "Combined Loading on Infilled Frames", Proceedings of the Institution of Civil Engineers, vol. 25, May 1963.

26. Holmes M., "Steel Frames with Brick Work and Concrete Infilling", Proceedings of the Institution of Civil Engineers, vol. 19, August 1961.

27. Igarashi S., Inoue K., Asano M., Ogawa K., "Restoring Force Characteristics of Steel Diagonal Bracings", Fifth World Conference on Earthquake Engineering, Rome, 1973.

28. Irwin A.W., Afshan A.B., "Performance of Reinforced Concrete Frames with Various Infills Subject to Cyclic Loading", Proceedings of the Institute of Civil Engineers, part 2, June 1979.

29. Kahn L., Hanson R., "Infilled Walls for Earthquake Strengthening", Journal of the Structural Division, ASCE, vol. 105, ST2, February 1979.

30. Kanaan A., Powell G.H., "General Purpose Computer Program for

Inelastic Dynamic Response of Plane Structures", University of California, Berkeley, EERC 73-6, April 1973.

31. Klinger R., Bertero V.V., "Infilled Frames in Aseismic Construction", Earthquake Engineering Research Center, Berkeley, EERC 76-32.
32. Kost G., McCue G.M., Simonson T.R., Rivera E., "The Interaction of Building Components During Seismic Action", Sixth World Conference on Earthquake Engineering, New Delhi, India, 1977, vol. II.
33. Kost G., Weaver W., Barber R., "Nonlinear Dynamic Analysis of Frames with Filler Panels", Journal of the Structural Division, ASCE, vol. 100, ST4, April 1974.
34. Krawinkler H., Bertero V.V., Popov E.P., "Shear Behavior of Steel Frame Joints", Journal of the Structural Division, ASCE, vol. 101, ST11, November 1975.
35. Lamar S., Fortanl C., "Brick Masonry Effect in Vibration of Frames", Fourth World Conference on Earthquake Engineering, Chile, January 1969, vol. II.
36. Lefter J., Calville J., "Reinforcing Existing Buildings to Resist Earthquake Forces", M.S. Thesis, Civil Engineering Deparment, University of Maryland, August 1974.
37. Liauw T.C., "Elastic Behavior of Infilled Frames", Proceedings of the Institution of Civil Engineers, vol. 46, July 1970.
38. Liauw T.C., Lee S.W., "On the Behavior and the Analysis of Multi-Story Infilled Frames Subjected to Lateral Loads",

Proceedings of the Institution of Civil Engineers, vol. 63, September 1977.

39. Mallick D.V., Severn R.T., "Dynamic Characteristics of Infilled Frames", Proceedings of the Institution of Civil Engineers, February 1968, vol. 39.

40. Mallick D.V., Severn R.T., "The Behavior of Infilled Frames Under Static Loading", Proceedings of the Institution of Civil Engineers, December 1967, vol. 38.

41. Mayes R.L., Clough R.W., "A Literature Survey: Compressive, Tensile, Bond, and Shear Strength of Masonry", Earthquake Engineering Research Center, University of California, Berkeley, EERC 75-15.

42. Mayes R.L., Clough R.W., "State of the Art in the Seismic Shear Strength of Masonry, An Evaluation and Review", Earthquake Engineering Research Center, Berkeley, EERC 75-21.

43. Mayes R.L., Clough R.W., Omote Y., "Cyclic Shear Test of Masonry Piers vol. 1 Test Results", Earthquake Engineering Reserch Center, Berkeley, EERC 76-8.

44. Meli R., "Comportamiento Sismico de Muros de Manposteria", Instituto de Ingenieria, Universidad Autonoma de Mexico, April 1975 (in Spanish).

45. Newmark N.M., Rosenblueth E., "Fundamentals of Earthquake Engineering", Prentice-Hall Inc., 1971.

46. Page A.W., "A Non-Linear Analysis of the Composite Action of Masonry Walls on Beams", Proceedings of the Institute of Civil Engineers, part 2, March 1979.

47. Page A.W., "Finite Element Model for Masonry", Journal of the Structural Division, ASCE, vol. 104, ST8, August 1978.

48. Paskaleva I., "Nonelastic Hysteretic Behavior of Reinforced Concrete Columns and Infilling Walls", Sixth World Conference on Earthquake Engineering, New Delhi, India, 1977, vol. II.

49. Penzin J., "Elasto-Plastic Response of Idealized Multi-Story Structures Subjected to a Strong Motion Earthquake", Second World Conference on Earthquake Engineering, Tokyo, vol. II, 1960.

50. Popov E.P., Bertero V., "Cyclic Loading of Steel Beams and Connections", Journal of Structural Division, ASCE, vol. 99, ST6, June 1973.

51. Popov E.P., Bertero V.V., Chandramanli S., "Hysteretic Behavior of Steel Columns", Earthquake Engineering Research Center, Berkeley, EERC 75-11.

52. Priestley M.J.N., "Seismic Design of Masonry Structures", Bulletin of the New Zealand National Society for Earthquake Engineering.

53. Ravara A., Mayorga A., Carvallo C., "Seismic Test of Infilled Reinforced Concrete Frames", Sixth World Conference on Earthquake Engineering, New Delhi, India, 1977, vol. II.

54. Roeder C., Popov E.P., "Eccentrically Braced Steel Frames for Earthquake", Journal of the Structural Division, ASCE, vol. 104, ST3, March 1978.

55. Sachanski S., "Analysis of Earthquake Resistance of Frame Buildings Taking into Consideration the Carrying Capacity of

the Filling Masonry", Proceedings of the Second World Conference on Earthquake Engineering, vol. III, Tokyo, 1960.

56. Sheppard P., Tercelj S., Turnselc V., "The Influence of Frequency on the Shear Strength and Ductility of Masonry Walls in Dynamic Loading Tests", Sixth World Conference on Earthquake Engineering, New Delhi, India, 1977, vol. II.
57. Sheppard P., Tercelj S., Turnselc V., "The Influence of Horizontally Placed Reinforcement on the Shear Strength and Ductility of Masonry Walls", Sixth World Conference on Earthquake Engineering, New Delhi, India, 1977, vol. II.
58. Stafford Smith B., "Behavior of Square Infilled Frames", Journal of the Structural Division, ASCE, vol. 92, ST1, February 1966.
59. Stafford Smith B., "Lateral Stiffness of Infilled Frames", Journal of the Structural Division, ASCE, vol. 88, ST6, December 1962.
60. Stafford Smith B., Carter C., "A Method of Analysis for Infilled Frames", Proceedings of the Institution of Civil Engineers, vol. 44, September 1969.
61. Storm J.H., "A Finite Element Model to Simulate the Nonlinear Response of Reinforced Concrete Frames with Masonry Filler Walls", Ph.D. Thesis, University of Illinois, Urbana, Illinois, 1973.
62. Velestos A.S., "Maximum Deformation of Certain Non-Linear Systems", Proceedings of the Fourth World Conference on Earthquake Engineering, Chile, vol. 2, January 1969.

63. Velestos A.S., Newmark N.M., Chelapati C.V., "Deformation Spectra for Elastic and Elastoplastic Systems Subjected to Ground Shocks and Earthquake Motions", Proceedings of the Third World Conference on Earthquake Engineering, vol. II, 1965.

64. Velestos A., Pennington V., "Response of Ground Excited Elastoplastic Systems", Journal of the Structural Division, ASCE, vol. 97, ST4, April 1971.

65. Walker W.H., Newmark N.M., Mosborg R.L., Velestos A.S., "Response Spectra for Two-Degree-of-Freedom Elastic and Inelastic Systems", vol. IV: Design Procedures for Shock Isolation Systems of Underground Protection Structures. RTD TDR-63-3096, Air Force Weapons Laboratory, 1965.

66. Wood R.H., "The Stability of Tall Buildings", Proceedings of the Institute of Civil Engineers, vol. 11, September 1958.

67. Wood R.H., "Plasticity, Composite Action, and Collapse Design of Unreinforced Shear Wall Panels in Frames", Proceedings of the Institute of Civil Engineers, part 2, June 1978.

68. Zienkiewiez O.C., "A New Look at the Nemark, Houbolt, and Other Time Stepping Formulas. A Weighted Residual Approach", Earthquake Engineering and Structural Dynamics, vol. 5, 1977.

69. Zigone M., Mancuso P., "Limit Analysis of Frame Systems Stiffened by Panels", Meccanica, vol. 9, March 1974.